ILLINOIS CENTER FOR TRANSPORTATION

CIVIL ENGINEERING STUDIES
Illinois Center for Transportation Series No. 22-007
UILU-ENG-2022-2007
ISSN: 0197-9191

Moisture Content and In-place Density of Cold-recycling Treatments

Prepared By
Imad L. Al-Qadi
Qingqing Cao
Lama Abufares
Siqi Wang
Uthman Mohamed Ali
Greg Renshaw
University of Illinois Urbana-Champaign

Research Report No. FHWA-ICT-22-007

A report of the findings of

ICT PROJECT R27-227
Moisture Content and In-Place Density of Cold Recycle Treatments

https://doi.org/10.36501/0197-9191/22-007

Illinois Center for Transportation

May 2022

TECHNICAL REPORT DOCUMENTATION PAGE

1. Report No.	2. Government Accession No.	3. Recipient's Catalog No.
FHWA-ICT-22-007	N/A	N/A

4. Title and Subtitle	5. Report Date
Moisture Content and In-place Density of Cold-Recycling Treatments	May 2022
	6. Performing Organization Code N/A

7. Authors	8. Performing Organization Report No.
Imad Al-Qadi (https://orcid.org/0000-0002-5824-103X), Qingqing Cao (https://orcid.org/0000-0002-9306-0306), Lama Abufares (https://orcid.org/0000-0002-9905-6930), Siqi Wang, Uthman Mohamed Ali, Greg Renshaw	ICT-22-007 UILU-2022-2007

9. Performing Organization Name and Address	10. Work Unit No.
Illinois Center for Transportation Department of Civil and Environmental Engineering University of Illinois at Urbana-Champaign 205 North Mathews Avenue, MC-250 Urbana, IL 61801	N/A **11. Contract or Grant No.** R27-227

12. Sponsoring Agency Name and Address	13. Type of Report and Period Covered
Illinois Department of Transportation (SPR) Bureau of Research 126 East Ash Street Springfield, IL 62704	Final Report 5/16/20–5/15/22 **14. Sponsoring Agency Code**

15. Supplementary Notes

Conducted in cooperation with the U.S. Department of Transportation, Federal Highway Administration.
https://doi.org/10.36501/0197-9191/22-007

16. Abstract

Cold-recycling treatments are gaining popularity in the United States because of their economic and environmental benefits. Curing is the most critical phase for these treatments. Curing is the process where emulsion breaks and water evaporates, leaving residual binder in the treated material. In this process, the cold-recycled mix gains strength. Sufficient strength is required before opening the cold-treated layer to traffic or placing an overlay. Otherwise, premature failure, related to insufficient strength and trapped moisture, would be expected. However, some challenges arise from the lack of relevant information and specifications to monitor treatment curing. This report presents the outcomes of a research project funded by the Illinois Department for Transportation to investigate the feasibility of using the nondestructive ground-penetrating radar (GPR) for density and moisture content estimation of cold-recycled treatments. Monitoring moisture content is an indicator of curing level; treated layers must meet a threshold of maximum allowable moisture content (2% in Illinois) to be considered sufficiently cured. The methodology followed in this report included GPR numerical simulations and GPR indoor and field tests for data sources. The data were used to correlate moisture content to dielectric properties calculated from GPR measurements. Two models were developed for moisture content estimation: the first is based on numerical simulations and the second is based on electromagnetic mixing theory and called the Al-Qadi-Cao-Abufares (ACA) model. The simulation model had an average error of 0.33% for moisture prediction for five different field projects. The ACA model had an average error of 2% for density prediction and an average root-mean-square error of less than 0.5% for moisture content prediction for both indoor and field tests. The ACA model is presented as part of a developed user-friendly tool that could be used in the future to continuously monitor curing of cold-recycled treatments.

17. Key Words	18. Distribution Statement
Cold In-place Recycling, Cold Central Plant Recycling, Emulsion, Moisture Content Curing, Ground Penetrating Radar, Density, Dielectric Constant, Simulations, Electromagnetic Mixing Theory	No restrictions. This document is available through the National Technical Information Service, Springfield, VA 22161.

19. Security Classif. (of this report)	20. Security Classif. (of this page)	21. No. of Pages	22. Price
Unclassified	Unclassified	69 + appendices	N/A

Form DOT F 1700.7 (8-72) **Reproduction of completed page authorized**

ACKNOWLEDGMENT, DISCLAIMER, MANUFACTURERS' NAMES

This publication is based on the results of **ICT-R27-227: Moisture Content and In-place Density of Cold Recycle Treatments**. ICT-R27-227 was conducted in cooperation with the Illinois Center for Transportation; the Illinois Department of Transportation; and the U.S. Department of Transportation, Federal Highway Administration.

Members of the Technical Review Panel (TRP) were the following:

- John Senger, TRP Chair, Illinois Department of Transportation
- Stephanie Drain, S Drain Engineering of IL
- Brian Hill, Illinois Department of Transportation
- Aaron Osman, Dunn Company
- Derek Parish, Illinois Department of Transportation
- Megan Swanson, Illinois Department of Transportation
- Marshall Thompson, University of Illinois Urbana-Champaign
- Ron Wagoner, Illinois Department of Transportation
- Jason Wielinski, Heritage Research Group
- Steve Worsfold, Illinois Department of Transportation
- Megan Yount, Heritage Research Group
- Tom Zehr, Illinois Department of Transportation

EXECUTIVE SUMMARY

Cold in-place recycling (CIR) and cold central-plant recycling (CCPR) are gaining wider use in the United States for rehabilitating existing hot-mix asphalt (HMA) pavements because of their economic and environmental benefits. The CIR or CCPR layer must be cured before the overlay is placed to avoid premature failure. During the curing process, water is steadily released from the emulsion and evaporates, enhancing layer stiffness and strength. For the emulsified asphalt, emulsion break and water evaporation occur in hours, days, or even weeks after compaction of the HMA mixture. If a CIR layer is overlaid while having a high moisture content, the retained moisture will affect the pavement-structure capacity and potentially cause HMA moisture damage. Therefore, monitoring moisture content during the curing period is important for selecting the optimum time to open the road for traffic and/or place the overlay on the constructed CIR or CCPR.

The curing time of asphalt emulsion depends on the type of emulsion, application rate, temperature of the pavement, and environmental conditions. Currently, moisture content can be measured by embedding capacitance moisture sensors at the midpoint and/or bottom of the CIR layer. A nuclear gauge can also measure moisture content; however, it is not accurate and is affected by the asphalt content. Ground-penetrating radar (GPR), which has been widely used in pavement engineering to predict pavement density and layer thickness, is a feasible technique for this application.

The objective of this study was to investigate the feasibility of estimating the moisture content in HMA pavement by using GPR. The methodology includes numerical simulation as well as lab and field tests. A numerical simulation model of HMA pavement with internal moisture was generated using mix-design information, and virtual GPR tests were performed using the finite-difference time-domain (FDTD) method. Based on the developed numerical model, the relationship between moisture content and GPR measurement was derived, and a testing protocol for predicting moisture content using GPR is suggested for CIR and CCPR pavement. Four slabs were built for the indoor lab tests to validate the relationship between moisture content and GPR measurements. Five field tests were performed using GPR on CIR- or CCPR-treated HMA pavement. GPR measurements, sand cone tests, and loose sample tests were implemented in the field. The field tests were used to calibrate numerical models and evaluate the performance of the moisture-prediction method. Based on the lab and field test results, the Al-Qadi-Lahouar-Leng (ALL) model, which was widely used to predict density for dry HMA pavement, was modified to predict pavement density when internal moisture exists.

The performance of the developed moisture content method was validated using data collected from field tests on CIR- and CCPR-treated layers. The average error of predicting moisture content for the five sites was similar and was around 0.33%. The ALL model was modified into the Al-Qadi-Cao-Abufares (ACA) model, which was used to predict moisture content from GPR measurements with a root-mean-square error (RMSE) of less than 0.5% and to predict pavement density with an average error of 2% for indoor and field CIR and CCPR projects.

TABLE OF CONTENTS

LIST OF FIGURES

LIST OF TABLES

CHAPTER 1: INTRODUCTION

BACKGROUND

The need to provide a safe, efficient, and cost-effective roadway system during a time of decreasing funds and growing demand on roadways has led to greater attention on rehabilitating existing pavements (ARRA, 2015). Therefore, new rehabilitation technologies and corresponding guidelines have been introduced. One of these technologies, which started in the 1970s, is recycling asphalt pavements. This technique has been gaining popularity because of its sustainability and economic benefits—especially cold recycling (CR), both in-place and at-plant practices.

There are several types of in-place recycling: CIR (cold in-place recycling), which involves no heat application; HIR (hot in-place recycling), which involves heat application to reclaimed asphalt pavement (RAP) for remixing and then repaving; and FDR (full-depth reclamation), which involves milling the whole depth of the asphalt layer at least 2 in. from the base/subgrade material. The selection among in-place rehabilitation methods is project specific and is based on traffic, severity of distresses, depth of milling, geometric features, limitations, and climatic conditions (NCHRP, 2011). As part of the decision making for a given project, all techniques should also be compared in terms of life cycle assessment and life cycle cost analysis.

Cold recycling of asphalt pavement is an economical and sustainable technique achieved without the application of heat to produce a rehabilitated pavement. Cold recycling can be done in-place or at a plant, referred to as cold central-plant recycling (CCPR). CIR is an on-site process that is conducted to a typical treatment depth of 3 to 4 in. but can also be done for depths as minimal as 2 in., provided underlying support is available and the depth is at least three times the nominal maximum aggregate size of the mixture to allow proper compaction. It could also be done to depths greater than 4 in. by treating the structure as a two-layer system (ARRA, 2015). CIR is conducted using a train of specialized equipment and utilizes emulsified or foamed asphalt technologies with or without stabilizers (e.g., lime and cement). The major benefit of CIR is reusing 100% of the milled material without transporting it to a plant location. CCPR, in contrast, uses a stationary cold mixture plant at a central location. The resulting mixure is laid into a pavement layer (AASHTO PP 86-17). A well-compacted CR mixture has a void percentage of 8%–16% or higher; hence, a surface overlay is usually required to protect the mixure from the intrusion of surface moisture. However, for pavements with low traffic volume, chip seals, slurry surfacing, and microsurfacing have all been proven to be sufficient (ARRA, 2015).

The CR technique is often used to address distresses like thermal cracking, raveling, and rutting in the surface layer and not for failures in bottom layers. If conducted early, CIR and CCPR could be considered preventive maintenance activities that aim to extend a pavement's service life until it needs major rehabilitation or full reconstruction. Cracked pavements that are structurally sound and have well-drained bases are the best candidates for CR (ARRA, 2015).

CIR is more common and usually preferred over CCPR because it is faster, more economical, less disruptive, and more environmentally friendly (ARRA, 2015; NCHRP, 2020). However, unlike CIR, CCPR

could offer improved aggregate gradation control by modifying the aggregate blend at the plant, but it requires the addition of slow-setting emulsions until the materials are transported to a construction site. According to ARRA, CCPR could offer the chance and time for stabilizing, replacing, or treating the base layers and/or foundation before the recycled layer is laid down. Moreover, CCPR allows the recycled pavement to be put in more than one lift. The reclaimed asphalt by CCPR could also be used in the rehabilitation of other pavement projects, not only the source pavement, preventing a valuable resource from being landfilled. Other than those differences, CIR and CCPR have similar mechanical properties (NCHRP, 2020). Please note that cold planing is at times considered a third type of CR technique, although it only consists of surface milling and preparation for resurfacing.

To ease the mixing and placement of stiff aged RAP in CIR and CCPR, there is a need to incorporate a recycling additive, softener, or a chemical stabilizing agent. Mechanical stabilization, in the form of compaction effort, is always needed and would be higher for CIR and CCPR than for conventional hot-mix asphalt (HMA) because of the colder mixing and placement temperature. Mechanical stabilization could also be achieved through the addition of imported granular materials to enhance interlock between aggregates. Chemical stabilization is achieved by adding one or a combination of Portland cement, fly ash, calcium chloride, magnesium chloride, and lime. Bituminous stabilization, the most common technique, consists of adding asphalt emulsions or foamed asphalt. A common practice in many U.S. states is to use a combination of bituminous and chemical stabilization for partial-depth recycling techniques (NCHRP, 2011). The resulting cold mixture consists of RAP, a recycling agent (emulsions or foamed asphalt), added water, added virgin binder, optional new aggregates, and other active chemical additives (e.g., cement, lime, and fly ash).

Asphalt emulsion is a stable dispersion of asphalt cement droplets in water. It contains asphalt binder, water, and emulsifying agents. Once asphalt emulsion is mixed with the aggregates, the water in the emulsion starts to break from the asphalt binder, and it behaves as free water. The emulsion starts to behave as pure asphalt binder after the evaporation of the free water during the curing process. Once all water evaporates, the emulsion sets, and the asphalt residue has the adhesion and durability of the original base asphalt binder. The asphalt emulsion or foamed asphalt have relatively low viscosity.

Curing is the most critical step in CR, as it assures achievement of adequate strength before opening the road to traffic. Curing also prevents raveling and facilitates placement of the final wearing course. The curing rate depends on multiple factors such as the nature of the stabilization, particularly if asphalt emulsions are used, as well as ambient temperature, humidity, and moisture content of the mixture. In addition, compaction level and drainage characteristics affect curing rate (FHWA, 2017). The Asphalt Recycling and Reclaiming Association (ARRA) requires CIR and CCPR to cure for a minimum of two to three days and the moisture content to be less than 3% before proceeding to secondary compaction or opening the road to traffic. Other states set the moisture content threshold at a different level. Failure to meet this requirement impacts the performance of the pavement and reduces its service life (ARRA, 2015).

There is a need to continuously monitor the curing phase in near real-time to assist with decision making about when to open a road for traffic and the suitable time to place an overlay. Ground-

penetrating radar (GPR) is a feasible technique for this application, as it has been widely used in pavement engineering to predict the density and thickness of HMA layers. GPR is a device that sends electromagnetic (EM) waves through an antenna, which penetrate the ground and reflect at interfaces of different dielectric materials. It provides insight about the underlying layer characteristics from the contrast of dielectric properties, such as their thickness, defects, density, and presence of water. GPR has been successfully used to predict the thickness of asphalt pavement layers (Leng & Al-Qadi, 2014), detect defects, localize rebar, and evaluate the dry density of asphalt pavements using the Al-Qadi-Lahouar-Leng (ALL) model (Leng et al., 2011).

The electric permittivity, ε, also referred to as relative dielectric constant or dielectric constant for simplicity, is one of the main constitutive parameters governing EM wave propagation in materials. It is defined as the measure of a material's ability to be polarized by an external electric field. The relative electric permittivity is defined by the equation in Figure 1:

$$\varepsilon_r = \varepsilon/\varepsilon_0$$

Figure 1. Equation. Relative electric permittivity.

where $\varepsilon_0 \simeq 8.85 \times 10{-}12$ Fm^{-1} is electric permittivity of free space. The velocity of propagation of EM waves, *v*, can be measured by dividing the speed of light in vacuum, *c*, by the square root of relative electric permittivity, as presented in the equation in Figure 2:

$$v = \frac{c}{\sqrt{\varepsilon_r}}$$

Figure 2. Equation. EM wave propagation speed as a function of relative permittivity.

The wave propagation speed is affected by the presence of moisture. The higher the moisture content, the higher the dielectric properties of the material and the lower the speed of EM waves in that medium, according to Figure 2. This concept is the basis for this study, where GPR was used to monitor the moisture content of pavement to decide when sufficient curing has occurred to open the road to traffic and/or construct an overlay.

OBJECTIVE AND SCOPE

The objective of this study was to investigate a new approach to continuously monitor the curing parameters that most affect CIR/CCPR pavement behavior, namely density and moisture content, using nondestructive large-coverage GPR. This will aid in decision making, such as determining the opening time for traffic and/or placing a surface overlay.

To meet this objective, the researchers conducted a series of field tests, including GPR survey, during the curing phase of emulsified asphalt to establish a correlation between a CIR/CCPR mixture's dielectric properties and its moisture content. This correlation could then be used to modify the ALL

density-prediction model to incorporate the effect of moisture. Finally, the results were presented in a user-friendly tool in near real-time.

The next chapter provides the current state of knowledge as well as details about cold-recycled mixtures, principles of GPR, GPR for density prediction, GPR for moisture content estimation, and decision making.

CHAPTER 2: CURRENT STATE OF KNOWLEDGE

This chapter summarizes the most relevant literature from recent studies and research on CR. The general process, in addition to advantages and disadvantages of CIR and CCPR, are first presented. A historic overview of the design and evaluation criteria of CR asphalt, including both CIR and CCPR, is presented along with current specifications. The chapter then focuses on the methods used to monitor density and moisture content of asphalt pavements and specifically GPR. Current practices for making decisions about curing time, which include when to open roads to traffic and/or the appropriate timing for placement of an overlay, are presented afterwards. Finally, this chapter dedicates a brief section to conclusions and recommendations based on the research to date in this field.

COLD RECYCLING

The general process of CIR and CCPR (Figure 3) starts with ripping/pulverizing the surface of existing pavements, producing RAP that can be used as base course material usually with the addition of an emulsion or a recycling agent. For CCPR, the mixing process is done at a central plant, whereas for CIR, either a single-unit recycler or a recycling train does the remaining processes on-site. A single-unit recycler mills the material, mixes the milled material with additives, and uses it for repaving either a stabilized base course or a wearing surface at a rate of 1 to 2 lane-miles/day. A recycling train consists of multiple separate construction units for milling, crushing, and screening as well as pugmill units for mixing with emulsions and additives. Conventional pavers then pave and compact the mixture. The speed of recycling trains depends on the thickness milled, equipment used, condition of existing pavement, terrain, and traffic. Modern CIR equipment can process up to 3 lane-miles/day (ARRA, 2015). The main advantages of using multi-unit trains are the higher level of process control and guaranteed maximum RAP size, but the length of the train results in less maneuverability and mobility.

Figure 3. Graph. CIR/CCPR schematic before (left) and after construction (right) (FHWA, 2017).

ARRA outlines requirements and guidelines for the use of in-place recycling processes. First, the road section should not have any subgrade- or base-related problems; otherwise, the problems should be repaired prior to CIR and CCPR. Second, there should be sufficient HMA thickness of 3 to 6 in., because CR is generally applied at a depth of 3 to 4 in. (FHWA, 2018), leaving at least 1 in. from the

HMA intact. ARRA (2015) requires the assessment of the remaining pavement and underlying materials after milling to make sure it can support the heavy loads of CR equipment. In general, the remaining 1 in. of HMA or 6 in. of stable granular base lowers the risk of equipment breaking through the pavement, if the subgrade is stable.

As the number of cold-recycling projects grows, more questions arise and more guidelines are needed. For example, NCHRP synthesis 421 did not recommend the use of CIR for roads with annual average daily traffic higher than 30,000 (NCHRP, 2011). CIR and CCPR techniques were traditionally limited to roadways with low to medium traffic volumes, but they have recently been used successfully on pavements with a higher traffic volume, including interstates (ARRA, 2015). The Virginia Department of Transportation recently completed two successful CR studies on high traffic applications: one on I-81 and another at the NCAT Test Track (FHWA, 2018). The studies concluded that there should be no upper limit for traffic levels for roadways to be treated with CIR and CCPR, provided a structural design is conducted and the recycled material is designed to have sufficient early- and long-term strengths.

There are many advantages associated with CR (ARRA, 2015; FHWA, 2017). Structural advantages of CR are listed as follows. First, CR improves pavement without changing horizontal and vertical alignments; hence, improving the original profile, crown, and slope of the pavement section. Second, CR treats existing crack patterns, including reflective cracking, by delaying the formation of new cracks. Third, CR treats pavement exhibiting a wide range of distresses, including rutting, through modification of existing aggregate gradation and binder properties. Fourth, CR does not disturb subgrade soils, unless full-depth reclamation (FDR) is performed. Other possible advantages of CR include improving surface friction, ride quality, and surface texture, all of which contribute to enhanced safety while improving pavement aesthetics by providing a new pavement surface.

CR mixes are also environmentally friendly, because the CR process eliminates RAP disposal problems, conserves higher energy compared to other maintenance and rehabilitation methods, and reduces greenhouse gases by 50% to 85% (ARRA, 2015). In addition, dust, fume, and smoke pollution are minimized. Likewise, natural petroleum, nonrenewable resources, and natural quarried aggregates are either not used or are employed in limited quantities, which helps preserve natural resources. CR followed by an asphalt overlay can also have a positive impact on tire-pavement noise levels.

CR hauling costs for materials are greatly reduced, especially for CIR. The corresponding equipment fuel consumption is thus reduced, resulting in 30% to 50% less total expenditure compared to other construction methods (ARRA, 2015). The production rate is high (up to 500 tons/hr), which makes this technique user convenient by minimizing construction time and delays. CIR also reduces the thickness of HMA overlay needed (or may eliminate it altogether) to obtain the desired life span, resulting in more savings.

There are, however, some limitations for the use of CR. Most of the limitations discussed hereafter were published in MnDOT (2000) and FHWA (2018) reports. Some structural drawbacks include material and construction variability, which is greater than that for conventional rehabilitation techniques. The variability makes the pavement's performance complicated and difficult to predict.

Additionally, CR mixes need to be cured for a period, which could extend to days, in order to gain strength. Cold-recycled mixtures were also shown to have lower stiffness than conventional HMA mixes (NCHRP, 2020). Improper application of CIR and CCPR can result in early failures that negatively impact economic and sustainable design aspects. Finally, there are limitations for CIR use imposed by roadway geometric attributes, such as tight turns, steep grades (> 5%), and presence of castings (such as manholes, catch-basins, valves, among others).

Other potential drawbacks include compaction delays to avoid producing a tender mix, which could take anywhere from 30 minutes to 2 hours, depending on the breaking properties of emulsions (ARRA, 2015). In addition, the construction process is influenced by ambient temperature and moisture conditions, especially the curing phase, as mentioned in Chapter 1. Extensively shaded areas that receive little or no direct sunlight take longer to cure, delaying traffic opening, and the construction of CR projects is often performed in stages, which can result in more traffic disruptions and delays in work zone areas.

OVERVIEW OF THE DESIGN AND EVALUATION OF COLD-RECYCLED ASPHALT

The mix design for CR varies by agency and project and is not yet well formulated. According to Wood et al. (1988), there was no standard reliable mix design practice for CR mixes until 1988. There were general design guidelines such as targeting the binder/additive ratio to be in the 1% to 3% range for asphalt emulsion. Survey responses in the same study also indicated varying laboratory compaction methods and efforts, such as using 50 Marshall blows, 75 Marshall blows, kneading, or gyratory compaction, with no distinct consensus on number of gyrations. Curing after compaction of design specimens was reported to be 1 hour, 5 hours, 16 hours, 1 day, 3 days, or 7 days. Curing temperatures included room temperature, 77°F, 105°F, 120°F, 140°F, and 250°F. These issues required further development and standardization.

Moreover, the responses from the same survey indicated the mix design procedure used by agencies and contractors was usually the Hveem or Marshall methods (Wood et al., 1988). However, AASHTO's most recent standard on the topic (AASHTO PP 86-17) offers a standard practice for CIR and CCPR mix designs. The standard recommends the use of either the Marshall or SuperPave approach for CR mix preparation. Considering that, most other asphalt mix designs shifted toward using SuperPave mix designs, because the SuperPave gyratory compactor can be portable, mimics field compaction better than other compactors, and causes less degradation to coarse aggregates than the Marshall hammer (Hainin et al., 2013). In addition, SuperPave mix design requirements consider the location's weather and more advanced performance-based testing.

In accordance with AASHTO PP 86-17, three test specimens of different emulsion percentages (between 1% and 4% with increments of 0.5 or 1.0) are to be compacted to 30 gyrations if using a SuperPave gyratory compactor or at 75 blows per side for the Marshall hammer. Lab tests associated with CIR and CCPR include bulk specific gravity, maximum specific gravity, stability, base bitumen requirements (AASHTO MP31-17), and optimum emulsion content. The Minnesota Department of Transportation (MnDOT, 2000) reported a summary of CIR lab testing methods developed by AASHTO, California, Ontario, Oregon, Pennsylvania, and the US Corps of Engineers. The Illinois

Department of Transportation (IDOT) specifies a minimum strength of 45 psi for an indirect tensile test or a minimum Marshall stability of 1,250 lb. More test requirements, such as those for the raveling test, can be found in AASHTO MP 31-17. However, according to MnDOT (2000), indirect tensile strength does not differ much among different emulsion contents and curing times of CR mixes. Nevertheless, remarkable differences were observed in failure modes; specimens with longer curing times hardly showed signs of failure once ultimate strength was reached. It was clear that the indirect tensile strength of a specimen is mainly a function of the air void percentage, and this called for tests and specifications for emulsified CIR and CCPR other than the indirect tensile test.

A 2020 NCHRP study proposed some AASHTO performance testing standards including thresholds for raveling and shear tests of CR mixes using three test replicates in the future. For the moment, CIR and CCPR AASHTO standard practices are more ambiguous compared to HMA guidelines and specifications. For example, typical air void content for CIR and CCPR is a range between 9% and 14% and is not a specific value like for HMA (4%). The resulting CIR and CCPR mix performance is highly variable and mainly depends on the RAP obtained, emulsions used, and curing conditions.

Volumetric mix design is more difficult for CR than HMA. According to ARRA, there are three theories used in designing CR (ARRA, 2015). The first theory assumes that RAP will act as black aggregates and the added binder should entirely coat the black aggregates. The second theory assumes complete softening of the aged binder in RAP using recycling agents. The third theory, which is the most realistic, is a combination of the first two assumptions, where some of the aged binder is softened and included in the design. However, this effective binder layer is still difficult to quantify.

The emulsions used with CIR and CCPR are usually engineered, meaning they have engineered properties including mixing and coating abilities, breaking times, curing times, moisture resistance, softening ability, and stiffness properties of the residual binder. Some of the engineered emulsions are proprietary, and their specific composition is unknown. Emulsions should be metered by the weight of RAP produced and accurately quantified by a computer-controlled measuring system to be added at a tolerance of $\pm$0.5%. Excess recycling agents could result in an unstable mix subjected to rutting and shoving, whereas insufficient recycling agents could result in segregation and raveling (ARRA, 2015).

The resulting pavement performance is governed by curing time and other key construction practices recommended by ARRA such as overlapping between adjacent CIR cold planer passes for at least 4 in.; avoiding overmixing, which results in loss of asphalt coating due to premature breaking of emulsions; and avoiding undermixing, which can cause poor coating of the aggregates (ARRA, 2015). To have good workability, compaction should start when emulsions start breaking. For curing, there is no protocol or agreed-on curing method in terms of temperature or duration for CR asphalt, but 14 days is generally considered adequate. Typical curing periods can be a few hours to several weeks (ARRA, 2015). For lab curing tests, curing with a drying oven appears to best represent actual field curing of CIR (Cox et al., 2016).

Furthermore, CIR and CCPR construction should always include field adjustments because these processes vary due to changes in the materials being recycled along the roadway, ambient temperature and humidity conditions, and speed of the equipment; therefore, the RAP gradation

from milling would also vary. Thus, field observations and adjustments are needed to assure good coating of the materials, workability of the HMA mixture, and quality construction, even though the optimum moisture, additive type and content, and other factors are predetermined through laboratory tests and are stated in the job-mix formula. These modifications and adjustments should be conducted by experienced field personnel who are continuously engaged in observing the material being placed behind the recycling train.

To evaluate CIR asphalt, recommendations for quality control approaches found in the literature include emulsion testing to determine the percentage of residue from distillation, which is now specified to be higher than 64% by AASHTO MP 31-17. Other field testing recommendations include measuring depth, monitoring compaction with a nuclear density gauge, and verifying moisture content before overlaying CIR and CCRP (NCHRP, 2011). Monitoring density and moisture content of CR mixes seem to be key points for performance evaluation. The next subsections present and compare state-of-the-art monitoring practices for density and moisture content.

PRINCIPLES OF GPR

GPR's premise is simple: it sends short EM waves, through an antenna, that are able to penetrate pavement layers. Whenever the waves enter a different medium (e.g., layer), part of the EM waves is reflected back and received by the antenna. The reflected signals help to detect different pavement layers or underground pipes and even some inhomogeneities within the pavement layer. Figure 4 presents the typical components of a GPR system: an antenna, a data acquisition system, and a distance-measuring instrument or GPS to synchronise data collected with the station or location. Note that the antenna can be ground- or air-coupled. An air-coupled antenna is preferred as it allows driving at highway speeds, although a ground-coupled antenna could offer higher penetration depth.

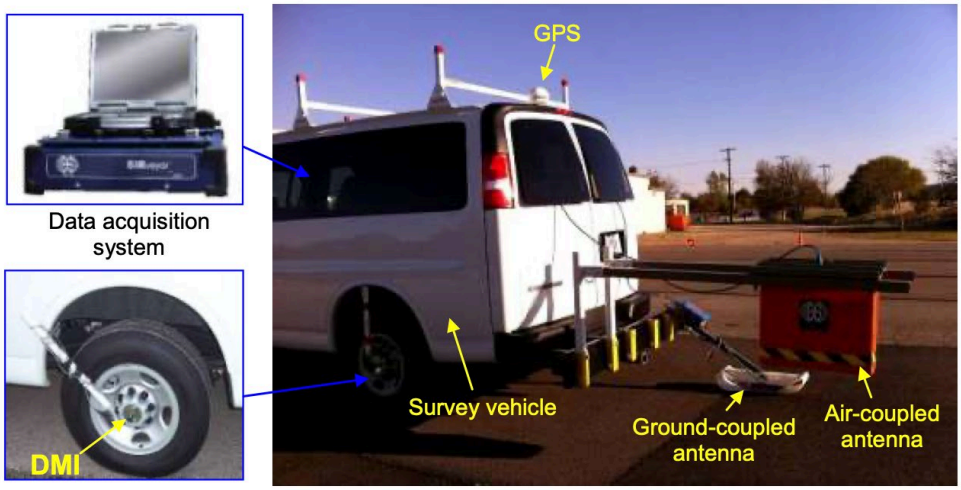

Figure 4. Photo. Components of a typical GPR system.

GPR offers advantages over other pavement evaluation devices. GPR is noninvasive, has wide coverage, can be used continuously, and is safe to use. However, GPR users still need some training and knowledge of EM waves and signal analysis.

Reflected GPR signals are used to calculate the (relative) dielectric constant of the medium, which is afterwards used to estimate other properties of the pavement like layer thickness and density. There are several methods to estimate the dielectric constant, the most common of which are reflection amplitude (RA) and two-way travel time (TWTT), which are applied in this study. For the reflection amplitude method, presented in Figure 5, two amplitude values are extracted from GPR scans and are used to calculate the dielectric constant. One value is the reflection amplitude from the pavement surface (A_p), and the other value is the reflection amplitude from a perfect reflecting surface like a copper plate (A_c).

$$\epsilon_r = \left(\frac{1+\frac{A_p}{A_c}}{1-\frac{A_p}{A_c}} \right)^2$$

Figure 5. Equation. Calculation of the dielectric constant using the reflection amplitude method.

This method is practical and simple to use. A calibration scan on top of the copper plate is obtained on-site and other amplitudes can be easily extracted from GPR scans. In this method, however, the surface dielectric constant is representing only the surface of the pavement and not the whole layer, which is a fair assumption for a newly constructed pavement, which could be assumed homogeneous along the depth. This may not be a proper assumption for older pavements, however, where aging of the surface causes inhomogeneity along the depth of the layer.

The TWTT method takes inhomogeneity of the layer into consideration. TWTT is the time needed for EM waves to go through a pavement layer and come back, which can be directly extracted from a GPR scan, using that time. The dielectric constant of the medium can be easily calculated, as presented in Figure 6.

$$\epsilon_r = \left(\frac{ct}{2d} \right)^2$$

Figure 6. Equation. Calculation of the dielectric constant by the two-way travel time method.

where *c* is speed of light ($1.18 * 10^{10}$ in./s), *t* is the two-way travel time (s), and *d* is the depth / thickness of the layer (in.). This method has shown to be accurate in many studies. However, it is not practical for a few reasons. First, the equation is highly sensitive to layer thickness, which is not always known accurately. Second, sometimes locating the reflection from the bottom layer in GPR scans is difficult, which jeopardizes determining the TWTT time. A reflector may be installed to avoid those two problems.

HMA DENSITY PREDICTION

Achieving adequate density is critical for the long-term performance of asphalt pavements. There have been extensive efforts to monitor field density of newly constructed pavements using different techniques such as coring and sand cone, which are traditional, reliable methods but are destructive,

time-consuming, labor intensive, and have limited coverage. Nuclear gauge, in contrast, has been extensively used because it is nondestructive. However, it also has limited coverage, requires special licensing, and is highly affected by the hydrogen present in the asphalt binder (NCHRP, 2020). Intelligent compaction (IC) for density monitoring during compaction has been used for a while. It uses mechanical waves to determine pavement layer responses due to specific loads and frequencies. The response is a function of density, Poisson's ratio, and the modulus of the pavement layer. However, the modulus and Poisson's ratio of asphalt are dependent on temperature and loading frequency, and temperature continuously changes when pavement cools down. This would limit the use of this technology, unless an advanced database is created that is a function of temperature. A lightweight deflectometer (LWD) has also been used to back-calculate the stiffness of the material. Its ability to measure an engineering property gives it an advantage over other methods, but it has limited coverage and causes traffic disturbance. The dynamic cone penetrometer (DCP) has shown good and reliable results (Diefenderfer et al., 2020); however, it does not measure an engineering property, has limited coverage, causes traffic disturbance, and is labor intensive. Finally, GPR is nondestructive, continuous, fast, and could provide near real-time measurements. GPR uses EM waves, which are temperature independent, at the frequency used and is solely a function of the volumetric and dielectric properties of the layer. GPR has been successfully used to determine the thickness of asphalt pavement layers (Leng & Al-Qadi, 2014), detect defects, locate rebar, and evaluate dry density of asphalt pavements using the ALL model (Leng et al., 2011). GPR, however, does need a specialized software to process data and signal-processing techniques to extract valuable results.

Compaction of CIR is believed to require more energy than conventional HMA or warm-mix asphalt because of the higher internal friction developed between the particles in a cold mix, the higher viscosity of the aged binder, and the cold compaction temperatures, as there is no heat applied for better workability (ARRA, 2015). There is no standard for the compaction process: it could be performed in one or two stages using a static steel roller and/or vibratory steel/pneumatic rollers. Some agencies reported success with a single stage of compaction but others indicated that a second stage is required after curing and before applying surface treatments to remove minor consolidation in wheel paths as a result of densification by traffic (ARRA, 2015). Although it is well-documented that improper compaction/density leads to poor HMA quality, the case is slightly different for CR asphalt pavements. Gaining strength occurs with time as curing proceeds, even when density remains almost constant (NCHRP, 2020), which urges researchers to identify another paramater to monitor: moisture content.

Because CR asphalt pavements differ from conventional asphalt in terms of compaction, the change in asphalt pavement density should be monitored after each roller pass in order to ensure successful compaction (i.e., real-time monitoring). It would be beneficial to develop a tool that can collect data continuously without contacting the pavement surface and interpret the data in real time. The operator of the compactor could then view the density in real time and adjust compaction parameters, such as vibration amplitude and frequency, rolling speed, number of rolling passes, sequence, and timing of rolling passes (Shangguan et al., 2014). To achieve that, a GPR system was mounted on a roller, and data were collected during compaction. Signal-processing techniques were also developed for noise cancellation during this process (Wang et al., 2019, 2020).

The ALL model (Leng et al., 2011)—represented in Figure 7—was developed at the Illinois Center for Transportation (ICT) and is a scientific fundamental approach that is not site specific. It relates the GPR reflected signal to the dry HMA bulk specific gravity (G_{mb}). The dielectric constant of the pavement structure obtained using the reflected GPR signal (ε_{AC}) is used to predict the density of the pavement using the dielectric properties and volumetric proportions of the pavement components. The larger the bulk dielectric constant, the higher the density of the pavement layer (assuming no moisture content). Other mix variables required as input for the ALL model include the maximum specific gravity of the HMA (G_{mm}), effective specific gravity of the aggregates (G_{se}), and percentage of asphalt content (P_b), all of which can be obtained from the contractor prior to compaction. Other parameters are the dielectric constant of binder (ε_b), which is set to three according to Leng and Al-Qadi (2014), and the dielectric constant of aggregates (ε_s), which could be obtained from coring or aggregate databases. The targeted G_{mb} changes air content, depending on compaction energy.

$$G_{mb} = \frac{\frac{\varepsilon_{AC}-\varepsilon_b}{3\varepsilon_{AC}-2.3\varepsilon_b}\frac{1-\varepsilon_b}{1-2.3\varepsilon_b+2\varepsilon_{AC}}}{(\frac{\varepsilon_s-\varepsilon_b}{\varepsilon_s-2.3\varepsilon_b+2\varepsilon_{AC}})(\frac{1-P_b}{G_{se}})-(\frac{1-\varepsilon_b}{1-2.3\varepsilon_b+2\varepsilon_{AC}})(\frac{1}{G_{mm}})}$$

Figure 7. Equation. The ALL density prediction model.

One of the techniques developed by ICT to predict asphalt pavement's bulk dielectric constant using GPR is the extended common midpoint method (CMP). This approach measures the bulk dielectric constant of the pavement, which can then be used to estimate the bulk density using the ALL model. A moisture-removal algorithm has also been introduced to remove the effect of "surface moisture" that is added through nozzles during compaction and to calculate the true dielectric constant of the asphalt mix (Shangguan et al., 2014). The ALL model for density prediction was verified using GPR for six different dry asphalt mixes varying in density (Fernandes et al., 2017). To date, the use of GPR has been limited to HMA (NCHRP, 2020). GPR has proven to be accurate and efficient in estimating density of dry asphalt, so this study aimed to explore its efficiency for cold-recycled emulsified mixtures.

FEASIBILITY OF GPR APPLICATION FOR MOISTURE CONTENT PREDICTION

Water is an important component in CR. It is added at several stages: before milling for dust control and lubrication to extend the life of the cutting teeth, during mixing to ease the mixing process and prevent premature breaking of emulsions, and at the time of compaction by a nozzle on the wheel of the compactor to prevent asphalt from sticking to the roller (ARRA, 2015).

Moisture is a key point where design and construction of cold-recycled mixtures disconnect; no design guideline controls the amount of water to be added in the field. Nevertheless, too much moisture can result in a tender mix, which could hinder compaction and cause moisture damage. Furthermore, if the moisture penetrates the granular layer, bearing capacity could be largely reduced.

As mentioned in Chapter 1, the curing time of asphalt emulsion depends on the type of emulsion and stabilizing agent. For example, Kim et al. (2011) recommended the use of different curing criteria for

foamed and emulsified asphalt. Curing time also depends on application rate, pavement temperature, moisture content, layer thickness, level of compaction, drainage characteristics, presence of active fillers, in-place air voids, and environmental conditions. Curing conditions for CIR were believed to range from a minimum of a few hours to a maximum of several weeks (ARRA, 2015).

Curing time affects other activities such as opening the road for traffic and timing for placing an overlay. Several studies have shown that when recycled materials lose moisture (i.e., cure), the particle bonds are enhanced and mix strength properties are increased (NCHRP, 2020). Decision making related to opening the road for traffic and timing for an overlay, based on curing status, will be discussed in the next section of this chapter.To date, no ASTM or AASHTO standards exist to determine curing status. A number of generic agreed-on temperatures for lab curing exist, but have not been proven to simulate field conditions (NCHRP, 2020).

There are several techniques to measure moisture content. One technique is embedded sensors, which are not practical for CR and are expensive. A time-domain reflectometer (TDR), which uses EM pulses to measure the dielectric constant by measuring the time needed for the pulse to traverse in the CIR layer, yields reliable results but has limited coverage. Nuclear gauges are not accurate, as discussed in the “HMA Density Prediction” section, and have limited coverage. Capacitance moisture sensors, found to be the most accurate technique in Kim et al. (2009), also calculate the dielectric constant by measuring the rate of change of voltage on a sensor, but sensors have limited coverage and are expensive.

A lightweight deflectometer was generally able to capture the curing of three test slab specimens with dimensions of 20 in. by 20 in. and a thickness of approximately 4.5 in. by back-calculating the modulus (Diefenderfer et al., 2020). To predict moisture evaporation, moisture content was found to be more related to pavement temperature than air temperature, wind speed, or humidity (Kim et al., 2009).

The key drawback of the aforementioned methods was mainly limited coverage. GPR, on the other hand, seems to be a feasible technique for this application, as it has been widely used in pavement engineering to predict pavement density and layer thickness, and, most importantly, its coverage is relatively high and could be planned for complete coverage. In addition, GPR uses EM waves to determine the dielectric properties of a layer at normal traffic speeds. However, when moisture is free (not bound in the emulsions), it masks the reflected signals, making them look higher in amplitude, which indicates false higher density. This is because the dielectric constant of water is 78 at ambient temperatures of 23ºC. (The dielectric constant changes slightly with temperature and is usually considered to be 81 at 20ºC.) This number is signficantly different from a typical HMA dielectric constant, which ranges from 3 to 10, depending on the aggregate type in the mix. (Limestone’s dielectric constant is greater than that for quartzite, for example.) This contrasting idea between dielectric properties of components was previously used between water and soil materials to determine partial water saturation (up to 60% only) using a square-root formula for soils and the dielectric properties obtained by GPR (Alharthi & Lange, 1987). GPR techniques are also widely used to infer the volumetric water content in sub-asphalt structural layers and to determine the performances of drainage systems (Al-Qadi et al., 2004).

According to the EM mixture theory, the dielectric constant of the emulsion asphalt mix may be greater than 12. This value is based on assuming the asphalt emulsion composes of 65% asphalt binder residue and 35% water and the asphalt emulsion content is 3% of the mix. As water evaporates, the dielectric constant of the emulsion asphalt mix becomes closer to the dielectric constant of the dry asphalt mixture. Thus, the dielectric constant can be used as an indicator of the moisture content, and GPR has the ability to monitor moisture content during emulsion breaking. Once the pavement is dry, the ALL model can be used to correlate the measured dielectric constant to pavement density (Leng & Al-Qadi, 2014).

GPR moisture estimation is dependent on the percentage of air voids and their connectivity. For example, if the pavement structure is highly porous, water would not accumulate and would be drained. In contrast, if the pavement structure has disconnected voids (in the case of low air void content), moisture would be trapped on the surface and would affect the GPR's surface reflection amplitude. A modified ALL model was developed to take into account the effect of surface water on the dielectric constant of an asphalt mixture (Shangguan et al., 2014). This model yielded an overall accuracy of about 98.8% in classifying air content of finite-difference time-domain (FDTD) simulated data into four categories: over compacted, well compacted, less compacted, and uncompacted. The thin, wet HMA layer in the simulation represents the surface moisture in the field. But this correlation is not yet validated for CR, because there are many variables other than percentage of voids and surface water that are not simulated such as emulsion-bound water, void connectivity, and heterogeneity of the asphalt layer.

In a recent study, GPR predicted the dielectric constant successfully and indicated the presence of moisture in six asphalt mix slabs with different densities and air void contents (Fernandes et al., 2017). The GPR readings were carried out moments after the application of water and were compared to those in the dry state. No correlation was found between the moisture content and parameters that were used to characterize the asphalt mixes (dielectric properties), which can indicate that the moisture required other complex variables for its assessment.

Other complications arise from using GPR to monitor moisture. One recent study showed that the higher the permittivity/dielectric constant of the layer (due to presence of moisture, for example), the more sensitive the GPR is to height swings and the greater the error in calculating layer characteristics (Frid & Frid, 2018). However, this could be addressed by using stable supports for the GPR antennas to try to minimize height swings as much as possible.

The major challenge of using GPR is that CR contains bound water within the emulsions before breaking, which makes the moisture composition more complicated and harder to detect using GPR, especially during the transition from bound to free to vapor.

TIME FOR OVERLAY CONSTRUCTION AND OPENING FOR TRAFFIC

The final goal of this study was to use the curing time estimated by GPR for decision making about when to open roads for traffic and indicate the optimum timing for an overlay/surface treatment. For the latter, there are some recommendations that differ by state, while for the former, there is not much previous work done in that area. However, they are both important, and they both affect the

performance of the pavement structure. If the CIR/CCPR layer is subjected to traffic for an extended period before an overlay is placed, the risk of premature failure increases.

The stiffness of the CR layer may not be a good measure of moisture loss, but it may be used as a measure to determine the optimum timing to place an overlay. Stiffness is mainly affected by temperature and secondarily by moisture (Kim et al., 2009). Laboratory test results confirm that curing time and moisture content affect the properties of CIR mixes. Increasing curing time and decreasing moisture content both increased the indirect tensile strength, dynamic modulus, and Marshall stability of foamed and emulsified CIR mixes (Kim et al., 2011). Special attention should be given to CIR/CCPR in terms of curing to build sufficient strength (NCHRP, 2020).

Curing is a critical step in CIR/CCPR, as it assures achievement of adequate strength before opening the road to traffic or else large distresses and performance issues could result early in the pavement's service life. Traffic is typically allowed back on CR pavements by the end of the day at reduced speeds to prevent raveling (FHWA, 2018). However, ARRA (2015) requires curing for at least two to three days and the moisture content to be less than 3% before proceeding to secondary compaction or opening to traffic. Placement of a surface layer on CR material with excessive moisture will delay strength gain and could cause premature failure of the surface layer (ARRA, 2015).

When asphalt emulsions or emulsified recycling additives are used, emulsion breaking could take anywhere from 30 minutes to 2 hours after laying it down, depending on the characteristics of the asphalt emulsion, thickness of the CIR mix, and environmental conditions (ARRA, 2015). The compacted mix must be adequately cured before a wearing surface is placed, and this could take several days to two weeks or more in case of rainfall events, depending on the variables discussed in the "Feasibility of GPR Application for Moisture Content Prediction" section. For example, Arizona, Iowa, South Dakota, Vermont, and Washington require that the CIR layer cure until the moisture of the CIR mixes is reduced to 1.5% or less. Colorado requires a moisture content of 1% and Kansas requires 2%. Delaware, Idaho, Maine, Maryland, Nebraska, Nevada, New Hampshire, New York, Ohio, Ontario, and Pennsylvania require a 4 to 45 day curing period before placing an overlay (Kim et al., 2011; Kim & Lee, 2006). But time requirements are highly inefficient; the materials could have developed sufficient strength much sooner than allowed by specifications (Diefenderfer et al., 2020) and sometimes roads are opened to traffic before sufficient strength is developed. This promoted the need for in situ tests. Dynamic cone penetrometer is the most sensitive in situ test for the existence of additives and curing of CR mixtures, with a mean between-specimen coeffecient of variation of less than 6%, in a study that included lightweight deflectometer, dynamic cone penetrometer, soil stiffness gauge, Marshall hammer, shear test, and raveling test (Diefenderfer et al., 2020). Some of those tests are laboratory tests only, some have limited coverage, and most are labor-intensive and disruptive to traffic.

As materials become better understood and contractors gain more experience, pavements may be open to light vehicles moving at slow speeds within hours of construction. Overlay may be placed several days later. For example, curing could be made faster using recycling additives like lime or cement or other active fillers, which are usually added at 1% (Diefenderfer et al., 2020). But, this process depends on many variables and needs to be monitored continuously before any decision is

made. Specifications from one owner agency might not be applicable to another owner agency in a different location because of the high dependency of CR on materials used and environmental conditions. This is where GPR is handy. This study aimed to extend the use of GPR to CR pavements using similar principles. If a correlation between the moisture content and GPR measurements was made, real-time decision making would be possible regardless of those variables, which was the final goal of this project.

SUMMARY

The main takeaways from the published literature are listed below:

- AASHTO PP 86-17 gives general guidelines for CIR and CCPR mix design. Additional guidelines concerning curing should be considered independently for each region or state. Similarly, more mix test requirements should be added to the specifications to complement the indirect tensile strength test, which was shown to be independent of curing time and emulsion content.

- The compaction of CIR and CCPR differs from the compaction of conventional HMA. Thus, to achieve the required field density, more attention is needed to monitor its density in order to avoid distresses, which can be done nondestructively and in real-time using GPR.

- Some local governments open roads to traffic within hours of construction, which might be detrimental to the pavement if sufficient curing did not take place. It is recommended to wait until the moisture content is below 3% before opening to traffic or at least three days. However, curing depends on many environmental and mix-related parameters, and, thus, it should be monitored continuously before decision making. Furthermore, roads should not be open to traffic in their weak state for a long time before an overlay is placed, especially CR mixes that are known to have 50% less stiffness than conventional HMA.

- Recommendations for when to place an overlay after CIR/CCPR construction differ by state. Recommendations for moisture content range from 1% to 2% or range in terms of time from 4 to 45 days. Real-time monitoring is needed, however, because of the high variation between projects.

- There is already a physical relationship that relates dielectric constant of the pavement obtained from the GPR and bulk dry density of the pavement: the ALL model, which could be modified to include the effect of moisture of CR on bulk density.

- There are some challenges that must be considered to using GPR to monitor moisture content of CIR/CCPR such as bound water vs. free water and heterogeneity of the layer. Likewise, GPR is highly sensitive to height changes at high reflection amplitudes, which could be caused by the presence of moisture.

CHAPTER 3: RESEARCH APPROACH

The methodology in this study was divided into simulation analysis and experimental studies. Predicting moisture content for a CIR or CCPR layer is a challenge because of the dielectric properties and space distribution of water inside HMA pavement. To better understand the effect of internal moisture content on the dielectric constant, GPR measurements on non-dry pavements were simulated using a numerical modelling approach, improving upon previous research by Al-Qadi and colleagues. Then, both indoor and field tests were implemented to validate the proposed simulation model. Based on the simulation, lab tests, and field tests, the ALL model was modified to accommodate internal moisture content in asphalt mixtures.

GPR MEASUREMENT SIMULATION

The discrete element method (DEM) and finite element method (FEM) are two numerical techniques that are widely used to conduct micromechanical analysis of heterogeneous materials such as HMA (Xu et al., 2017). The finite-difference time-domain (FDTD) method, in contrast, concentrates on the simulation of EM wave propagating in the material and not the mechanics of the aggregates' interlocking. Hence, the model needs to provide an effective and accurate simulation of volumetric properties of each component in a 2D space. The theoretical background of the heterogeneous FDTD model is the dielectric mixing theory, which uses volume fractions and the dielectric constant of each component of the heterogenous material to derive an approximation of the material's bulk dielectric constant. An accurate density-prediction method for dry asphalt pavement has been extensively studied by Al-Qadi and colleagues (Cao & Al-Qadi, 2021; Leng et al., 2011; Leng & Al-Qadi, 2014; Shangguan et al., 2016; Shangguan & Al-Qadi, 2015; Zhao et al., 2018), based on the dielectric mixing theory. The presented work shows numerical implementation of the mixing theory in FDTD simulation and extends the numerical model from simulating a dry asphalt mixture to a wet mixture.

Among the limited studies on heterogeneous numerical models of construction material using the FDTD method, Lachowicz and Rucka (2019) and Zadhoush et al. (2021) developed heterogeneous numerical models of concrete materials. However, the simulated aggregates in concrete overlapped, so precise volumetric properties of components could not be guaranteed, hindering its application for investigating dielectric properties of an asphalt mixture. Benedetto et al. (2018) proposed a random sequential adsorption (RSA) method for railway ballast simulation, which allows non-overlapping particle generation. Cao and Al-Qadi (2021) later developed a similar method for generating a heterogeneous numerical model of a dry asphalt mixture, which was composed of aggregate, asphalt binder, and air voids. The presented work extends the model to simulate GPR surveys on non-dry asphalt pavement.

In this study, the development of a dielectric model for a heterogeneous asphalt mixture was performed in two steps. First, a geometric model of a heterogeneous asphalt mixture was developed based on the RSA method. Then, the geometric information of the generated model was imported to GprMax, an FDTD simulation tool (Warren et al., 2016). An FDTD method was used to simulate GPR surveys on asphalt pavement. The asphalt mixture's dielectric constants were calculated from the received GPR signals.

The dry asphalt mixture is composed of aggregate, asphalt binder, and air voids. Once the mixture is saturated, the air void space is replaced by water. Figure 8 presents a phase diagram of the mixture with internal moisture. The volumetric contributions of each component to the entire mixture are represented by V.

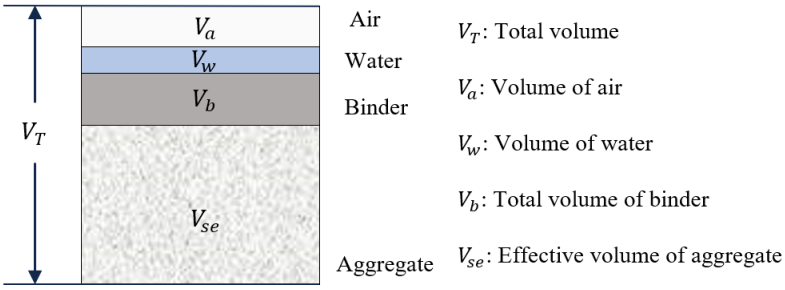

Figure 8. Graph. Composition and parameters of a non-dry asphalt mixture.

The saturation ratio, SR, is defined as the ratio between volumes of water and all voids (water and air) (Figure 9). From Figure 8, the volume of voids in the asphalt mixtures is the summation of the volumes of the air voids, V_a, and water, V_w.

$$SR = \frac{V_w}{V_w + V_a} \times 100\%$$

Figure 9. Equation. Definition of the saturation ratio.

Moisture content indicates the quantity of water contained in the asphalt mixture. It is defined as the ratio between the weights of water, W_w, and the dry asphalt mixture, W_{dry}. The relationship and its derivation between the moisture content, MC, and saturation ratio is presented in Figure 10.

$$MC = \frac{W_w}{W_{dry}} \times 100\% = \frac{\rho_{wa} V_w}{\rho_{dry} V_T} = \frac{\rho_{wa} V_T P_a * SR}{\rho_{wa} G_{mb} V_T} = \frac{P_a * SR}{G_{mb}} = \frac{P_a * SR}{(1 - P_a) G_{mm}}$$

Figure 10. Equation. Conversion between moisture content and saturation ratio.

Here ρ_{wa} is density of water, and ρ_{dry} is density of the dry asphalt mixture. P_a is percentage of air voids before moisture saturation. G_{mb} is bulk specific gravity of HMA, and G_{mm} is theoretical maximum specific gravity of the asphalt mixture.

The geometry of a heterogeneous mixture model was developed based on the RSA method (Benedetto et al., 2018; Cao & Al-Qadi, 2021; Feder, 1980). Sets of spherical particles were randomly generated so that the distribution of the sphere diameters is coherent to the distribution of the aggregate gradation. Given that aggregate shape has no effect on GPR measurement at the considered central frequency and aggregate size, the aggregate can be safely simulated as spheres (Cao & Al-Qadi, 2021; Zadhoush et al., 2021). Then, each particle was positioned in the geometrical

domain following the RSA algorithm so that no particles overlapped. The detailed development procedures are summarized as follows:

- According to the prescribed pavement layer thickness, aggregate gradation, and sample size, calculate the number of particles corresponding to each sieve fraction.

- Randomly generate the 2D coordinates of the spherical particles within the simulation domain. The radii of the particles are chosen as the mean values between the adjoining sieve sizes. If an attempt to deposit a particle would result in an overlap with any already deposited particles, then the attempt is rejected. Otherwise, the particle is irreversibly adsorbed. Thus, its position becomes fixed and cannot be moved from the model. Its coordinates and radius are stored in a list of adsorbed particles. For particle p_1, with coordinates x_i, y_i, and radius r_1, and particle p_2, with coordinates x_j, y_j and radius r_2, the nonoverlap condition required is presented in Figure 11.

$$\sqrt{(x_i - x_j)^2 + (y_i - y_j)^2} > r_1 + r_2$$

Figure 11. Equation. Nonoverlap condition for simulation particles.

- To accommodate the grid shape in the FDTD model in the next step, the simulation domain is discretized using 0.004 in. × 0.004 in. unit square elements, and the generated spherical particles are approximated using the unit squares. Figure 12 presents an example of the particles before and after discretization. According to the RSA algorithm, the simulation domain will reach a jamming limit, in which no more particles can be adsorbed (Feder, 1980). Given that the depositing particles are polydisperse, jamming usually occurs during the generation of fine aggregate. Once the jamming limit is reached, the aggregate gradation is checked, and unit squares are complemented as fine aggregate. After the generation of aggregates, the positions of unit squares are stored and labeled as “aggregate.”

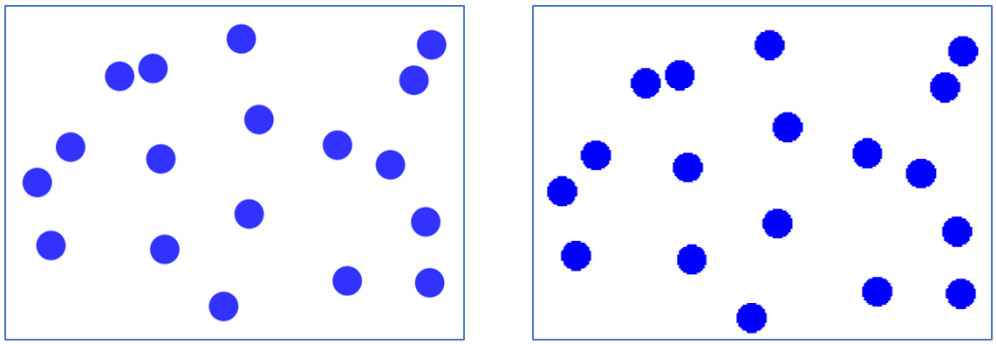

Figure 12. Graph. Particles before and after discretization in the geometric model.

- The region in the simulation domain not occupied by aggregates is set as “effective” asphalt binder, which is not adsorbed by the aggregate. Note that the actual aggregate volume is greater than the one used in the model because of the adsorbed portion of the asphalt binder by the aggregate. Air voids are generated by deleting the asphalt binder elements randomly. Then, parts of air voids are converted into moisture elements according to the saturation ratio. The positions of unit squares belonging to each material are stored and labeled.

Figure 13 presents the generated dry mixture, water distribution, and a combination of these two—an asphalt mixture with internal moisture. The output of the numerical modeling was encoded in a zipped data file. The file includes all geometric information of every component in an HMA pavement as well as the label information of geometric coordinates. It can be read in the FDTD model without losing accuracy in the next stage.

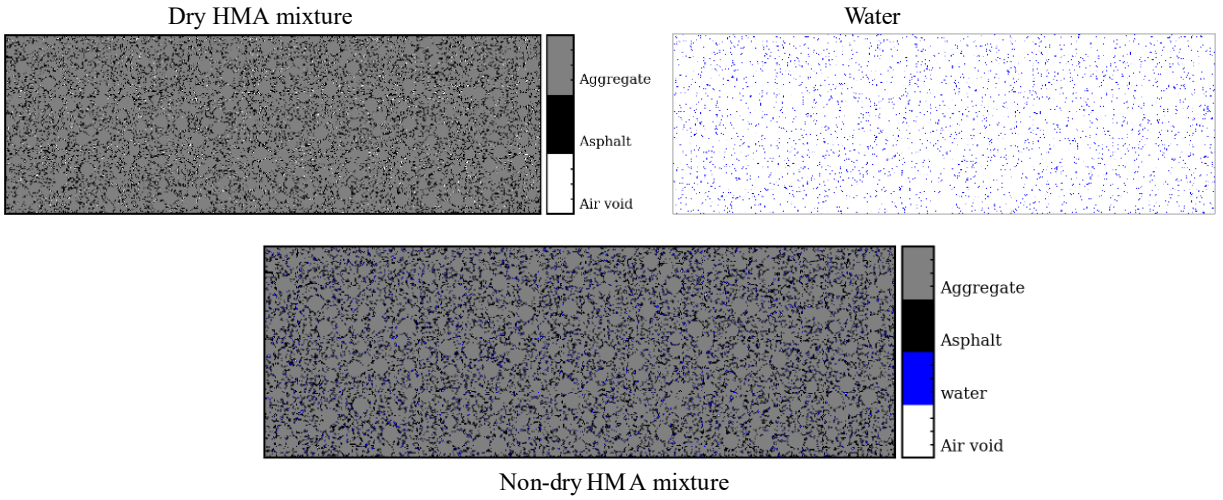

Figure 13. Graph. Visualization of a heterogenous dry asphalt mixture, water component, and a non-dry HMA mixture numerical model.

To simulate EM waves interacting with heterogenous asphalt pavement, the geometric model of the mixture was embedded into a numerical model that reproduces GPR surveys by the FDTD technique (Yee & Chen, 1997). The FDTD method, also known as Yee’s algorithm, is a differential equation-based solver that provides numerical solutions for Maxwell’s equations in complex geometries. The FDTD method uses second-order accurate derivatives in space and time. It utilizes a mesh built from the rectangular, or Yee, cells in which field values are updated time-step by time-step as EM waves propagate through a structure. Two-dimensional FDTD simulations have been proven to have similar results as that of 3D simulations for the considered application (Benedetto et al., 2018; Shangguan & Al-Qadi, 2015). Hence, 2D FDTD simulations were performed considering the computational intensity of 3D simulations.

A virtual 2D asphalt pavement, consisting of asphalt surface and base layers, was constructed in GprMax. The asphalt layer was replaced with the heterogeneous model generated by the RSA method. Figure 14 presents a diagram of the FDTD model and its dimensions. *Tx* is the transmitter,

and *Rx* is the receiver antenna. Depicting the actual distance between the transmitter and receiver, the distance between the transmitter and receiver antennas was set at 15 in. in the simulation. The excitation of the antenna was a Hertzian dipole with the Ricker function as the excitation signal. The model was discretized using a grid with spatial steps of 0.004 in. × 0.004 in. The perfect matched layer (PML) was used to cancel out any reflections on its interface. The model with PML can simulate EM wave propagation in an infinite space (Giannopoulos, 2005).

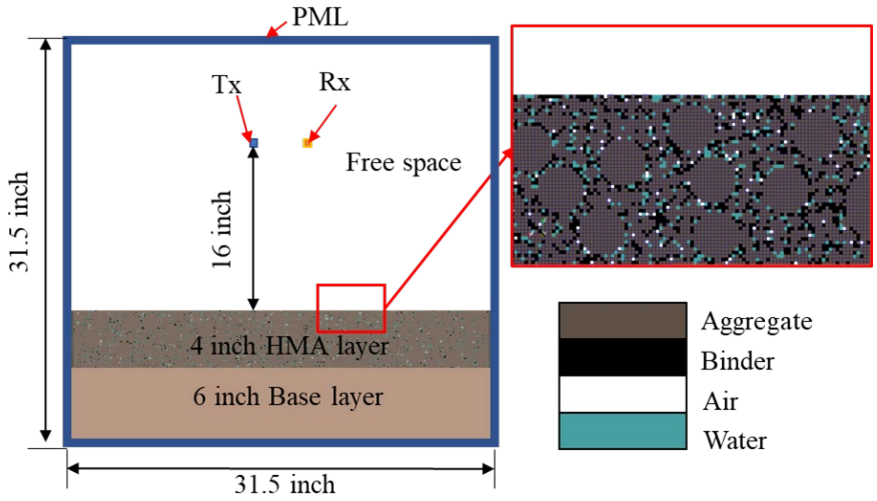

Figure 14. Graph. Diagram of an FDTD model in GprMax.

After the geometry of the FDTD model was determined, dielectric properties of the materials were assigned to the model. The asphalt layer contains elements of the aggregate, binder, water, and air voids generated using the RSA method. Dielectric properties of the aggregate, binder, and air are not subjected to temperature and frequency changes in the GPR frequency range. Thus, they were assumed to be constant. The dielectric constants are three and one for binder and air, respectively. The dielectric constant of the aggregate can be back-calculated from the field samples through an iterative process to minimize the deviation between real and virtual GPR measurements (Cao & Al-Qadi, 2021) or it could be obtained from a database (Leng & Al-Qadi, 2014).

The dielectric property of water, $\epsilon_{r,w}$, a lossy material, is more complicated than the dielectric properties of aggregate, binder, and air, which are non-lossy materials. Pure water, subjected to variation in frequency and temperature, can be well represented by the Debye relaxation function (see Figure 15) (Kaatze, 1989; Liebe et al., 1991). The real part, $\epsilon'_{r,w}$, is a dielectric constant, which shows the ability of an object to store electrical energy in an electric field. The imaginary part, $\epsilon''_{r,w}$, is called a loss factor, which is associated with dielectric loss. The loss factor can be related to the conductivity, σ, of the material. Their relations are presented in Figure 15.

$$\epsilon_{r,w}(f) = \epsilon_{r,w}(\infty) + \frac{\epsilon_{r,w}(0) - \epsilon_{r,w}(\infty)}{1 + i2\pi f\tau} = \epsilon'_{r,w} - i\epsilon''_{r,w} = \epsilon'_{r,w} - \frac{i\sigma}{2\pi f}$$

Figure 15. Equation. Complex dielectric constant of water by Debye.

Here f is frequency, provided in Hz. $\epsilon_{r,w}(0)$ is the zero-frequency relative dielectric constant, and $\epsilon_{r,w}(\infty)$ is the dielectric constant at infinite frequency. τ is Debye relaxation time, and $i = \sqrt{-1}$.

$\epsilon_{r,w}(0)$, $\epsilon_{r,w}(\infty)$, and τ are temperature dependent. Using the empirical formulas derived by Kaatze, the dielectric property of pure water as a function of temperature in 2 GHz is presented in Figure 16. The loss factor of pure water is much smaller than the complex dielectric constant, and it remains almost constant when the temperature is higher than 104°F.

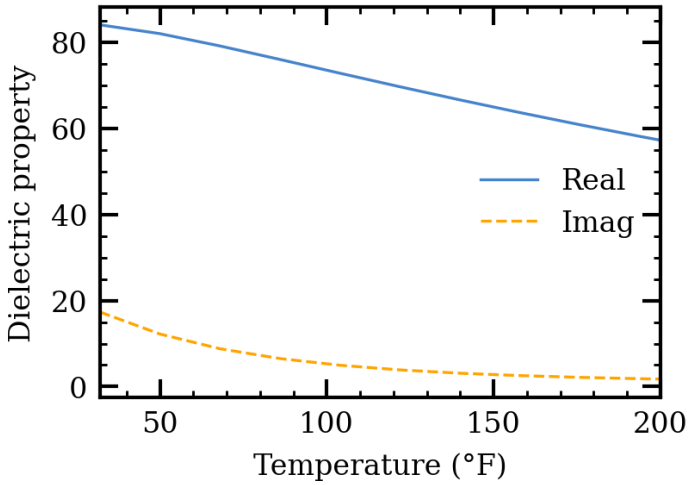

Figure 16. Chart. Dielectric property of water changing with temperature in 2 GHz.

The RA and TWTT methods were used to calculate the dielectric constant of the asphalt mixture. For the RA method, simulations were performed on the numerical models of pavement and pavement with a perfect electrical conductor on top. The amplitude of the EM wave reflected from the top of the pavement layer and the copper plate are recorded as A_p and A_c, respectively. The dielectric constant $\epsilon_{r,AC}$ of the asphalt pavement layer can be calculated using Figure 5.

The TWTT method derives the material's dielectric constant from the average velocity of EM waves in the material. The travel speed of EM waves in an asphalt pavement layer is calculated using the known pavement layer thickness, d, and the time interval, t, between pulses reflected from the top and bottom of pavement layers, where *c* is the speed of light (see Figure 6). The TWTT method uses the average speed of an EM wave within the material, so the dielectric constant measured using this method is the average or bulk dielectric constant of the material (Benedetto & Pajewski, 2015).

MODEL DEVELOPMENT

The effect of moisture on GPR signals was investigated in terms of amplitude and travel time features. The effect of aggregate gradation and saturation ratio on the asphalt pavement dielectric constants was discussed using RA and TWTT methods, respectively. Finally, an empirical formula was derived to correlate moisture and dielectric constants of non-dry asphalt pavement, and an application of the derived formula on internal moisture-content prediction was introduced.

Numerical models were utilized to investigate the effect of moisture on GPR signals. To differentiate the reflection from the surface and bottom of the surface layer, a numerical model was constructed with an 8 in. thick heterogeneous asphalt layer and a 4 in. thick base layer. The area of the calculation model was 32 in. × 32 in., and the antennas were 16 in. above the pavement's surface. An aggregate dielectric constant $\epsilon_a = 4.3$, water dielectric constant $\epsilon'_{r,w} = 81$, and loss factor $\epsilon''_{r,w} = 4$ were used in the simulation. Figure 17 presents the received GPR signals on the pavement with different saturation ratios.

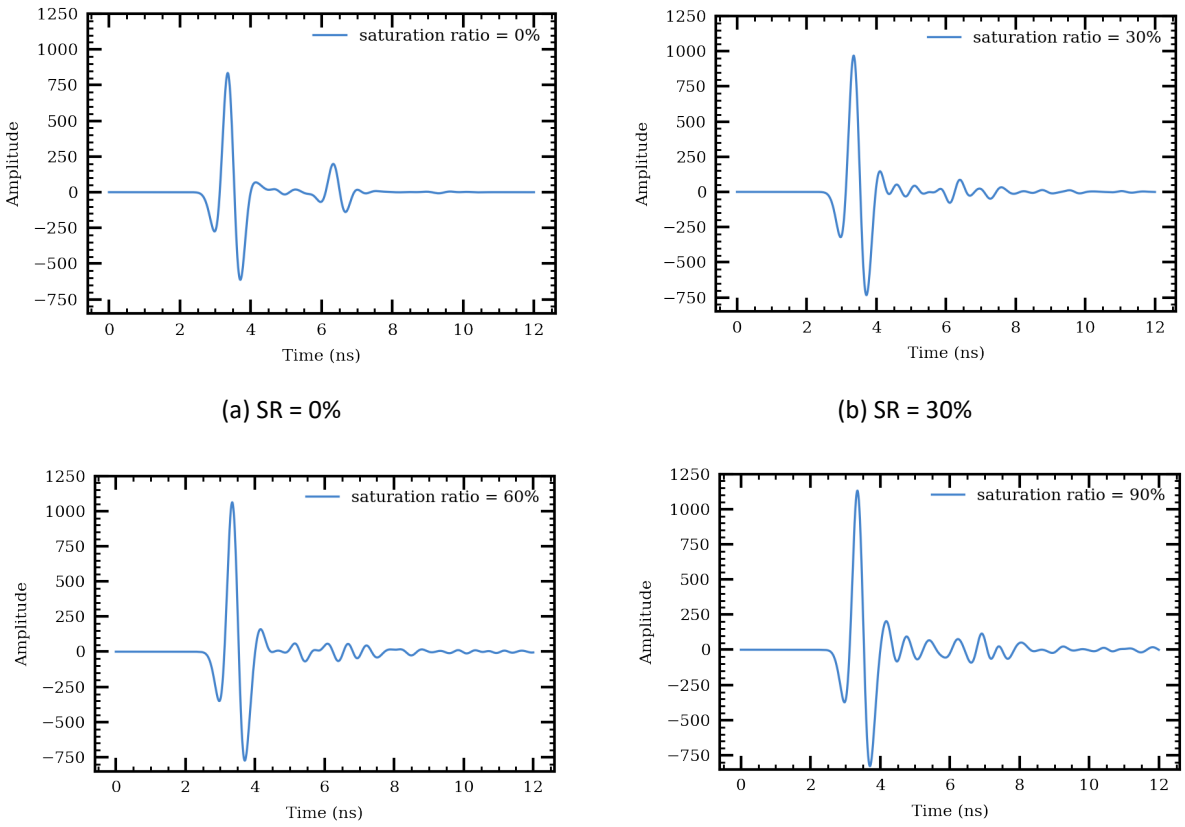

(a) SR = 0%

(b) SR = 30%

(c) SR = 60%

(d) SR = 90%

Figure 17. Chart. GPR signals on pavement with different saturation ratios.

When the asphalt pavement is dry or the saturation ratio is 0%, the reflections from the top of the pavement layer and bottom of the asphalt pavement layer (top of the base layer) are at around 3 ns and 6.5 ns, respectively. As the saturation ratio increases, the amplitude of reflection from the top of the pavement layer is amplified, while the reflection from the bottom is attenuated. The amplification of surface reflection explains the increasing dielectric constants with more internal water in the medium, as indicated from Figure 5 and reported in previous studies (Fernandes et al., 2017; Plati & Loizos, 2013). At the same time, more distortions are observed for signals reflected from the medium underneath the pavement surface. The signal attenuation and distortion observed from the simulation are consistent with those noted in other studies (Kaplanvural et al., 2018;

Lachowicz & Rucka, 2019). Additionally, the EM depth of penetration in a wet asphalt layer is smaller than that in the same layer but in dry conditions, and the difference increases with higher saturation (Al-Qadi et al., 1991). Hence, it is more difficult to detect the bottom of an asphalt layer. To overcome this issue, a perfect electrical conductor (PEC) was inserted at the top of the base layer (at the bottom of the asphalt layer), to enhance the signal reflection in the simulation. Figure 18 presents the simulation results.

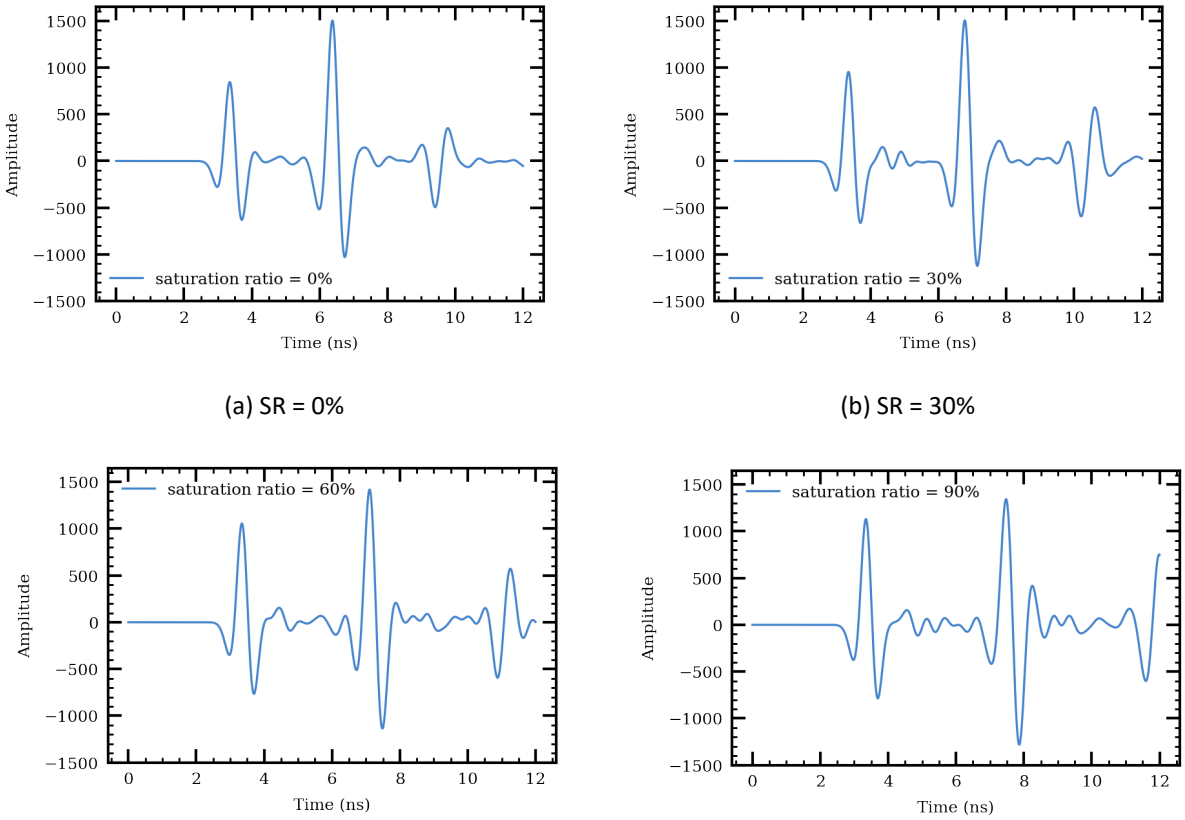

(a) SR = 0%

(b) SR = 30%

(c) SR = 60%

(d) SR = 90%

Figure 18. Chart. GPR signals on PEC-embedded pavement with different saturation ratios.

The reflection from the bottom of the surface layer has been amplified with the reflector (Figure 18). The third pulse is caused by the signals reflecting twice from the bottom of the pavement layer. The time interval between the first and second pulse is the TWTT of the EM wave in the asphalt layer. As the saturation ratio increases, travel time increases and the velocity of the EM wave in the medium decreases. The effects of moisture on the EM wave and the dielectric constant of the asphalt pavement's travel times are square-root reciprocal, as indicated in Figure 6.

Effects of Aggregate Gradation and Saturation Ratio on Calculated Asphalt Mixture Dielectric Constant

A sensitivity analysis was performed to investigate the effects of aggregate gradation and saturation ratio on the asphalt mixture's dielectric constants using the Monte Carlo method (Benedetto et al.,

2018). Three aggregate gradations—dense- (Mix 1), gap- (Mix 2), and open-graded (Mix 3) HMA mixtures—were simulated in the numerical models (Table 1). The aggregate sizes 16 and 13.2 mm were used for simulation purposes only. Figure 19 presents the results.

Table 1. Aggregate Gradation of Three HMA

Sieve size (mm)	Mix 1 % passing	Mix 2 % passing	Mix 3 % passing
16	100.0	100.0	100.0
13.2	95.0	97.9	97.8
9.5	76.5	63.5	63.3
4.75	53.0	29.0	18.8
2.36	37.0	25.8	15.0
1.18	26.5	22.7	11.5
0.6	19.0	19.5	8.7
0.3	13.5	16.3	6.1
0.15	10.0	13.2	5.4
0.075	6.0	10.0	4.6

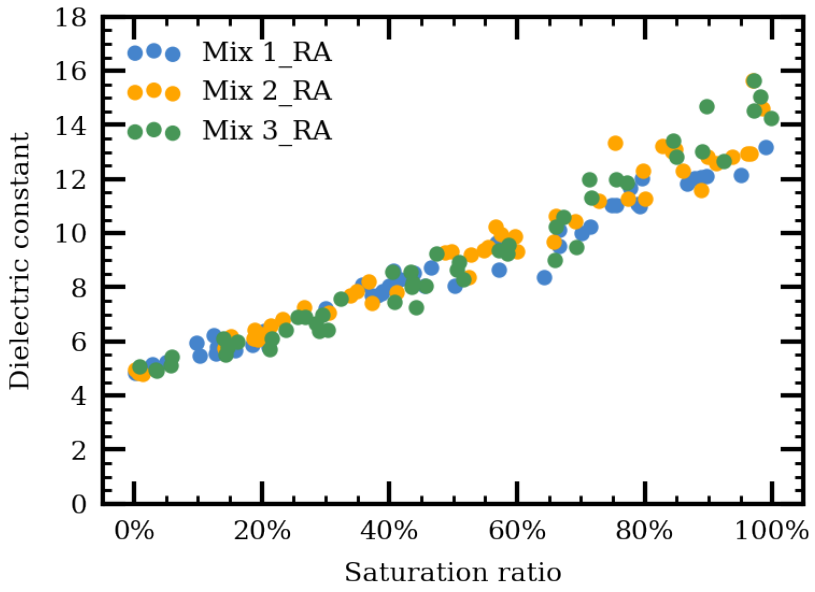

Figure 19. Chart. Effects of gradation and saturation ratio on dielectric constant using RA method.

Aggregate gradation has no effect on the reflected amplitude and, accordingly, the calculated dielectric constant regardless of the water saturation level, similar to simulation results on dry HMA pavement (Cao & Al-Qadi, 2021). The dielectric constant increases from 5 to 16 when the saturation ratio increases from 0% to 100%.

Relationship between Moisture Content and Dielectric Constant

To quantify the effect of internal moisture on the dielectric constant, numerical models were generated with different air voids and saturation ratios. The dielectric constants were calculated using the RA method (Figure 20). As expected, the dielectric constant of the asphalt mixture decreases as air void increases. For the same air void content, as moisture increases, the asphalt mixture's dielectric constant increases. The dielectric constant of the asphalt mixture with higher air voids, however, exceeds the dielectric constant of the asphalt mixture with lower air voids when the saturation ratio is greater than 20% (Figure 20). This is because the effect of water surpasses the effect of air voids on the dielectric constant. Additionally, larger air voids lead to larger water volume when saturation ratios are the same.

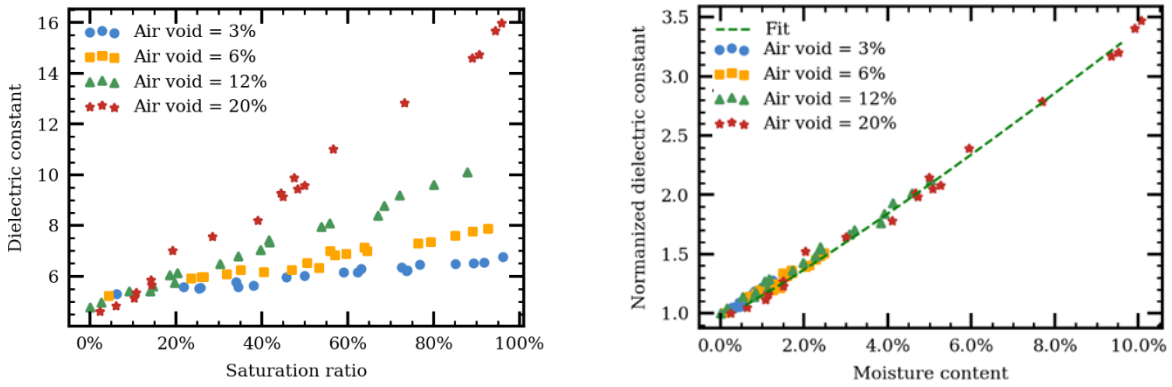

(a) Before axes' conversion

(b) After axes' conversion

Figure 20. Chart. (a) Effects of saturation ratio and air voids on dielectric constant, and (b) effects of moisture content and air voids on normalized dielectric constant.

To exclude the effect of air voids on the quantitative relationship between dielectric constant and moisture content, the dielectric constant of HMA is normalized using Figure 21, where the reference is the dielectric constant of a dry asphalt mixture. The moisture content is converted from the saturation ratio using Figure 10, and $G_{mm} = 2.38$ was assumed.

$$\epsilon_{r,norm} = \frac{\epsilon_{r,AC}}{reference}$$

Figure 21. Equation. Normalization of the dielectric constant using the reference dry condition.

After normalization and conversion from the saturation ratio to the moisture content, the relationship between the normalized dielectric constant, $\epsilon_{r,norm}$, and moisture content, MC, could be fitted using a power function with different air voids (see Figure 22). Parameters A_ϵ, B_ϵ, and C_ϵ depend on the asphalt binder content and the dielectric properties of each component in the numerical model. Using the calibrated model from Illinois Route 61 (IL-61), which will be discussed in Chapter 4, the parameters are $A_\epsilon = 23.475, B_\epsilon = 1.025$, and $C_\epsilon = 1.008$. Compared with an

exponential function or an inverse function, the power function has a higher R^2 value at 0.997 for curve fitting.

$$\epsilon_{r,norm} = A_\epsilon * MC^{B_\epsilon} + C_\epsilon$$

Figure 22. Equation. Normalized dielectric constant as a power law function of moisture content.

Prediction of Asphalt Mixture Moisture Content from GPR Data

Over the last four decades, many studies have demonstrated the high sensitivity of GPR to water in soil and building materials. There are two existing methods to estimate the underlying moisture content. The first method is to correlate the moisture content with the material dielectric constant. For example, Topp's equation (Topp & Davis, 1985) is the most used model in geophysics to estimate soil moisture (Liu et al., 2017; Tosti & Slob, 2015) from the dielectric constant. However, there is no established universal model for asphalt pavement. The relationship between moisture content and dielectric constant is site-dependent, which requires regression from a large amount of collected samples (Klewe et al., 2021). Another method is to correlate the moisture content with the GPR signal features on the frequency domain (Benedetto & Benedetto, 2011). This method is usually used to make a qualitative rather than a quantitative estimation of moisture content. The first study in the field was conducted by Al-Qadi et al. (1991) and used a focused frequency-step antenna at a high frequency.

In this study, the proposed relationship between dielectric constant and moisture content, derived from FDTD simulations, has been used to predict moisture content inside HMA pavement. Compared with the aforementioned methods to estimate moisture content, the method in this study is based on EM mixing theory and provides a quantitative prediction of moisture content. Compared with existing regression models, this study's numerical model is time- and cost-efficient and can also be easily applied to different project sites, and it only needs two samples in the calibration process.

Moisture content was predicted using Figure 23, which is the inverse of Figure 22.

$$MC = \left(\frac{\epsilon_{r,norm} - C_\epsilon}{A_\epsilon}\right)^{\frac{1}{B_\epsilon}}$$

Figure 23. Equation. Moisture content as a function of the normalized dielectric constant.

The proposed numerical model allows better control of an asphalt mixture's structural and material properties. It can be further used to study GPR surveys on unevenly compacted pavement and nonuniformly distributed moisture content.

EXPERIMENTAL PROGRAM

Indoor Tests

Variability is naturally encountered for field tests; different day-by-day weather conditions like rain, ambient temperature, relative humidity, cloudiness, and solar radiation could affect the curing process of CR mixes and cause variability in moisture content between the different spots tested. Other location-specific factors like shade from trees could also affect curing by slowing down evaporation. Consequently, an indoor test procedure was proposed, the goal of which was to limit the variability of the results by testing CR asphalt slabs under controlled environmental conditions. Inside the lab, shade is always provided, no rain is encountered, and fewer changes in temperature and relative humidity are expected. However, because of a lack of solar radiation indoors, curing and evaporation of free water are expected to take longer than in the field, allowing the slabs' curing to be monitored more closely.

One remarkable note is that emulsions are proprietary, and their exact composition is unknown. In emulsions, water is initially bound to the asphalt binder before it breaks into free water. This phase change is expected to also change EM properties measured by GPR. To first understand this difference between bound and free water, the research team investigated the behavior of conventional HMA with added free water. Afterwards, they used GPR to test and monitor emulsified CR mixes during the curing process.

The indoor tests included constructing and testing four different slabs with similar dimensions: 4 ft. × 4 ft. × 4 in., where 4 in. is the depth of the slab. The choice of these dimensions was not arbitrary; the width and length of the slab was wide enough to cover the full footprint of the 2 GHz GSSI horn antenna used in the experiment. The antenna was mounted at a height of 18–20 in., a typical height for air-coupled antennas, and 4 ft × 4 ft is enough to protect the GPR signals from side effects of the wood frame at this height. The depth was similar to the layer thicknesses treated in the visited cold-recycling projects, which were in the 3–4 in. range.

All slabs had similar a construction process, starting with building the wood frame according to the aforementioned dimensions, cutting and lining the wood frame with a waterproof membrane to make sure water does not leak or get absorbed by the wood frame, and cutting and inserting a copper plate to accurately detect the bottom layer reflection. This would allow the researchers to apply the TWTT method. TWTT will be compared to the RA method, which will be used in the field. The asphalt mix was placed in slabs after mixing and/or reheating in a mini mixer. Finally, the mix was compacted either manually by tampers or by using a mini-roller compactor. Figure 24 presents the various construction processes of the slabs.

(a) Building wood frame

(b) Lining with a waterproof membrane

(c) Insertion of a copper plate

(d) Heating/mixing

(e) Placing the mix

(f) Compaction

Figure 24. Photo. Indoor slab construction process.

Slab 1

The first slab was built using conventional HMA. The asphalt mix was stored at the lab from a previous project. Appendix A presents the mix design sheet. A series of lab tests was conducted to verify the mix properties, especially the ones needed for the ALL density model. Those properties are P_b, which was obtained by extraction; G_{mm}, which was obtained using the conventional rice test method (AASHTO T 209); and effective specific gravity of aggregates (G_{se}), which was calculated using the previous two properties, as in Figure 25. Aggregate gradation was also measured as a check to ensure accurate properties are used in the analysis.

$$G_{se} = \frac{100 - P_b}{\frac{100}{G_{mm}} - \frac{P_b}{G_b}}$$

Figure 25. Equation. Calculation of the effective specific gravity of the aggregates.

where G_b is specific gravity of the asphalt binder, usually taken as 1.02.

After compaction by the mini roller, a dry reference GPR scan was taken. The slab was then submerged in water for four consecutive days, as presented in Figure 26. The height of water was approximately 0.8 in. above the surface at all times. The antenna was mounted in the center above the slab using shelves (Figure 27). The plan was to monitor the evaporation of water from the slab using GPR while it dries every two hours. A fan was used to speed up the drying process for one hour on and one hour off. The fan's position was alternated between both sides of the slab. GPR scan collection started right after drying the surface of the slab with a cloth until the measured dielectric constant was almost stabilized. The slab was monitored for three days. Figure 28 presents the results; the dielectric constant of the wet slab reached the dry reference dielectric constant (the red star in Figure 28) in less than one hour. This suggested that the water was not actually penetrating the slab and stayed on the surface. This was verified through cores obtained after the tests were completed. The core air void percentages were determined in accordance with the AASHTO T 166 specification. Three cores were extracted, and the average air void percentage was 3.3%. The air voids appeared to be disconnected, and the slab was almost impermeable. Connected air voids are needed to ensure water penetration through the slab. Fernandes et al. (2017) reported that even at a 6% air void, water infiltration was not guaranteed because of incomplete void connectivity.

Figure 26. Photo. Slab 1 submerged in water for four days.

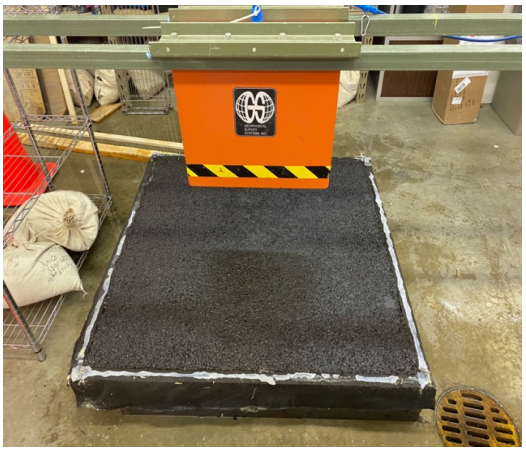

Figure 27. Photo. GPR antenna mounted on top of a slab for measurements.

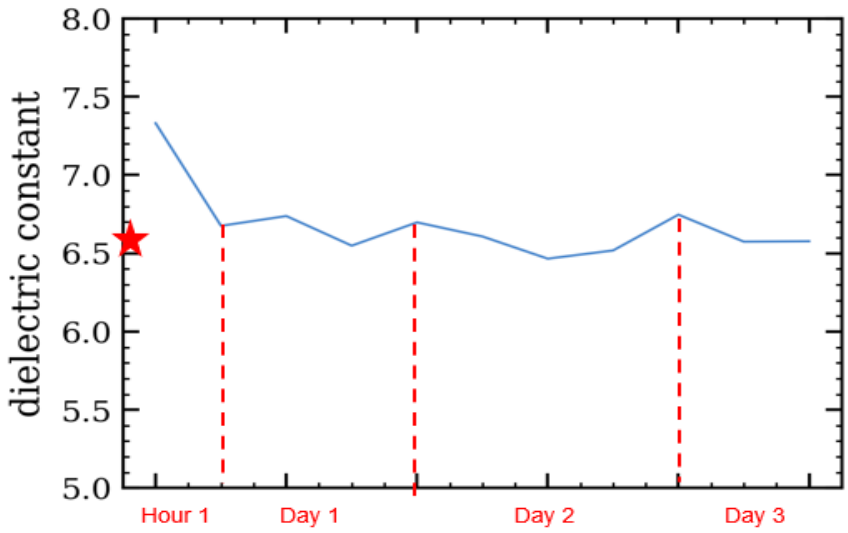

Figure 28. Chart. Slab 1 dielectric constant trend with drying.

A water leak was noticed in slab 1. This was due to water movement through the membrane, which was folded around the wood frame's sides (Figure 29). This problem was addressed in constructing slab 2; less compaction was applied, and the membrane was not folded over the wood frame's edges.

Figure 29. Photo. Water leaking from the membrane folded over the wood frame's edges.

Slab 2

The HMA for slab 2 was sampled from an Open Roads plant in Champaign, Illinois. The mix properties were provided by the plant and measured in the lab for consistency. A similar construction procedure was followed, but less compaction was applied. Tamping was used in lieu of roller compaction (Figure 30). Also, silicon was used to seal the joints, and extra folded membrane materials were removed using a heat gun and cutter to minimize water leakage (Figure 31).

Figure 30. Photo. Manual tamping for slab 2 compaction.

Figure 31. Photo. Using a heat gun to remove excess membrane.

The testing procedure was different for slab 2. A graduated flask (Figure 32) was used to calculate moisture content at each GPR scan. Additionally, a time domain reflectometer (TDR) was used to estimate the volumetric moisture content (VMC) of the slab by embedding it in predrilled holes at the four corners of the slab (Figure 33).

Figure 32. Photo. Adding water using a graduated flask.

(a) Pre-drilled holes for TDR probes (b) Taking a measurement

Figure 33. Photo. Using TDR to measure VMC of the slab.

The results of slab 2 showed a trend of the dielectric constant increasing when increasing the amount of water added for both the RA and TWTT methods. No leaking was encountered, and data points of known moisture content and calculated bulk dielectric constant were obtained. The results formed the basis for the model development stage. Figure 34 presents the data. The big jump in reflection amplitude dielectric constant toward the end is expected because the slab was almost saturated then and water was on the surface.

The TDR is typically used to determine the VMC of unbound materials like soils in agricultural applications. For use in the indoor test slabs, the TDR was calibrated for asphalt mixes. The calibration process yielded a parabolic polynomial (second degree) calibration curve (Figure 35). However, even after calibration, the TDR was deemed to be inappropriate for use in asphalt mixes, as it gave unreasonable results. For example, it had a calibrated estimated VMC of 10% when the slab was completely dry (see Figure 36). Many factors could have affected TDR accuracy in the indoor test, including varying insertion depth of the probes in the drilled holes, the holes drying faster than the rest of the slab, and water potentially being pumped out by the probes. In general, the TDR readings were constantly lower than the ground truth and were not representative of actual moisture level in the slab.

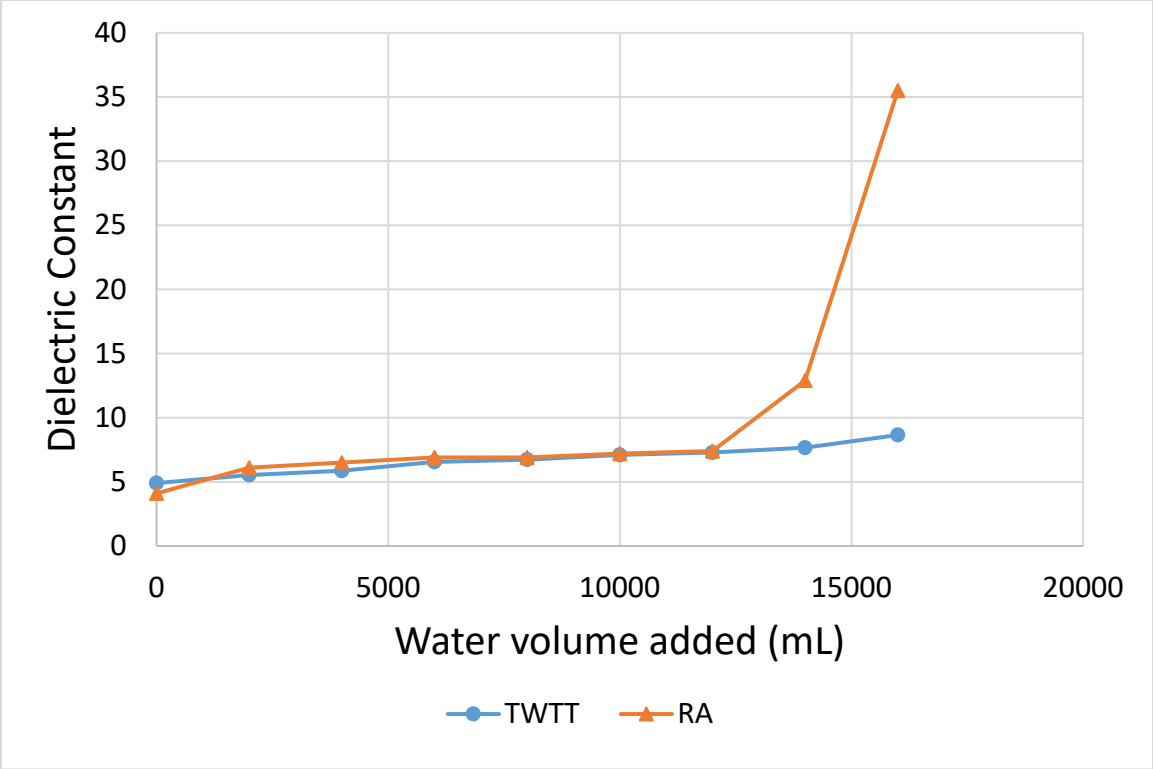

Figure 34. Chart. Slab 2 dielectric constant trend vs volume of water added.

(a) Calibration of TDR for HMA

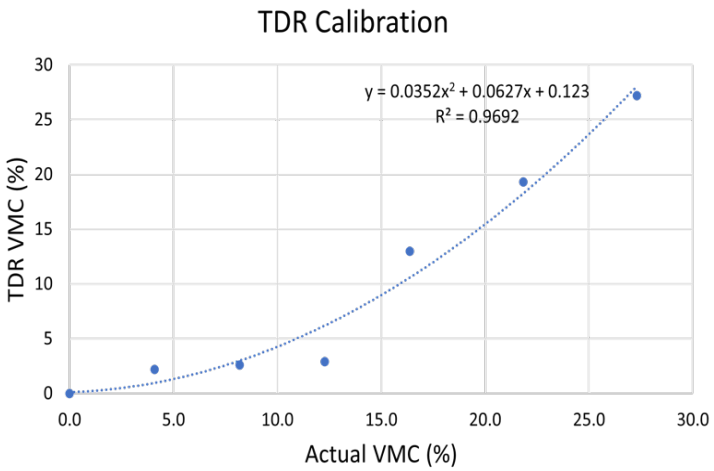

(b) Calibration curve

Figure 35. Photo and chart. Calibration of TDR for asphalt mixes.

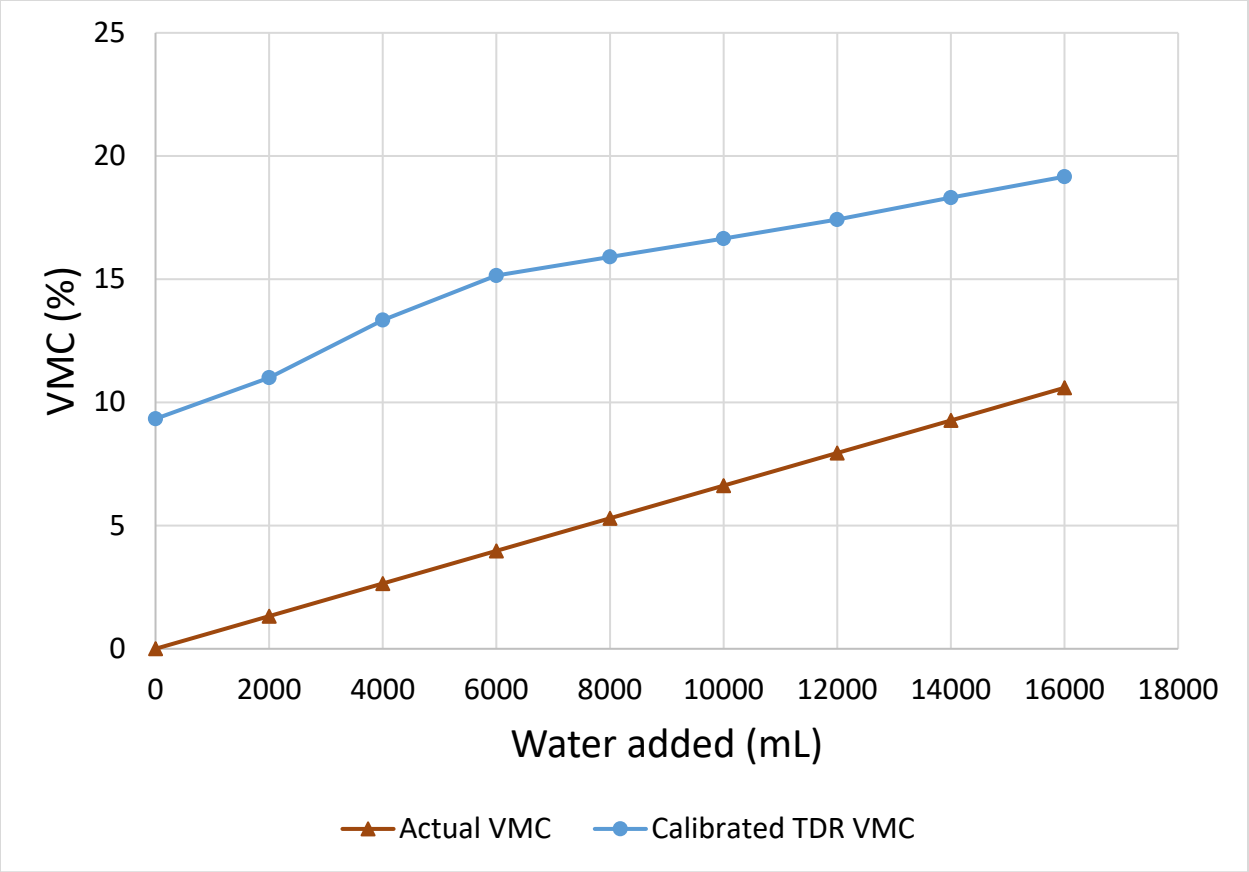

Figure 36. Chart. TDR results for slab 2.

Slabs 3 and 4

After getting acceptable results from HMA slabs, curing of cold-recycled emulsified mixes was investigated. A CCPR mix was sampled from Indianapolis. To imitate various field conditions, slab 3 was built with a waterproof membrane, while slab 4 was built without a membrane. Both slabs were compacted in the same way using a mini roller. After compaction, GPR scans were taken for 40 days; many scans were obtained in the first day to capture the curing process. After 14 days, the calculated dielectric constant for both slabs was almost constant. This suggests that entrapped moisture evaporated, and the mix was cured. The trend of the calculated dielectric constant (obtained using the TWTT method) over time was the same for both slabs. As expected, the dielectric constant decreased as moisture content decreased (Figure 37).

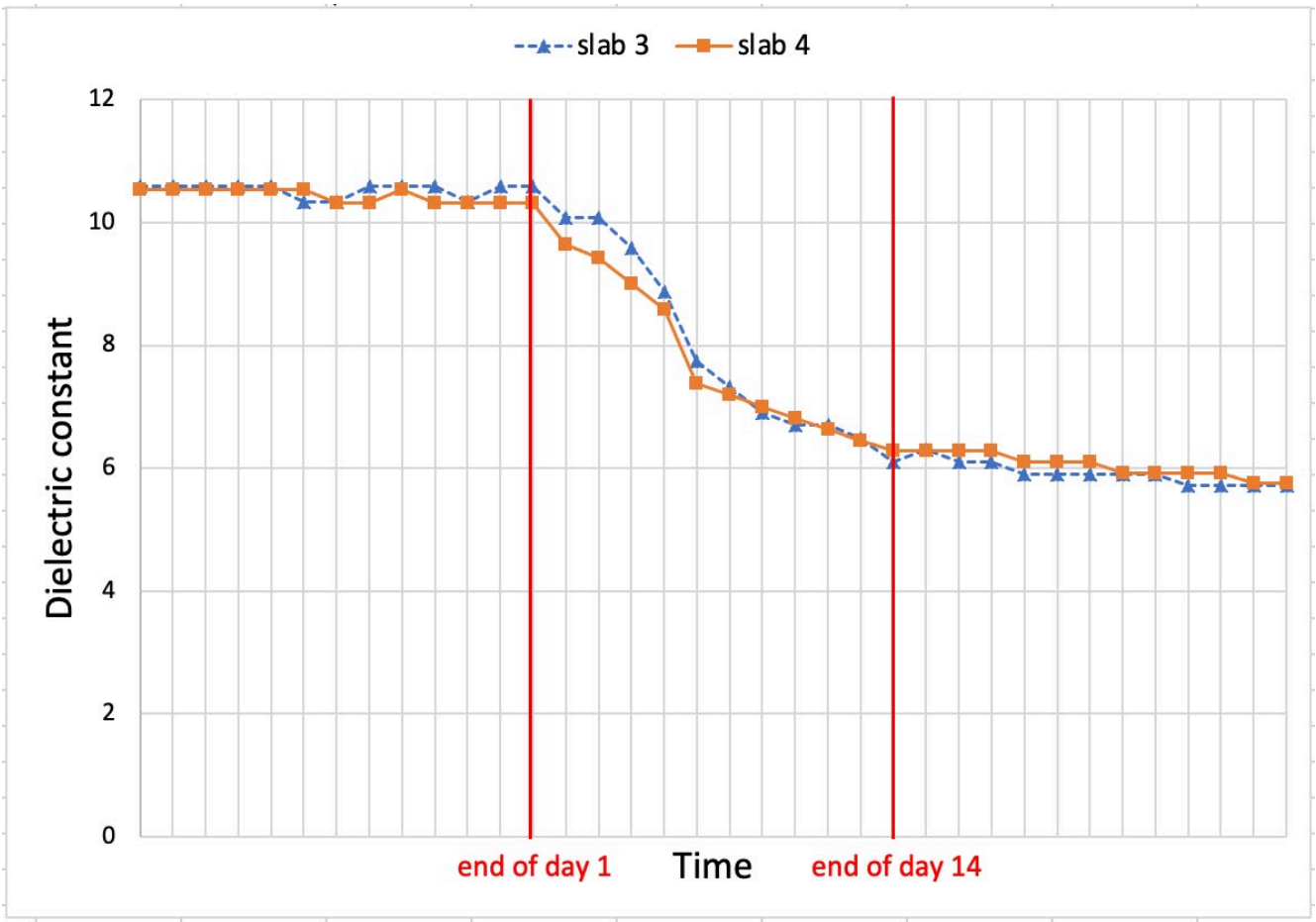

Figure 37. Chart. CCPR slabs 3 and 4 dielectric constant trend during curing.

TDR was used to monitor the change in moisture content of the CCPR slabs through drilled holes at the four corners of each slab. As concluded earlier, TDR may not be used for bound materials like asphalt mixes.

Analysis of Indoor Tests Measurements

Slab 1 data were not used in the analysis because of the slab's over-compaction; hence, water did not infiltrate the slab. For slab 2, known volumes of water were added and GPR scans were collected after each change in moisture level. The equations presented in Figures 9 and 10 were used to transform the volume of water added to the moisture content.

Figure 38 presents the dielectric constant versus gravimetric moisture content for slab 2. Results followed the expected trend, suggesting that the bulk dielectric constant of asphalt mixes is capable of predicting moisture content.

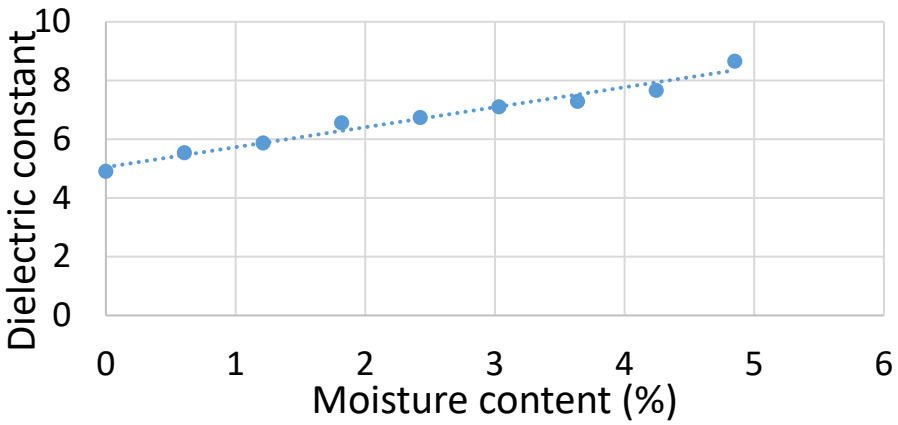

Figure 38. Chart. Dielectric constant vs moisture content for slab 2.

The developed simulation model was validated using the slab's test results. Figure 39 illustrates the predicted dielectric constant from the simulation models, which has the same volumetric properties as the lab test mixture. The ground-truth dielectric constants were calculated from the GPR scans of the slabs. The predicted dielectric constants aligned well with the ground-truth results.

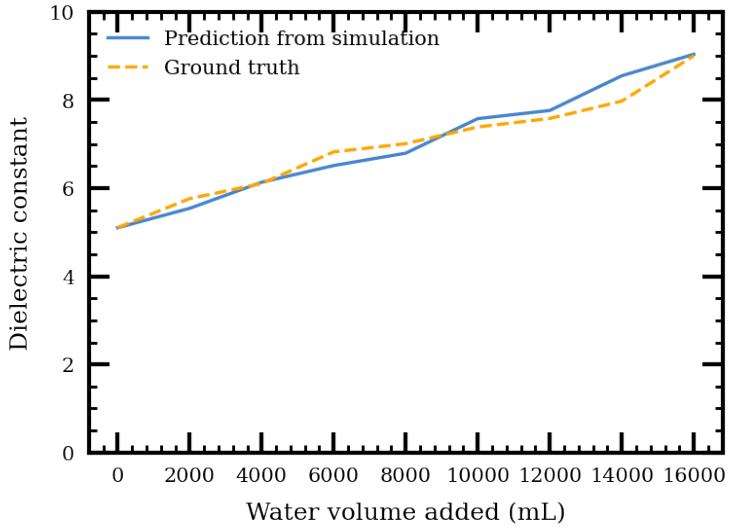

Figure 39. Chart. Comparison of simulated and ground truth determined dielectric constant.

Figure 40(a) presents the calculated dielectric constants from slabs 3 and 4. Slab 3 was built with a waterproof membrane at the bottom, while slab 4 was built without a membrane. The dielectric constants decrease from day 0 to day 10. After day 10, the reduction rate of the dielectric constants was relatively low and approaching zero. Using Figure 23, the moisture contents were predicted, as presented in Figure 40(b). For these two slabs, the ground-truth original moisture content was around 5.6%, which was measured using an oven. The gap between the ground-truth moisture content and predicted initial moisture content could be due to moisture loss during mixture transportation.

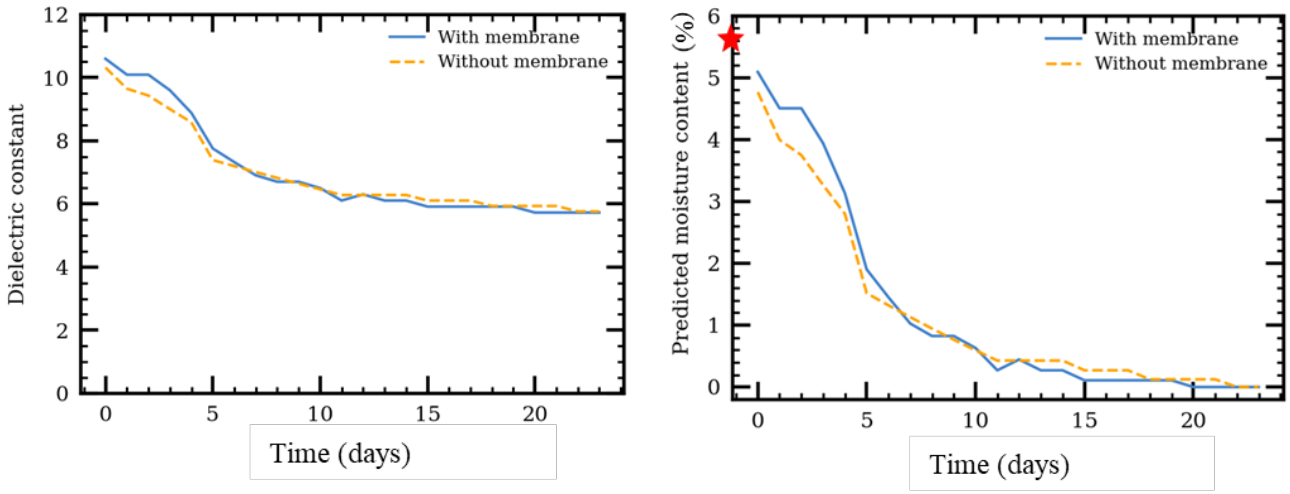

(a) Dielectric constant variation (b) Predicted moisture content variation

Figure 40. Chart. (a) Dielectric constant variation over time and (b) predicted moisture content variation over time for slabs 3 and 4.

ACA Model Development

The Al-Qadi-Lahouar-Leng (ALL) model, developed by Leng et al. (2011), is used to predict in situ asphalt mixture density from component and bulk dielectric constants (Figure 41). The ALL model was developed based on the Bottcher model and a shape factor introduced for asphalt mixes.

$$G_{mb} = \frac{\frac{\varepsilon_{AC} - \varepsilon_b}{3\varepsilon_{AC} - 2.3\varepsilon_b} - \frac{1 - \varepsilon_b}{1 - 2.3\varepsilon_b + 2\varepsilon_{AC}}}{\frac{\varepsilon_s - \varepsilon_b}{\varepsilon_s - 2.3\varepsilon_b + 2\varepsilon_{AC}} \frac{1 - P_b}{G_{se}} - \frac{1 - \varepsilon_b}{1 - 2.3\varepsilon_b + 2\varepsilon_{AC}} \frac{1}{G_{mm}}}$$

Figure 41. Equation. Al-Qadi-Lahouar-Leng model.

where G_{mm} is maximum specific gravity of an HMA mixture, G_{se} is effective specific gravity of aggregates, P_b is binder content of an HMA mixture, ε_b is dielectric constant of an asphalt binder, and ε_s is aggregate dielectric constant.

The HMA volumetric values may be obtained from the mix plant prior to pavement compaction, while aggregate dielectric constant may be obtained from a database or field cores. The air void is derived from G_{mm} and G_{mb} using Figure 42.

$$Air\ void = \frac{G_{mm} - G_{mb}}{G_{mm}} * 100\%$$

Figure 42. Equation. Air void calculation from G_{mm} and G_{mb}.

The ALL model does not consider internal moisture content in asphalt pavement. Thus, it may not be extended to CIR/CCPR pavement because of moisture presence. In this study, the ALL model was modified to allow consideration of internal moisture content in asphalt mixes, including CIR and CCPR.

The bulk dielectric constant of an asphalt mixture, ε_{AC}, is composed of a background material with *N* inclusions of different dielectric constants, as given in Figure 43. Herein, asphalt binder is assumed to be the background material because it is connected and spherical-shaped aggregates, air, and water are the inclusions.

$$\frac{\varepsilon_{AC} - \varepsilon_b}{3\varepsilon_{AC} - 2.3\varepsilon_b} = V_{se}\frac{\varepsilon_s - \varepsilon_b}{\varepsilon_s - 2.3\varepsilon_b + 2\varepsilon_{AC}} + V_a\frac{\varepsilon_a - \varepsilon_b}{\varepsilon_a - 2.3\varepsilon_b + 2\varepsilon_{AC}} + V_w\frac{\varepsilon_w - \varepsilon_b}{\varepsilon_w - 2.3\varepsilon_b + 2\varepsilon_{AC}}$$

Figure 43. Equation. ALL model with volumetric properties.

V_{se}, V_a, and V_w are partial volumes of aggregate, air, and water, respectively. Using an asphalt mixture's volumetric properties, the partial volume of components could be calculated as presented in Figures 44–46.

$$V_{se} = \frac{G_{mb}(1 - P_b)}{G_{se}}$$

Figure 44. Equation. Calculate V_{se} from G_{mb}, P_b, and G_{se}.

$$V_w = w * G_{mb}$$

Figure 45. Equation. Calculate V_w from G_{mb} and w.

$$V_a = 1 - \frac{G_{mb}}{G_{mm}} - w * G_{mb}$$

Figure 46. Equation. Calculate V_a from G_{mb}, G_{mm}, and w.

Substituting Figures 44–46 in Figure 43, G_{mb} (including the moisture) may be calculated as follows:

$$G_{mb} = \frac{\frac{\varepsilon_{AC} - \varepsilon_b}{3\varepsilon_{AC} - 2.3\varepsilon_b} - \frac{1 - \varepsilon_b}{1 - 2.3\varepsilon_b + 2\varepsilon_{AC}}}{(1 + w)\left(\left(\frac{\varepsilon_s - \varepsilon_b}{\varepsilon_s - 2.3\varepsilon_b + 2\varepsilon_{AC}}\right)\left(\frac{1 - P_b}{G_{se}}\right) - \left(\frac{1 - \varepsilon_b}{1 - 2.3\varepsilon_b + 2\varepsilon_{AC}}\right)\left(\frac{1}{G_{mm}}\right) - w\left(\frac{1 - \varepsilon_b}{1 - 2.3\varepsilon_b + 2\varepsilon_{AC}} - \frac{81 - \varepsilon_b}{81 - 2.3\varepsilon_b + 2\varepsilon_{AC}}\right)\right)}$$

Figure 47. Equation. Final form of the ACA model, when internal water is included.

To determine internal moisture in asphalt mixes, including CIR and CCPR, the Al-Qadi-Cao-Abufares (ACA) model is introduced. Figure 48 is a simplified symbolic form of Figure 47. This simplification is used afterwards in the ACA model to calculate the moisture content of asphalt mixtures using Figure 49.

$$G_{mb} = \frac{A}{(1+w)(B-C-wD)}$$

Figure 48. Equation. Simplified symbolic version of the modified ALL model.

$$w = -\frac{((G_{mb}(C+D-B))^2 - 4DG_{mb}(A+G_{mb}(C-B)))^{1/2} + G_{mb}(B-C-D)}{2DG_{mb}}$$

Figure 49. Equation. ACA model for determining moisture content of asphalt mixtures.

Table 2 presents the results of using Figure 47 to predict G_{mb} (including internal moisture) from GPR measurements for slab 2. The ground truth of G_{mb} is 2.185 (using Corelok method—AASHTO T-331). The root-mean-square error (RMSE) of the G_{mb} prediction is 0.06.

Table 2. Predicted G_{mb} from GPR Measurements for Indoor Slabs

Moisture Content (%)	Predicted G_{mb}	Error (%)
0.0	2.185	0.0
0.6	2.238	2.5
1.2	2.231	2.2
1.8	2.293	5.0
2.4	2.247	2.9
3.0	2.235	2.3
3.6	2.189	0.2
4.2	2.173	0.5
4.9	2.246	2.8

Figure 50 presents the results of predicted moisture content from GPR measurements using Figure 48 for slab 2. The predicted moisture content using the ACA model is approximately 0.2% greater than the actual values. This could be viewed as conservative when used for CIR and CCPR moisture prediction. The R^2 and RMSE of predicted moisture are 0.97 and 0.46%, respectively.

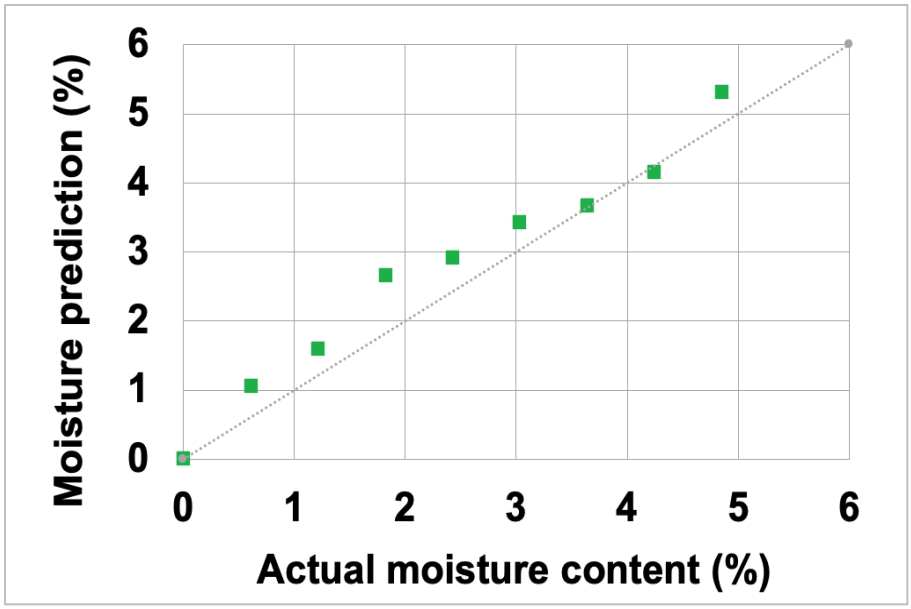

Figure 50. Chart. Predicting moisture content using the ACA model.

Field Tests

Testing Site Characteristics

A field investigation to validate the ACA model was conducted on CIR construction sites in District 4 and one CCPR site in District 5 between May 2020 and September 2020. In addition, one CIR construction site was investigated in District 2 in July 2021. The CIR sites in Illinois were IL-91, IL-116, IL-100, and IL-61 in District 4 and IL-64 in District 4. The CCPR site is RT-509 in District 4. Figure 51 presents a diagram of the six construction sites. Table 3 presents the field-data collection schedule for each project.

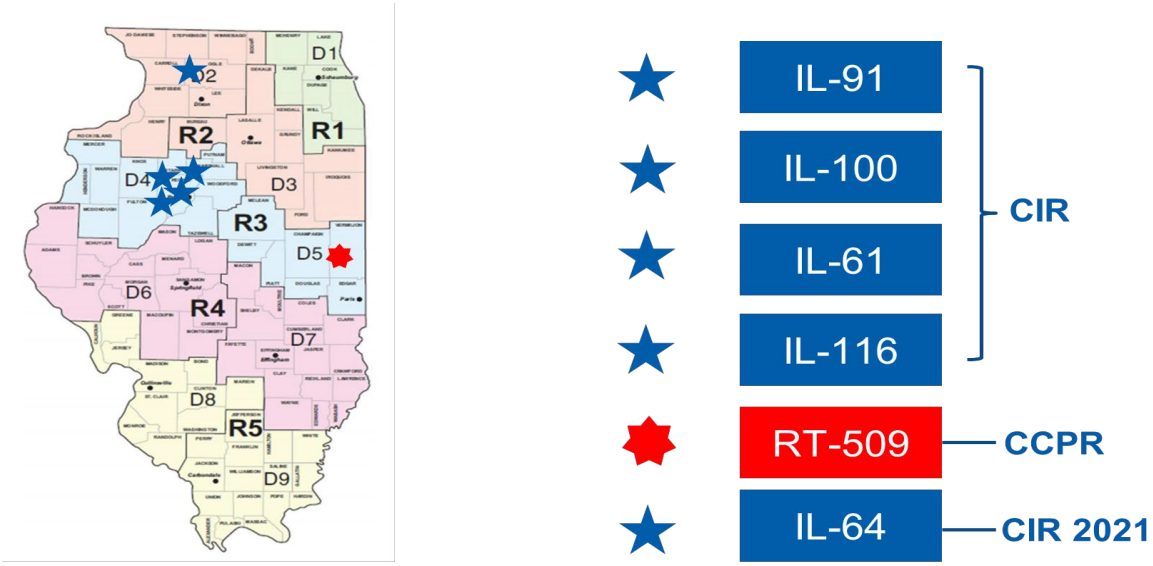

Figure 51. Graph. Diagram of CIR and CCPR construction sites.

Table 3. Schedule of Field Data Collection

Construction Site	Time (mm/dd/yy–mm/dd/yy)
IL-91	05/27/2020–06/08/2020
IL-116	06/17/2020–06/26/2020
IL-100	07/06/2020–07/13/2020
IL-61	08/12/2020–08/19/2020
IL-64	07/14/2021–07/21/2021
RT-509	09/09/2020–09/14/2020

The details of each construction site are provided below:

- IL-91: The total rehabilitation length was 4.1 miles on a two-lane, two-way road, starting from Station 149+35 and ending at 368+00. Existing pavement includes 12 ft wide driving lanes, 3 ft wide shoulders, and a 1.5% cross slope. The CIR depth is 4 in., and engineered emulsion was used.

- IL-116: The total rehabilitation length was 6.43 miles on a two-lane, two-way road, starting from Station 1084+28 and ending at 1425+50. Existing pavement includes 13 ft wide driving lanes, 3 ft wide shoulders, and a 1.5% cross slope. The CIR depth is 4 in., and an engineered emulsion was used.

- IL-100: The total rehabilitation length was 10.545 miles on a two-lane, two-way road, starting from Station 759+40 and ending at 1320+56. Existing pavement includes 10 ft wide driving lanes, 3 ft aggregate shoulder, and 1 ft wide HMA shoulder. The cross slope is 1.5%, and the CIR depth is 4 in., and engineered emulsion was used.

- IL-61: The total rehabilitation length was 4.003 miles, on a two-lane, two-way road, starting from Station 827+50 and ending at 1039+05. Existing pavement includes 13 ft wide driving lanes, 3 ft 7 in. wide shoulders, and a 1.5% cross slope. The CIR depth is 4 in., and engineered emulsion was used.

- IL-64: The total rehabilitation length is 4.80 miles on a two-lane, two-way road, starting from Station 4+00 and ending at 263+20. Existing pavement includes 13 ft wide driving lanes, 3 ft wide shoulders, and a 1.5% cross slope. The CIR depth is 4 in., and engineered emulsion was used.

- RT-509: The total rehabilitation length is 2.854 miles on a two-lane, two-way Portland cement concrete road, starting from Station 39+62.50 and ending at 191+79. Existing pavement includes 12 ft wide driving lanes, 4 ft wide shoulders, and a 1.5% cross slope. The CCPR depth was 3 in., and engineered emulsion was used. The recycled HMA mixtures were retrieved from a mobile plant by Heritage Group.

Field Test Measurements

Field data collections were performed before and after CR construction. Only GPR measurements were obtained one day before or on the same day as the CR process. GPR and sand-cone test data were collected after final compaction passes for all sites. Because the study was conducted during the COVID-19 pandemic, face masks and social distancing were observed during all tests (presented in Figure 52). Hourly weather information was documented, and an example is presented in Table 4. Table 5 illustrates the testing schedule for IL-61; similar schedules were applied to other sections.

Table 4. Temperature Documentation of IL-61 on August 12, 2020

Wind Speed	Wind Gust (mph)	Pressure altimeter (in)	Precipitation (in)	Condition
7	0	29.19	0.0	Fair
3	0	29.21	0.0	Cloudy
5	0	29.21	0.0	Partly Cloudy
6	0	29.22	0.0	Mostly Cloudy
6	0	29.22	0.0	Fair
6	0	29.23	0.0	Cloudy
5	0	29.23	0.0	Cloudy
8	0	29.23	0.0	Mostly Cloudy
7	0	29.23	0.0	Mostly Cloudy
5	0	29.24	0.0	Cloudy
6	0	29.24	0.0	Cloudy
7	0	29.23	0.0	Mostly Cloudy
7	0	29.24	0.0	Partly Cloudy
6	0	29.23	0.0	Fair
8	0	29.23	0.0	Fair
8	17	29.23	0.0	Partly Cloudy
10	0	29.23	0.0	Mostly Cloudy
9	0	29.23	0.0	Mostly Cloudy
9	0	29.22	0.0	Partly Cloudy
9	0	29.21	0.0	Mostly Cloudy
8	0	29.20	0.0	Partly Cloudy
8	0	29.19	0.0	Fair
10	0	29.17	0.0	Fair
7	0	29.17	0.0	Fair
7	0	29.18	0.0	Mostly Cloudy
6	0	29.18	0.0	Mostly Cloudy
6	0	29.17	0.0	Fair
6	0	29.18	0.0	Fair
6	0	29.20	0.0	Fair
3	0	29.23	0.0	Fair
7	0	29.23	0.0	Fair
7	0	29.23	0.0	Fair

Figure 52. Photo. Face masks and social distancing during field testing.

Table 5. Field Data Collection Schedule for IL-61

Location #	1	2	3	4	5	6	7
Station	848+00 SB	849+50 SB	851+00 SB	852+50 SB	1034+00 NB	1032+50 NB	1031+00 NB
Transverse	LWP	RWP	LWP	RWP	LWP	CL	RWP
8/12/2020	0h	0h	0h	0h			
8/13/2020	1D	1D	1D	1D	0h	0h	0h
8/14/2020	N/A	N/A	N/A	N/A	N/A	N/A	N/A
8/15/2020	N/A	N/A	N/A	N/A	N/A	N/A	N/A
8/16/2020	N/A	N/A	N/A	N/A	N/A	N/A	N/A
8/17/2020	5D	5D	5D	5D	4D	4D	4D
8/18/2020	N/A	N/A	N/A	N/A	N/A	N/A	N/A
8/19/2020	7D	7D	7D	7D	6D	6D	6D

Test procedures were as follows:

Before CIR/CCPR placement, researchers either arrived on-site one day prior to or early on the same day of CIR/CCPR construction. Continuous GPR surveys were performed on existing pavement sections at a minimum speed of 30 mph. The GPR van was equipped with work zone safety lights. Location, starting and ending points, and weather information were documented.

A walk-around inspection of the construction site was performed on the rehabilitation day. A schedule of the recycling process was obtained to identify test locations. Once the testing locations were decided, buckets of loose CIR mixtures were obtained from the mix conveyer (Figure 53). These data were the ground-truth readings for moisture content at hour 0. In general, four locations were selected on the first construction day and three were selected for the second day for each project. The collected loose samples were later used as a filling material of the ground-truth test location holes.

Figure 53. Photo. Loose mix from conveyer in the CIR train.

Test locations were identified when the final compaction pass was completed. The conducted tests included sand cone for density, dynamic cone penetrometer (DCP) for qualitatively estimating the structural bearing capacity, lightweight deflectometer (LWD) for estimating the section's structural capacity, and GPR static scans. In addition, GPR scanning of the whole rehabilitated section was performed. Generally, the control section was 600–1000 ft long, depending on the geometry of the pavement section. Tests were performed on the section, following protocols presented in Figure 54, and traffic control was provided.

The obtained sand cone density results were lower than those of field cores density results measured by Heritage Research Group. This observation was further verified in the lab using indoor slabs. However, limited core data were available to correct the sand cone measurements. In addition, the cores were taken after the treated cold-recycled mat was preliminarily consolidated by traffic. Hence, an inherent error is expected that may impact the model's outcome. To quantify the potential risk of the inherent error caused by using the sand cone data, sensitivity analysis was performed and presented at the end of the analysis section.

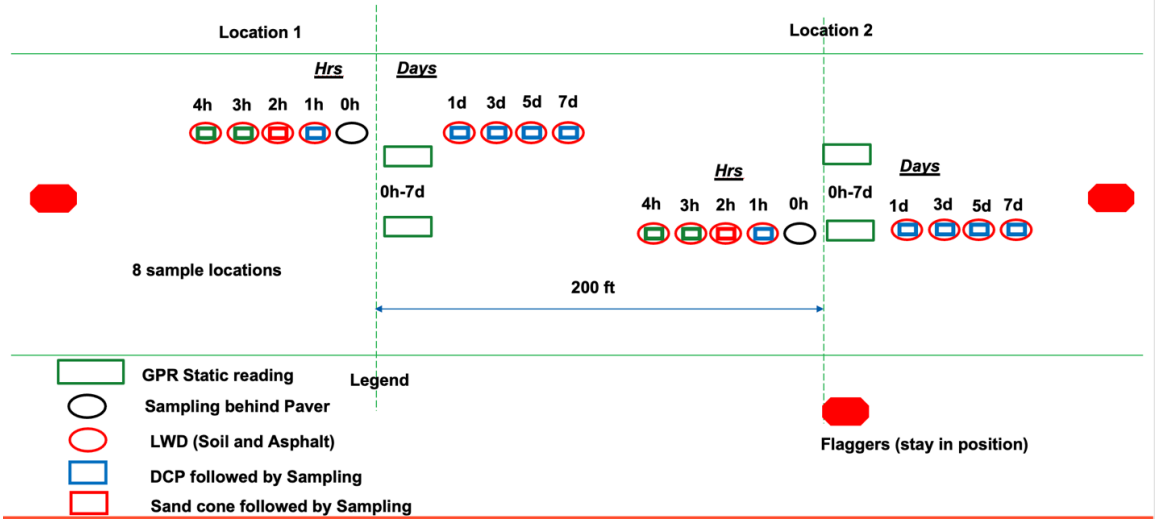

Figure 54. Graph. Diagram of testing protocols on selected locations.

GPR static surveys were performed, as presented in Figure 55. Air-coupled horn antennas with a central frequency of 2.0 GHz, manufactured by Geophysical Survey Systems, Inc., were used in the study. Before testing, the GPR system was turned on and warmed up for 20–30 min. The distance-measuring instrument and GPS were connected and calibrated. The time mode was selected during testing. The duration of each scan was at least 1 min.

Figure 55. Photo. GPR static survey at a test location.

GPR test spots were marked using paint spray. Samples were obtained from nearby locations. Four in. deep holes were dug, and samples were collected. The collected samples were sealed and secured in two plastic bags to maintain the moisture level. An oven was used to obtain the moisture content level. Although a microwave was used in the field, the data used herein were obtained from the lab oven following the current procedures (Figure 56[a]). Sampling holes were filled and patched (Figure 56[b]) using the collected loose mix. When performing LWD, a thermal gun was used to measure pavement surface temperature for later modulus data-processing purposes. LWD and DCP tests are presented in Figure 56(c) and Figure 56(d). However, more results are presented in Appendix B. In some locations, the sand cone test was performed to measure in situ density, Figure 56(e).

(a) Collecting field samples

(b) Filling and patching sampling spots

(c) LWD testing

(d) DCP testing

(e) Sand cone test

Figure 56. Photo. Field sampling.

The same approach was followed in all other test sections. Other antenna configurations were explored for calculation of the dielectric constant from GPR data, including the extended common midpoint method (XCMP) which is presented in Appendix D.

Model Validation

Field Measurements

To validate the numerical model, an investigation was performed at the IL-161 CIR construction site in May 2020 (Figure 57). GPR surveys were performed after paving and compacting the CIR layer. Table 6 summarizes the testing parameters. The existing pavement was Portland cement concrete with an HMA overlay. The proposed CIR treatment included HMA surface removal, 4 in. CIR, followed by a 1.5 in. HMA overlay. Table 6 summarizes the information from the field test. Table 7 presents the aggregate gradation of the CIR mixture. After CIR layer compaction and prior to HMA overlay surface placement, static GPR measurements were conducted at seven locations. The measurements were repeated various times until the CIR moisture content reached a predefined threshold: 2%. DCP, LWD, and sand cone tests were also conducted in the same vicinity.

Figure 57. Photo. GPR antenna calibration with a copper plate before measurement.

Table 6. Summary of Test Information

Information	Value	Information	Value
Antenna central frequency	2 GHz	Samples/scan	512
Scans/sec	100	Time range	12 ns
CIR layer thickness	100 mm	Binder residue content	64.5%
Maximum theoretical specific gravity	2.38	Emulsion target (based on dry weight)	2.5%
Bulk specific gravity	2.05	Optimum water for mixing	2.0%

Table 7. Aggregate Gradation of the IL-161 CIR Mixture

Sieve Size (mm)	37.5	25	19	12.5	9.5	4.75	2.36	1.18	0.6	0.35	0.15	0.075
% Passing	100	99.0	90.8	77.3	63.8	45.9	33.1	18.1	8.2	4.1	2.7	1.9

Utilizing the test and mixture information, the geometry of the heterogeneous CIR pavement layer was generated and input into the FDTD model. Two sand cone samples were used to calibrate the material dielectric properties of the numerical model. Air void and moisture content data were obtained from the sand cone test results. The dielectric constants of the CIR layer were predicted at adjacent locations where the two samples were taken. Using Figures 9 and 10, the volumes of air void and internal water could be calculated. The volumetric data were incorporated into the numerical model to obtain a simulated dielectric constant of the CIR layer in virtual GPR measurements. This process allowed the back-calculation of water dielectric constant, $\epsilon'_{r,w} = 42$, and the substitute dielectric constant of the aggregate-binder component, $\epsilon_{ab} = 4.3$. The back-calculated dielectric constant of water is close to the value used in a recent simulation study (Lachowicz & Rucka, 2019). The loss factor of water, $\epsilon''_{r,w} = 4$, is chosen from Figure 7 because of the small change in the loss factor in the field temperature range; the ambient temperature was around 86°F.

Validation of the Numerical Model

Figure 58(a) presents a comparison between simulated and measured GPR reflected amplitudes with direct coupling removal. The simulated GPR signals matched the field GPR measured ones. Comparisons were done between the dielectric constants from the field tests and simulations (Figure 58[b]). The simulated dielectric constant of the non-dry HMA mixture matches well with the field data. The average relative error between the simulated and measured results is 5.1%.

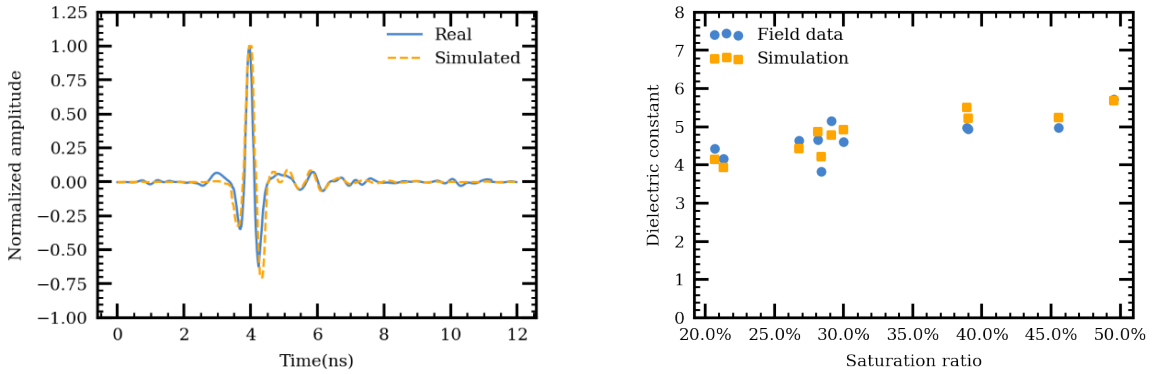

(a) GPR signal (b) Dielectric constants

Figure 58. Chart. Comparisons between field test results and simulation outcome.

ANALYSIS OF FIELD TEST RESULTS

Moisture Content vs. Dielectric Constant

Field Tests on IL-100

On construction day, three GPR measurements were conducted three, four, and five hours after mixture placement to monitor moisture-content variation. Because of the construction schedule, GPR scans could not be collected earlier than three hours after mixture placement. Figure 59(a) presents the moisture-content reduction with time, as measured from loose samples.

Moisture content in the CIR mix decreased over time for all locations during the seven-day monitoring period. As expected, initial moisture content was the highest at hour zero. The decrease in moisture content is due to emulsion breaking and water evaporating from the mixture. Three hours after the mixture placement, the moisture content decreased by approximately 1%–2%. The rate of moisture-content reduction varied per location. For example, location 7 had similar moisture content at hours three and five, while location 3's value decreased from 4% to 3%. After one day, the moisture-content reduction rate slowed, at approximately 0.2% per day. A similar reduction has been reflected in the calculated dielectric constant of the CIR layer (Figure 59[b]). In general, all locations showed a decrease in dielectric constant over the seven-day measurement, except location 4, where the dielectric constant increased after one day. This could be attributed to dripping water from the testing vehicle's air conditioner.

Analyzed GPR measurements accurately showed the moisture-content level at various locations, suggesting moisture loss values and rates. For example, the reduction of dielectric constants from hours three to five at location 3 is greater than for the same period at location 7. Similarly, the rapid decrease of the dielectric constant at day zero was compared to later days' readings. The dielectric constant value may not be the same at various locations because of differences in moisture content and density. Both density and moisture content contribute to the bulk dielectric constant simultaneously.

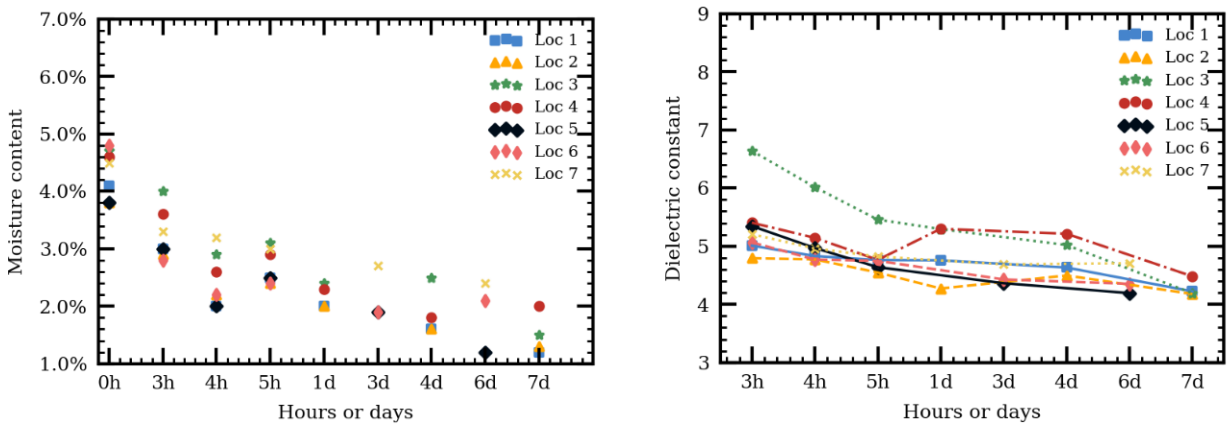

(a) Moisture content (b) Dielectric constant

Figure 59. Chart. (a) Moisture content progression with time and (b) dielectric constant progression with time for IL-100.

Field Tests on IL-61

Figure 60 illustrates moisture content and dielectric constant progression over time for IL-61. As noted at IL-100, moisture content at hour zero was the highest, reaching approximately 4.6%–5.6%. Six hours after mix placement, the moisture content dropped to approximately 3.0%–4.0%. After one day, the moisture content dropped another 0.5% and reached around 2.0% at days six and seven. The dielectric constant decreased over time for all locations. On construction day, the dielectric constant at some locations (e.g., location 3 and 7) increased slightly. That could be explained by moisture evaporation and accumulation at the upper part of the CIR layer. The calculated dielectric constants,

using the equation presented in Figure 1, can be impacted by the material's heterogeneous properties. The contribution of the shallow part is more pronounced than that of the deeper part.

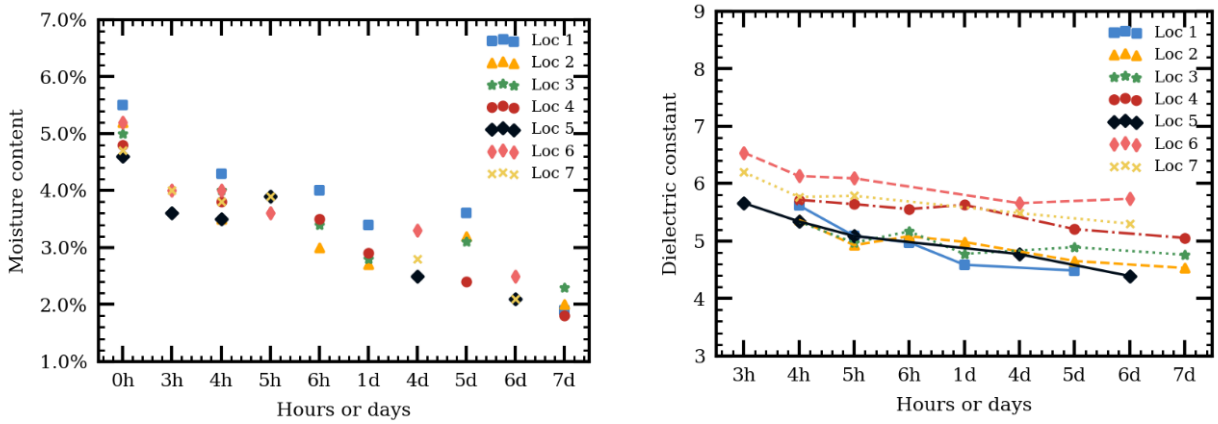

(a) Moisture content (b) Dielectric constant

Figure 60. Chart. (a) Moisture content progression with time and (b) dielectric constant progression with time for IL-61.

Field Tests on Rt-509

Figure 61 presents the moisture content and dielectric constant progression from tests on Rt-509. At hour zero, the moisture content of locations 1, 2, and 3 was already around 3.0%. For these locations, the moisture content decreased more slowly than for locations with higher initial moisture content, such as locations 5, 6, and 7. A similar trend may be observed in the dielectric constant progression, where locations 5, 6, and 7 had a relatively greater dielectric constant dropping rate.

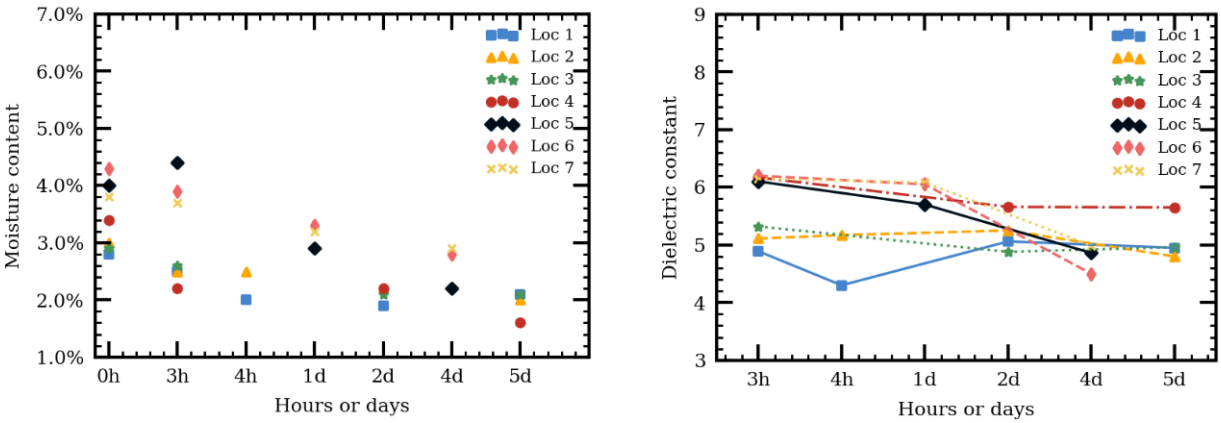

(a) Moisture content (b) Dielectric constant

Figure 61. Chart. (a) Moisture content progression with time and (b) dielectric constant progression with time for Rt-509.

Field Tests on IL-116

Figure 62 presents the moisture content and dielectric constant progressions from tests on IL-116. The measurements started on June 18, 2020, and there was rain on June 22. Several locations were impacted by the rainfall, including locations 1 and 3. Their moisture content increased after day three, as shown by direct moisture measurement and calculated dielectric constant. As expected, this impacted the calculated dielectric constant because of the accumulation of free water on the pavement surface, especially when using the reflection amplitude approach.

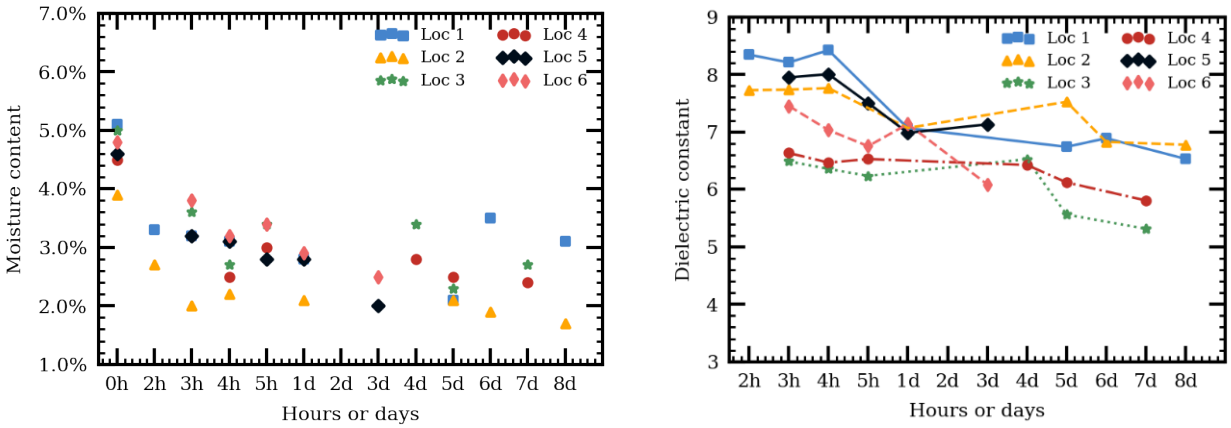

(a) Moisture content (b) Dielectric constant

Figure 62. Chart. (a) Moisture content progression with time and (b) dielectric constant progression with time, both on IL-116.

Field Tests on IL-64

Figure 63 presents the moisture content and dielectric constant progressions at locations 1–7 on IL-64. The measurements started on July 14, 2021, and there was heavy rainfall two days after the first compaction. Measurements were taken at locations 1 to 4 during these days. As expected, measurements were affected by the rainfall. The moisture content increased at day two, as shown by the direct moisture measurement and calculated dielectric constant. Measurements were made at locations 5 to 7 after the rainfall. The same trend was noticed, but to a lesser degree. In general, all locations showed a parallel reduction in moisture content and dielectric constant after the rainfall.

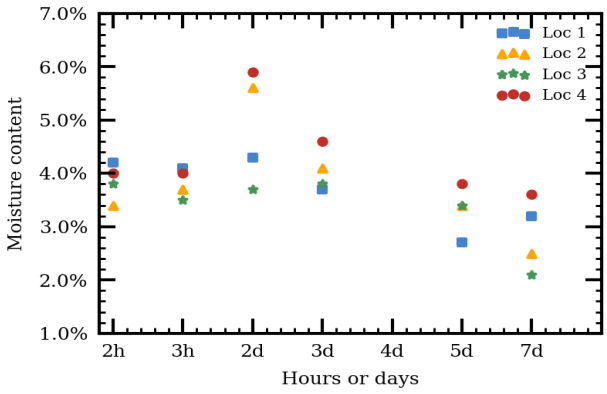

(a) Moisture content

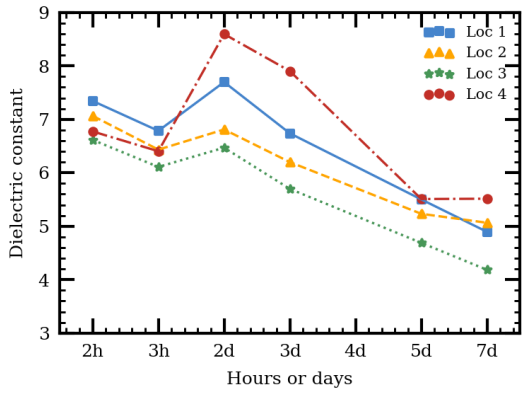

(b) Dielectric constant

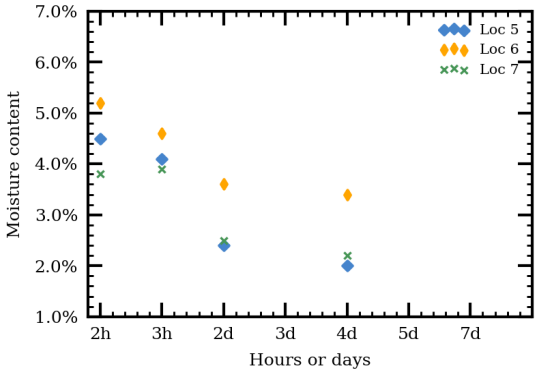

(a) Moisture content

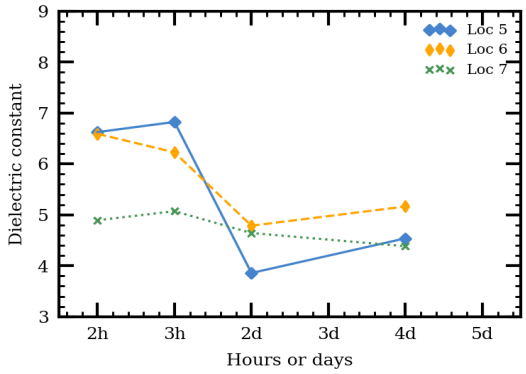

(b) Dielectric constant

Figure 63. Chart. (a) Moisture content progression with time at locations 1–4, (b) dielectric constant progression with time at locations 1–4, (c) moisture content progression with time at locations 5–7, and (d) dielectric constant progression with time at locations 5–7 at IL-116.

Moisture Content Prediction

The in situ moisture content was predicted from GPR scans and compared with measured moisture content obtained from loose samples at all five field tests (Figure 64). The numerical model (Figure 14) was calibrated using two sand-cone test results from IL-61. The calibrated parameters were $A_\epsilon = 23.475, B_\epsilon = 1.025$, and $C_\epsilon = 1.008$.

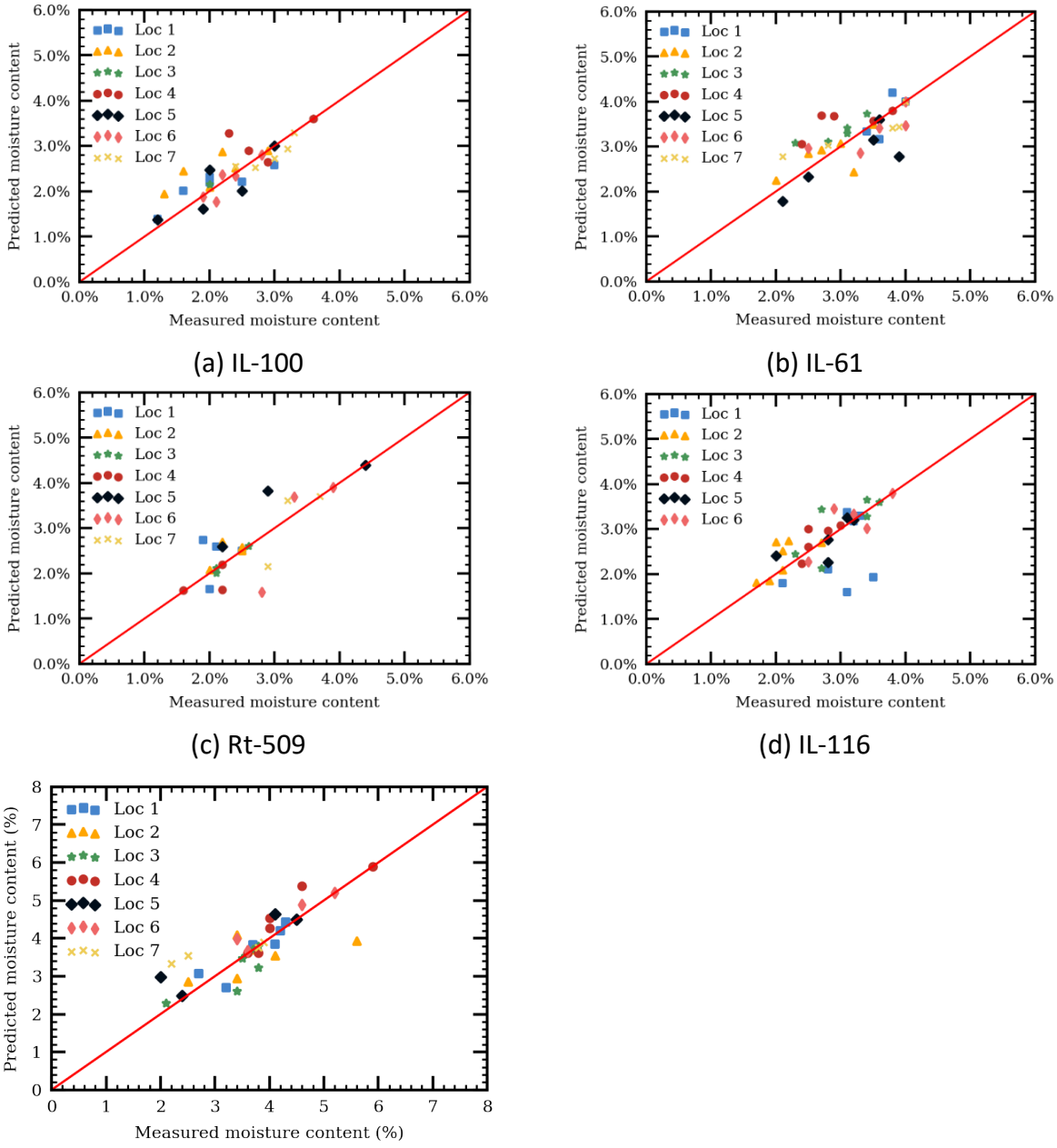

(a) IL-100

(b) IL-61

(c) Rt-509

(d) IL-116

(e) IL-64

Figure 64. Chart. Comparison between predicted and measured moisture content.

Table 8 presents the absolute and average errors for the four field tests. The average absolute errors were calculated for each location. The moisture content predictions at the four field sites have similar average errors. At some locations, the absolute error of the moisture content prediction reached more than 0.50%, as at location 4 at IL-100, location 4 at IL-61, locations 1 and 6 at Rt-509, and location 1 at IL-116. These locations were reported to have water dripping from the testing van's air conditioner or rainfall.

Table 8. Absolute Error of Predicted Moisture Content for Each Location at the Five Field Test Sites

Location	Error (%)	Avg. Error (%)	Location	Error (%)	Avg. Error (%)
IL-100			**IL-61**		
1	0.29	0.33	1	0.33	0.36
2	0.39		2	0.27	
3	0.39		3	0.28	
4	0.62		4	0.59	
5	0.28		5	0.39	
6	0.12		6	0.32	
7	0.17		7	0.35%	
Rt-509			**IL-116**		
1	0.56	0.33	1	0.63	0.32
2	0.16		2	0.26	
3	0.03		3	0.30	
4	0.20		4	0.17	
5	0.44		5	0.23	
6	0.53		6	0.30	
7	0.38				
IL-64					
1	0.08	0.30			
2	0.64				
3	0.17				
4	0.16				
5	0.31				
6	0.11				
7	0.59				

Density and Moisture Content Prediction Using ACA Model

Table 9 presents the prediction of CIR layer density using the ACA model for four projects, and Figure 65 presents predicted moisture content for those projects using the ACA model.

Table 9. Predicted G_{mb} from GPR Measurements for CIR Projects

Moisture content (%)	Sand cone* G_{mb}	Predicted G_{mb}	Error (%)
1.9	1.956	1.959	0.2
2.5	1.880	1.916	1.9
3.1	1.906	1.869	1.9
1.8	1.980	1.955	1.3
2.7	1.954	2.016	3.1
4.0	2.001	1.964	1.8
3.8	1.929	1.925	0.2
2.1	2.017	2.016	0.1
2.7	1.833	1.817	0.9
3.4	1.904	1.968	3.4
5.6	1.775	1.769	0.3
3.4	1.771	1.724	2.7
2.5	1.796	1.778	1.0
3.7	1.855	1.891	2.0
2.1	1.902	1.819	4.4
4.0	1.857	1.891	1.8
5.9	1.884	1.938	2.9
3.8	1.814	1.727	4.8
4.5	1.797	1.791	0.4
2.4	1.780	1.781	0.1
2.0	1.787	1.806	1.0
5.2	1.762	1.732	1.7
3.8	1.727	1.692	2.0
2.5	1.785	1.808	1.3
2.2	1.714	1.794	4.7
2.0	1.946	1.939	0.3
2.2	1.941	1.907	1.8
2.9	1.940	2.029	4.6
2.6	1.873	1.924	2.7
2.0	1.999	1.955	2.2
2.2	1.955	1.907	2.4
3.2	1.915	1.882	1.7
2.0	1.883	1.945	3.3
3.2	1.900	1.865	1.8

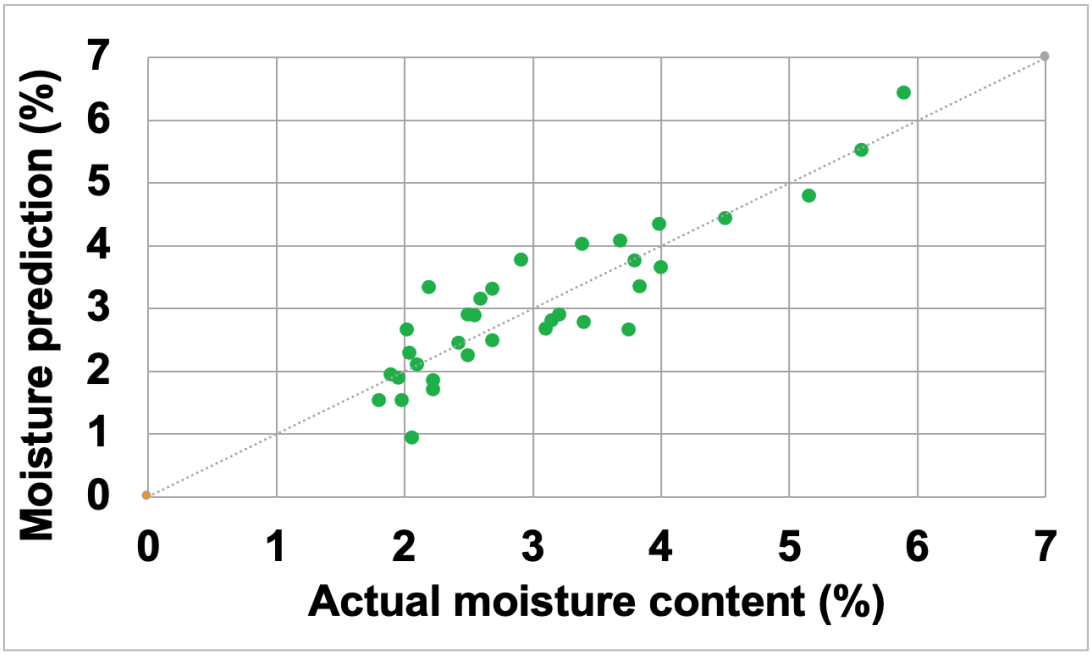

*Sand cone data were lower than extracted core data obtained after traffic application. Sensitivity was conducted to identify the impact of the inherent error.

Figure 65. Chart. Predicting moisture content using the ACA model for CIR projects.

The dry density is predicted with an average error of 2.0% and an RMSE of 0.047 using the ACA model. The model also predicts the moisture content of CIR data, with an RMSE of 0.5%, and the data explanation has an R^2 of 0.81. Notably, a few data points were excluded from the CIR projects; most of the omitted data were collected during the first two hours of construction. During the first two hours of treatment, some water might have been still bound to the emulsion. Bound water has a significantly lower dielectric constant than free water. This would affect the calculated bulk dielectric constant and, hence, hinders moisture prediction with the ACA model, as the ACA model predicts free moisture content.

Table 10. Predicted G_{mb} from GPR Measurements for CCPR Project

Moisture content (%)	Sand cone G_{mb}	Predicted G_{mb}	Error (%)
1.95	1.732	1.713	1.1
2.52	1.720	1.702	1.0
3.66	1.652	1.699	2.8

The dry density is predicted with an average error of 1.7% and an RMSE of 0.036.

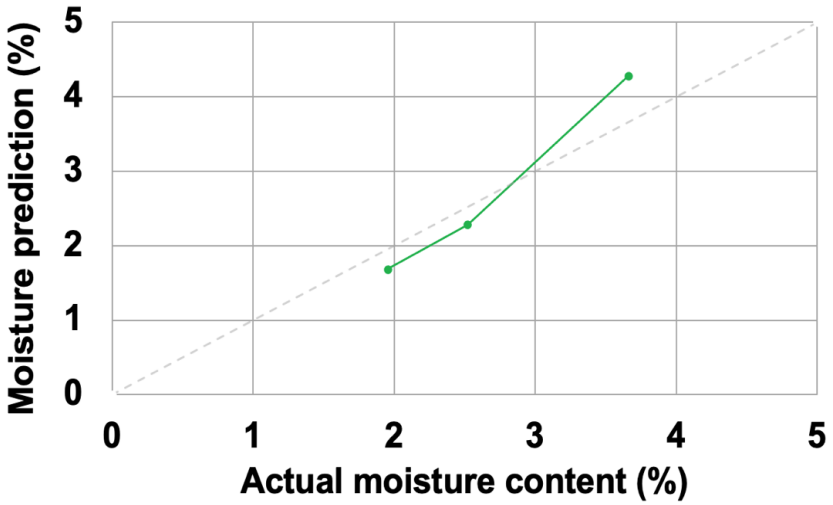

Figure 66. Chart. Predicting moisture content using the ACA model for CCPR project.

The ACA model can accurately predict the moisture content in CCPR with an RMSE of 0.47%, and an R^2 of 0.99. An RMSE of less than 0.5% is considered satisfactory for curing monitoring application.

ACA Model Sensitivity Analysis

The sensitivity of the ACA model to density input was evaluated. Sensitivity analysis, by definition, is quantifying the uncertainty or expected error in the output due to uncertainty or error in the input. In this case, the error in moisture content prediction, by the ACA model, was quantified. The RMSE was obtained for different levels of density input. Monte Carlo simulations were used to accomplish this task. The input density varied from a corresponding air void level of 10% to 20%, the expected air void range for CR treatments. Other variables in the ACA model were kept constant per the collected field data. Figure 67 illustrates the results of the sensitivity analysis.

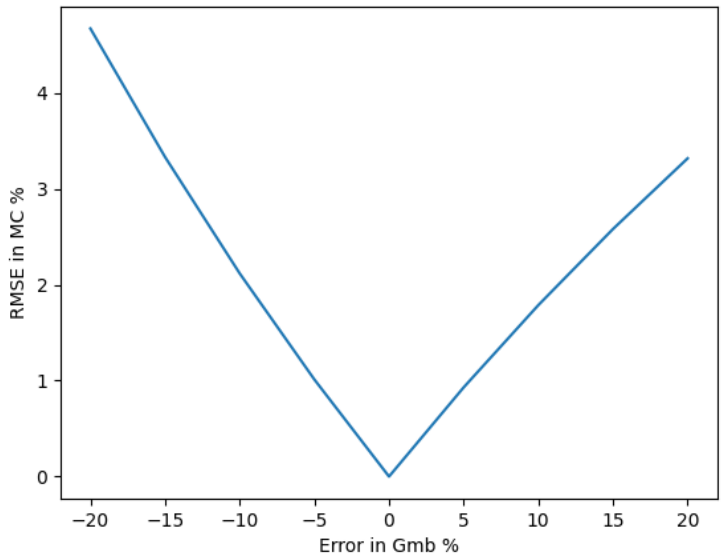

Figure 67. Chart. ACA model sensitivity analysis results.

As expected, the ACA model is sensitive to input density (Figure 67). An average error of 5% in measured/calculated bulk dry density (G_{mb}) could result in a 1% RMSE of predicted moisture content. This means if the actual moisture content is 2%, then the prediction can be 1%–3%.

DATA-PROCESSING TOOL

A data-processing tool (GPR-Density), developed and owned by ICT, has been modified to meet the objectives of this project and has become applicable to predict moisture for cold-recycling treatments of asphalt pavements. GPR-Density was developed using MATLAB APPDESIGNER (MathWorks 2021). This tool is a stand-alone file, meaning Internet connection is not needed nor previous installation of MATLAB to use the tool. Additionally, programming skills and theoretical knowledge about GPR are also not needed. The tool's interface, presented in Figure 68, is user friendly, with help features for all input parameters when the user hovers over them.

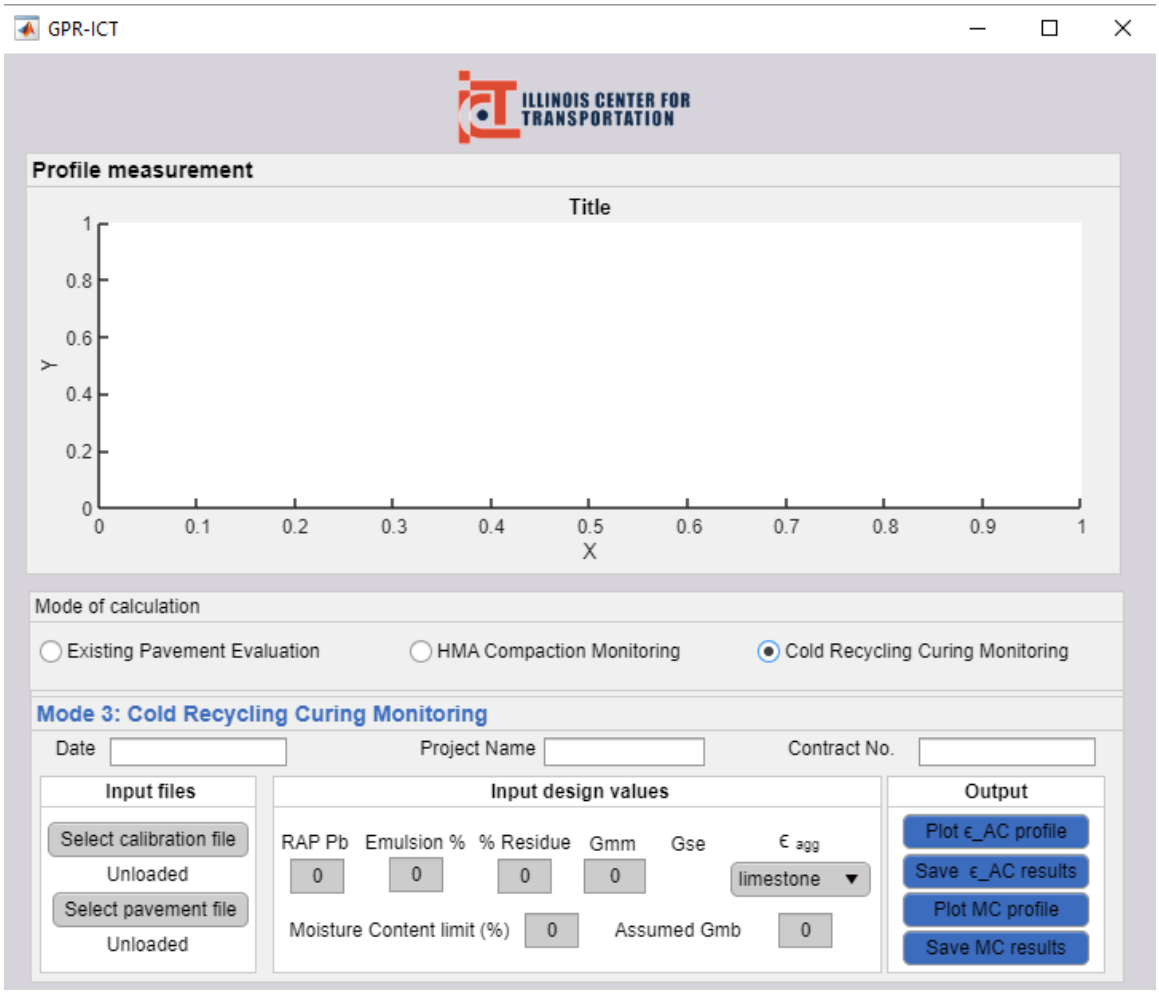

Figure 68. Photo. GPR-Density tool with a user-friendly interface.

The interface includes three separate computation modules: 1) existing pavement evaluation, 2) HMA compaction monitoring, and 3) cold-recycling curing monitoring. The last model was added for this project. All models have two input sections, GPR data and material characteristic values, and one output section for plotting and saving results.

In this section, module 3 (shown in Figure 68) is explained briefly. For documentation, the user may insert project-specific information (i.e., date, project name, and contract number), which is used as the default name of the output of the saved results.

In general, the computation uses the reflection amplitude method for dielectric constant calculation, the wavelet transform decomposition approach for dielectric constant smoothing, and the ACA model for moisture content estimation.

For input, two files are needed: a calibration file (on top of a perfect reflector such as copper) and a pavement scan. The measurements should be at the same antenna height and in a "csv" format. Additional material characteristics are listed as follows:

- RAP binder content (RAP P_b), which refers to the original binder content of the milled pavement.
- Percent of emulsions used in the mix, which is typically around 2%–3%.
- Percent residue, which corresponds to the percent binder in the added emulsion. This value is required to be a minimum of 64 by AASHTO MP 31-17.
- Maximum theoretical specific gravity (G_{mm}) of the CR.
- Type of dominant aggregate. Typical aggregate types in Illinois are listed in the drop-down menu: limestone, dolomite, granite, and trap rock.
- Moisture content limit in percent, which is the threshold below which sufficient curing is expected. This value is usually 1.5%–2.5%.
- Assumed specific gravity of the CR mix. The CR specific gravity could be estimated from the mix design or from field values. The CR specific gravity affects the moisture content prediction, as shown in the sensitivity analysis, so the input value should be as accurate as possible.

The dielectric constant profile, along the scan path, would be plotted by clicking the "plot ε_{AC} profile" button. The tool presents both the raw and smooth dielectric constant profiles. The smooth results could be saved in a "csv" format. Upon clicking "plot MC profile," the moisture content profile appears, and a moisture content indicator appears. The moisture content indicator will appear green, yellow, or red when moisture content is below, around, or above the set threshold ($\pm$1%), respectively. Figure 69 illustrates an example of moisture content estimation.

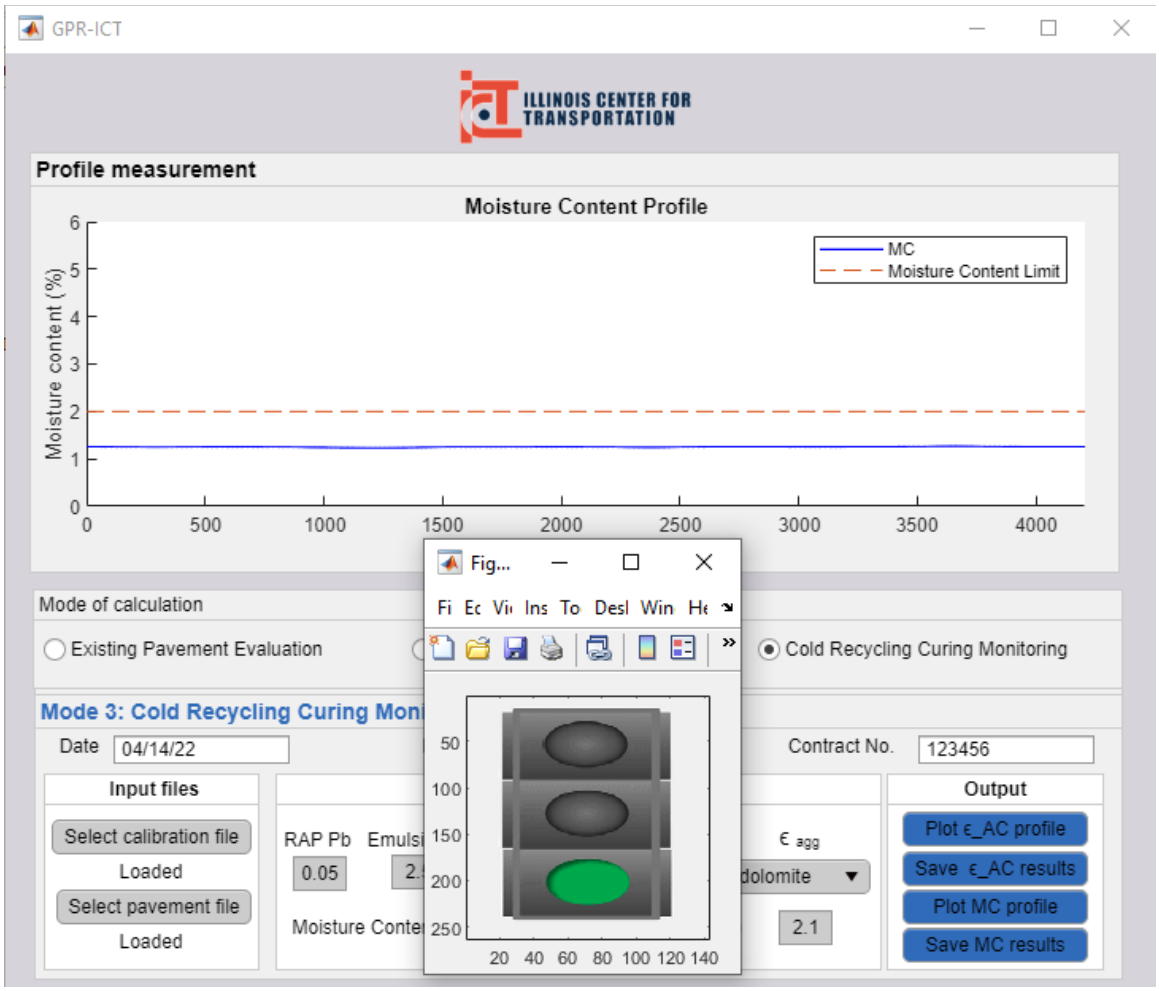

Figure 69. Photo. Moisture content output example.

Appendix C provides more information about the tool's structure as well as its algorithms, other modes of computation, and a simplified installation user guide.

CHAPTER 4: FINDINGS, CONCLUSIONS AND RECOMMENDATIONS

SUMMARY

Cold recycling (CR), e.g., cold in-place recycling (CIR) and cold central-plant recycling (CCPR), is gaining wider acceptance and use in the United States as a rehabilitation approach of existing asphalt pavements because of its economic and environmental benefits. A CR layer must be cured before an overlay is placed to avoid premature failure. During the curing process, water is steadily released from the emulsion and evaporates, enhancing layer stiffness and strength. Emulsion breaking and water evaporation occur in hours, days, or even weeks after compaction of the CR mixture. If a CR layer is overlaid while having a high moisture content, the retained moisture would affect the pavement structure capacity and potentially cause asphalt pavement damage. Therefore, monitoring moisture content during the curing period is important for identifying the optimum time to open the road for traffic and/or place an overlay on the constructed CIR or CCPR.

Two methods—coring and nuclear gauge—are traditionally used to measure the moisture content of flexible pavements. Both methods have limitations. Coring is destructive to the pavement, and it reflects the moisture information only at the locations where the cores are taken. In addition, the process affects the accuracy of moisture prediction. The nuclear density gauge uses radioactive material. It requires special licensing to transport and operate, which leads to increased operational costs. In addition, the nuclear gauge's accuracy in measuring moisture content is affected by the asphalt content of the pavement; hence, it has not been commonly used for this application.

Ground-penetrating radar (GPR), in contrast, has the potential for such application. It is a nondestructive testing method based on the propagation and reflection of electromagnetic (EM) waves. It has been widely applied in geoscience and civil engineering. Over the past few decades, many studies have already demonstrated the high sensitivity of GPR to water in soil and building materials. The relative permittivity or relative dielectric constant, which is commonly used as the dielectric constant, is a critical material property in the practical application of GPR measurements. The dielectric constant is 1 for air and approximately 81 for pure water at 68°F. For asphalt pavement, the dielectric constant is in the range of 3–12. Therefore, a relatively small increase in moisture content could alter the bulk dielectric constant of asphalt materials. Hence, GPR could be a feasible tool to predict moisture in asphalt pavements.

One challenge arises for monitoring moisture content in asphalt pavements: the complicated nature of water inside the asphalt pavement. The dielectric properties of water change with the environment temperature and frequency of GPR. In addition, the dielectric constant of free and bound water is highly different, which is an important factor in CR pavements. Given the complexity of estimating moisture content using GPR, simulations and numerical models were developed and used to better understand the effect of internal moisture content on asphalt pavement's dielectric properties. The finite-difference time-domain (FDTD) method, which simulates EM wave propagation, has been successfully used to interpret GPR data. The FDTD method allows simulation of a considerable number of samples from the same initial mixture components and properties. Recently, Al-Qadi and colleagues have applied the FDTD method to evaluate the dielectric properties of dry

asphalt pavement and compaction progression of asphalt pavement. In addition, analyses were conducted to remove surface moisture due to compaction, to allow for dry density prediction. This study extends this effort to predict the internal moisture of an asphalt mixture.

To achieve the research objective of quantifying in situ CR moisture content, a numerical method was developed to simulate EM wave propogation in non-dry asphalt pavement. The heterogeneous dielectric model of asphalt pavement was generated using the random sequential adsorption (RSA) method, followed by an FDTD simulation. A power function relationship between moisture content and dielectric constant was derived from the simulation.

The simulation model was validated with field data, and a relationship between moisture content and dielectric constant was developed. A comparison between lab- and field-measured and GPR-predicted moisture content values indicated the simulation model was effective in predicting in situ CR moisture content.

Based on the lab tests, the Al-Qadi-Lahouar-Leng (ALL) model was modified and used to predict pavement density for non-dry flexible pavements. The new model, Al-Qadi-Cao-Abufares (ACA), can be used to predict pavement density when internal moisture content is present. The performance of the ACA model was verified by using field data collected from CR pavement. A user-friendly tool was also developed to assist pavement engineers with predicting moisture content and pavement density as well as using GPR in practice.

MAJOR FINDINGS

The findings on predicting moisture content of asphalt and CR pavements are summarized below:

1. The bulk dielectric constant of a CR layer is highly correlated with its moisture content. This correlation has been supported by simulation and laboratory and field test results. Aggregate gradation of asphalt layers has no effect on the calculation of the dielectric constant because the EM wavelength (2.2 in.) to maximum aggregate size is more than two.

2. Sensitivity analysis showed that high moisture content inside asphalt pavements would increase surface amplitude reflection, while reducing the speed of EM waves in the pavement layer and increasing their attenuation. The heterogeneous numerical model was validated using GPR surveys of CR (CIR and CCPR) pavements. The average relative error between simulated and measured dielectric constants was 5.1%.

3. Internal moisture content of CIR and CCPR was predicted from dielectric constants using a formula derived from an FDTD simulation model. The average error is around 0.33%. The developed ACA model was used to predict G_{mb} from GPR measurements with a root-mean-square error (RMSE) of 0.06 and an average error of 2.04% and to predict moisture content with R^2 of 0.97 and RMSE of 0.46% for indoor tests. The ACA model was applied on field tests, with an average error of 3.9% and average RMSE of 0.09 for G_{mb} prediction and average RMSE of 1% and average R^2 of 0.5 for moisture content prediction.

RECOMMENDATIONS

A data-driven method to decouple the effect of air voids and moisture content should be developed. The numerical model proposed in this study can be used to generate a synthetic database of non-dry asphalt pavement, which can be used for training on the data-driven approach. Additionally, further validation of the ACA model is needed.

REFERENCES

AASHTO MP 31-17. (2017). Standard Specification for Materials for Cold Recycled Mixtures with Emulsified Asphalt.

AASHTO PP 86-17. (2017). Standard Practice for Emulsified Asphalt Content of Recycled Mixture Designs.

Alharthi, A., & Lange, J. (1987). Soil water saturation: Dielectric determination. *Water Resources Research*, *23*(4), 591–595, https://doi.org/10.1029/WR023i004p00591

Al-Qadi, I. L., Ghodgaonkar, D. K., Varada, V. K., & Varadan, V. V. (1991). Effect of moisture on asphaltic concrete at microwave frequencies. *IEEE Transactions on Geoscience and Remote Sensing*, *29*(5), 710–717. https://doi.org/10.1109/TGRS.1991.817705

Al-Qadi, I., Lahouar, S., Loulizi, A., Elseifi, M. A., & Wilkes, J. A. (2004). Effective approach to improve pavement drainage layers. *Journal of Transportation Engineering*, *130*(5), 658–664. https://doi.org/10.1061/(ASCE)0733-947X(2004)130:5(658)

Asphalt Recycling and Reclaiming Association (ARRA). (2015). *Basic asphalt recycling manual*, 2nd ed. U.S. Department of Transportation. Federal Highway Administration.

Benedetto, A., & Benedetto, F. (2011). Remote sensing of soil moisture content by GPR signal processing in the frequency domain. *IEEE Sensors Journal*, *11*(10), 2432–2441. https://doi.org/10.1109/JSEN.2011.2119478

Benedetto, A., Ciampoli, L. B., Brancadoro, M. G., Alani, A. M., & Tosti, F. (2018). A computer-aided model for the simulation of railway ballast by random sequential adsorption process. *Computer-Aided Civil and Infrastructure Engineering*, *33*(3), 243–257. https://doi.org/10.1111/mice.12342

Benedetto, A., & Pajewski, L. (Eds.). (2015). *Civil engineering applications of ground penetrating radar*. Springer, Cham. https://doi.org/10.1007/978-3-319-04813-0

Cao, Q., & Al-Qadi, I. L. (2021). Development of a numerical model to predict the dielectric properties of heterogeneous asphalt concrete. *Sensors*, *21*(8), 2643. https://doi.org/10.3390/s21082643

Cox, B., Howard, I., & Campbell, C. (2016). Cold in-place recycling moisture-related design and construction considerations for single or multiple component binder systems. *Transportation Research Record*, *2575*(1), 27–38. https://doi.org/10.3141/2575-04

Diefenderfer, B., Boz, I., Habbouche, J., Jones, D., & Hand, A. (2020). Development and assessment of rapid tests for construction of asphalt-treated cold recycled pavements. *Transportation Research Board*, *2674*(3), 189–198. https://doi.org/10.1177/0361198120908867

Feder, J. (1980). Random sequential adsorption. *Journal of Theoretical Biology*, *87*(2), 237–254. https://doi.org/10.1016/0022-5193(80)90358-6

Federal Highway Administration. (2017). *A life-cycle methodology for energy-use by in-place pavement recycle techniques* (Report No. ICT-20-018). Illinois Center for Transportation, University of Illinois at Urbana-Champaign. https://doi.org/10.36501/0197-9191/20-018

Federal Highway Administration. (2018). *Overview of project selection guidelines for cold in-place and*

cold central plant pavement recycling (Report No. FHWA-HIF-17-042). US Department of Transportation.

Fernandes, F. M., Fernandes, A., & Pais, J. (2017). Assessment of the density and moisture content of asphalt mixtures of road pavements. *Construction and Building Materials*, *154*, 1216–1225. https://doi.org/10.1016/j.conbuildmat.2017.06.119

Frid, A., & Frid, V. (2018). Irregular changes in antenna height during high speed scanning as a source of essential errors in measuring the thickness of asphalt. In *2018 17th International Conference on Ground Penetrating Radar (GPR)*, 1–4, https://doi.org/10.1109/ICGPR.2018.8441565

Giannopoulos, A. (2005). Modelling ground penetrating radar by GprMax. *Construction and Building Materials*, *19*(10), 755–762. https://doi.org/10.1016/j.conbuildmat.2005.06.007

Hainin, R., Jaya, P., Yaacob, H., Ismail, R., Hassan, A., Akhir, M., & Mohammed, I. (2013). Aggregate degradation characteristics of stone mastic asphalt mixtures. *Jurnal Teknologi*, *65*(3). https://doi.org/10.11113/jt.v65.2155

Kaatze, U. (1989). Complex permittivity of water as a function of frequency and temperature. *Journal of Chemical & Engineering Data*, *34*(4), 371–374. https://doi.org/10.1021/je00058a001

Kaplanvural, İ., Pekşen, E., & Özkap, K. (2018). Volumetric water content estimation of C-30 concrete using GPR. *Construction and Building Materials*, *166*, 141–146. https://doi.org/10.1016/j.conbuildmat.2018.01.132

Kim, Y., Im, S., & Lee, H. (2009). *Examination of curing criteria for cold in-place recycling* (Report No TR-553). Iowa highway Research Board. http://publications.iowa.gov/id/eprint/20058

Kim, Y., Im, S., & Lee, H. (David). (2011). Impacts of curing time and moisture content on engineering properties of cold in-place recycling mixtures using foamed or emulsified asphalt. *Journal of Materials in Civil Engineering*, *23*(5), 542–553. https://doi.org/10.1061/(ASCE)MT.1943-5533.0000209

Kim, Y., & Lee, H. (2006). Development of mix design procedure for cold in-place recycling with foamed asphalt. *Journal of Materials in Civil Engineering*, *18*(1), 116–124. https://doi.org/10.1061/(ASCE)0899-1561(2006)18:1(116)

Klewe, T., Strangfeld, C., & Kruschwitz, S. (2021). Review of moisture measurements in civil engineering with ground penetrating radar—Applied methods and signal features. *Construction and Building Materials*, *278*, 122250. https://doi.org/10.1016/j.conbuildmat.2021.122250

Kleyn, E. G. (1975). *The use of the dynamic cone penetrometer* (DCP). Transvaal Roads Department, South Africa.

Lachowicz, J., & Rucka, M. (2019). A novel heterogeneous model of concrete for numerical modelling of ground penetrating radar. *Construction and Building Materials*, *227*, 116703. https://doi.org/10.1016/j.conbuildmat.2019.116703

Leng, Z., & Al-Qadi, I. L. (2014). An innovative method for measuring pavement dielectric constant using the extended CMP method with two air-coupled GPR systems. *NDT & E International*, *66*, 90–98. https://doi.org/10.1016/j.ndteint.2014.05.002

Leng, Z., Al-Qadi, I. L., & Lahouar, S. (2011). Development and validation for in situ asphalt mixture density prediction models. *NDT & E International*, *44*(4), 369–375. https://doi.org/10.1016/j.ndteint.2011.03.002

Liebe, H., Hufford, G., & Manabe, T. (1991). A model for the complex permittivity of water at frequencies below 1 THz. *International Journal of Infrared and Millimeter Waves*, *12*, 659–675. https://doi.org/10.1007/BF01008897

Liu, X., Chen, J., Cui, X., Liu, Q., Cao, X., & Chen, X. (2017). Measurement of soil water content using ground-penetrating radar: A review of current methods. *International Journal of Digital Earth*, *12*, 1–24. https://doi.org/10.1080/17538947.2017.1412520

MathWorks. (2021). MATLAB Documentation: Create a Simple App Using GUIDE. Accessed January 27, 2021. https://www.mathworks.com/help/matlab/creating_guis/about-the-simple-guide-gui-example.html

Minnesota Department of Transportation. (2000). *Cold in-place recycling literature review and preliminary mixing design procedure* (Report No. MN-RC-2000-21). University of Minnesota, Department of Civil Engineering.

National Cooperative Highway Research Program. (2011). *Synthesis 421: Recycling and reclamation of asphalt pavements using in-place methods*. Transportation Research Board.

National Cooperative Highway Research Program. (2020). *Proposed AASHTO practice and tests for process control and product acceptance of asphalt-treated cold recycled pavements*. National Academy of Sciences.

Plati, C., & Loizos, A. (2013). Estimation of in-situ density and moisture content in HMA pavements based on GPR trace reflection amplitude using different frequencies. *Journal of Applied Geophysics*, *97*, 3–10. https://doi.org/10.1016/j.jappgeo.2013.04.007

Shangguan, P., Al-Qadi, I. L., Leng, Z., Schmitt, R. L., & Faheem, A. (2013). Innovative approach for asphalt pavement compaction monitoring with ground-penetrating radar. *Transportation Research Record*, *2347*(1), 79-87. https://doi.org/10.3141/2347-09

Shangguan, P., Al-Qadi, I. L., & Lahouar, S. (2014). Pattern recognition algorithms for density estimation of asphalt pavement during compaction: A simulation study. *Journal of Applied Geophysics*, *107*, 8–15. https://doi.org/10.1016/j.jappgeo.2014.05.001

Shangguan, P., Al-Qadi, I. L., Coenen, A., & Zhao, S. (2016). Algorithm development for the application of ground-penetrating radar on asphalt pavement compaction monitoring. *International Journal of Pavement Engineering*, *17*(3), 189–200. https://doi.org/10.1080/10298436.2014.973027

Shangguan, P., & Al-Qadi, I. L. (2015). Calibration of FDTD simulation of GPR signal for asphalt pavement compaction monitoring. *IEEE Transactions on Geoscience and Remote Sensing*, *53*(3), 1538–1548. https://doi.org/10.1109/TGRS.2014.2344858

Topp, G. C., & Davis, J. L. (1985). Measurement of soil water content using time-domain reflectrometry (TDR): A field evaluation. *Soil Science Society of America Journal*, *49*(1), 19–24. https://doi.org/10.2136/sssaj1985.03615995004900010003x

Tosti, F., & Slob, E. C. (2015). Determination, by using GPR, of the volumetric water content in structures, sub-structures, foundations and soil-ongoing activities in working project 2.5 of COST action TU1208. Geophysical Research Abstracts, 17, EGU General Assembly, Vienna, Austria, 12-17 April 2015; EGU2015-15199.

Wang, S., Zhao, S., & Al-Qadi, I. L. (2019). Real-time monitoring of asphalt concrete pavement density during construction using ground penetrating radar: theory to practice. *Transportation Research Record*, *2673*(5), 329–338. https://doi.org/10.1177/0361198119841038

Wang, S., Al-Qadi, I. L., & Cao, Q. (2020). Factors impacting monitoring asphalt pavement density by ground penetrating radar. *NDT & E International*, *115*, 102296, https://doi.org/10.1016/j.ndteint.2020.102296

Warren, C., Giannopoulos, A., & Giannakis, I. (2016). gprMax: Open source software to simulate electromagnetic wave propagation for ground penetrating radar. *Computer Physics Communications*, *209*, 163–170. https://doi.org/10.1016/j.cpc.2016.08.020

Wood, L., White, T., & Nelson, T. (1988). Current practice of cold in-place recycling of asphalt pavements. *Transportation Research Record*, 1178, 31–37. http://onlinepubs.trb.org/Onlinepubs/trr/1988/1178/1178-005.pdf

Xu, W., Xu, B., & Guo, F. (2017). Elastic properties of particle-reinforced composites containing nonspherical particles of high packing density and interphase: DEM–FEM simulation and micromechanical theory. *Computer Methods in Applied Mechanics and Engineering*, *326*, 122–143. https://doi.org/10.1016/j.cma.2017.08.010

Yee, K. S., & Chen, J. S. (1997). The finite-difference time-domain (FDTD) and the finite-volume time-domain (FVTD) methods in solving Maxwell's equations. *IEEE Transactions on Antennas and Propagation*, *45*(3), 354–363. https://doi.org/10.1109/8.558651

Zadhoush, H., Giannopoulos, A., & Giannakis, I. (2021). Optimising the complex refractive index model for estimating the permittivity of heterogeneous concrete models. *Remote Sensing*, *13(*4), 723. https://doi.org/10.3390/rs13040723

Zhao, S., Al-Qadi, I. L., & Wang, S. (2018). Prediction of thin asphalt concrete overlay thickness and density using nonlinear optimization of GPR data. *NDT & E International*, *100*, 20–30. https://doi.org/10.1016/j.ndteint.2018.08.001

APPENDIX A: MIX DESIGN DATA

IDOT Lab Verification Nbr ---> | Ver.: 11-01-07.07.14 | DATE: 08/18/14

Producer Number & Name --> 5116-06 Sandeno East | Plant Location --> Hazel Crest

Material Code Number --> 19524R HMA SC N70 D REC 9.5mm

TPN7030%

48BITVS89

48BITS7M

Plant Bin #	#7	#6	#5	#4	#3	#2	#1	MF	RCY	RCY	RAS #2	RAP #1	ASPHALT
Source (PROD #)			032CM16	025FM39	027FM03		004MP01				01TPM80	01TPM490	19129
(NAME)			80312-04	80112-04	53606-06			80312-04			6416-06	80315-12	Seneca
(LOC)			Hanson	Hanson	Mercer LA			Hanson			Southwind	Sandeno East	1707-06
(ADD. RAP0)			Thornton	Thornton	Niles, MI			Thornton			Thornton	Hazel Crest	Lamont
									0.0	0.0	25.0	4.5	PG 64-28
												Plan PG Grade >	PG 64-28
Aggregate Blend:	0.0	0.0	0.0	62.0	13.0	10.0	0.0	1.0	0.0	0.0	4.0	10.0	Tmax-F 100.0
Mixture Blend:	0.0	0.0	0.0	58.4	12.2	9.4	0.0	0.9	0.0	0.0	5.0	9.9	Tmax-C 100.0

Agg. No. / Sieve Size	#7	#6	#5	#4	#3	#2	#1	MF	RCY	RCY	RAS #2	RAP #1	Aggregate Blend	Mixture Comp Spec
1" (25.0mm)	100.0	100.0	100.0	100.0	100.0	100.0	100.0	100.0	100.0	100.0	100.0	100.0	100	
3/4"(19.0mm)	100.0	100.0	100.0	100.0	100.0	100.0	100.0	100.0	100.0	100.0	100.0	100.0	100	
1/2" (12.5mm)	100.0	100.0	100.0	100.0	100.0	100.0	100.0	100.0	100.0	100.0	100.0	100.0	100	100
3/8" (9.5mm)	100.0	100.0	100.0	95.0	100.0	100.0	100.0	100.0	100.0	100.0	100.0	100.0	97	90-100
No.4 (4.75mm)	100.0	100.0	100.0	29.0	16.0	97.0	100.0	100.0	100.0	100.0	95.0	74.0	53	32-67
No.8 (2.36mm)	100.0	100.0	100.0	7.0	91.0	87.0	100.0	100.0	100.0	100.0	85.0	54.0	33	32-67
No.16 (1.18mm)	100.0	100.0	100.0	5.0	60.0	77.0	100.0	100.0	100.0	100.0	67.0	40.0	25	15-37
No.30 (600µm)	100.0	100.0	100.0	4.0	31.0	57.0	100.0	100.0	100.0	100.0	50.0	30.0	18	
No.50 (300µm)	100.0	100.0	100.0	4.0	18.0	23.0	100.0	100.0	100.0	100.0	40.0	19.0	12	4-18
No.100 (150µm)	100.0	100.0	100.0	3.0	10.0	3.0	100.0	98.0	100.0	100.0	35.0	12.0	7	3-10
No.200(75µm)	100.0	100.0	100.0	3.0	6.3	1.1	100.0	90.0	100.0	100.0	25.0	8.8	5.5	4-8
Bulk Sp. Gr	1.000	1.000	1.000	2.669	2.675	2.891	1.000	2.990	1.000	1.000	2.580	2.640	2.656	Dust/AB
Absorption, %	1.00	1.00	1.00	1.70	1.20	1.20	1.00	1.00	1.00	1.00	1.00	SP GR AB	1.031	1.42	Ratio	0.54

SUMMARY OF SUPERPAVE GYRATORY DESIGN DATA

DATA for N-ini.	7													
	AB, %MOX	Gmb	Gmm	Voids (Pa)	VMA	VFA	Vbe	Pbe	Gse	Pba				
MIX 1	6.3	2.140	2.519	15.1	23.7	36.5	8.66	4.57	2.740	1.19				
MIX 2	6.8	2.155	2.499	13.8	23.6	41.6	9.80	4.88	2.739	1.18				
MIX 3	6.3	2.159	2.479	12.9	23.3	48.3	10.35	5.23	2.736	1.14				
MIX 4	6.8	2.158	2.461	12.3	24.0	48.9	10.51	5.23	2.736	1.16				

DATA for N-des.	70													
	AB, %MOX	Gmb	Gmm	Voids (Pa)	VMA	VFA	Vbe	Pbe	Gse	Pba				
MIX 1	6.3	2.378	2.519	5.6	15.2	63.2	8.62	4.17	2.740	1.19				
MIX 2	6.8	2.397	2.499	4.1	15.0	72.8	10.50	4.68	2.739	1.18				
MIX 3	6.3	2.409	2.479	2.8	15.1	81.3	12.22	5.20	2.736	1.14				
MIX 4	6.8	2.419	2.461	1.7	15.1	88.7	13.42	5.72	2.738	1.16				

OPTIMUM DESIGN DATA @ %des													
GYRATIONS	AB	Gmb	Gmm	%VOIDS (Pa)	VMA	VFA	Gse	Gsb	TSR	RCY AB	Virgin AB	ABR
	5.55			Target								
70	6.8	2.398	2.488	4.0	15.0	73.3	2.729	2.659	0.88	1.70	4.13	29.2

REMARKS LINE 1

REMARKS LINE 2

BITUMINOUS MIXTURE ADDED: 1 HOURS @ 295

Hamburg Wheel Information	
Sample No. Passes	10000
Sample Wheel Depth	2.18

TSR Information	
Conditioned	124.9
Unconditioned	141.2
TSR	0.88
CA Strip Rating	1
FA Strip Rating	1
Additive Prod #	
Additive Product Name	
Additive %	

Lab Preparing Design: pp

Designating Lab Mbr#: TPN7030%

Designating Lab Name: D Con

Tested by:

Reviewed by:

Verified by:

Blend Assessed:

APPENDIX B: FIELD TEST RESULTS

For the lightweight deflectometer (LWD) data, the Boussinesq half-space equation is used to calculate the modulus using a Poisson's ratio = 0.25. The results are converted to the reference temperature at 20°C.

For the dynamic cone penetrometer (DCP) data presented herein, DCP test results were used to estimate calculate CBR values using the South Africa correlation by Kleyn (1975).

IL-61

Asphalt LWD results, with temperature correction:

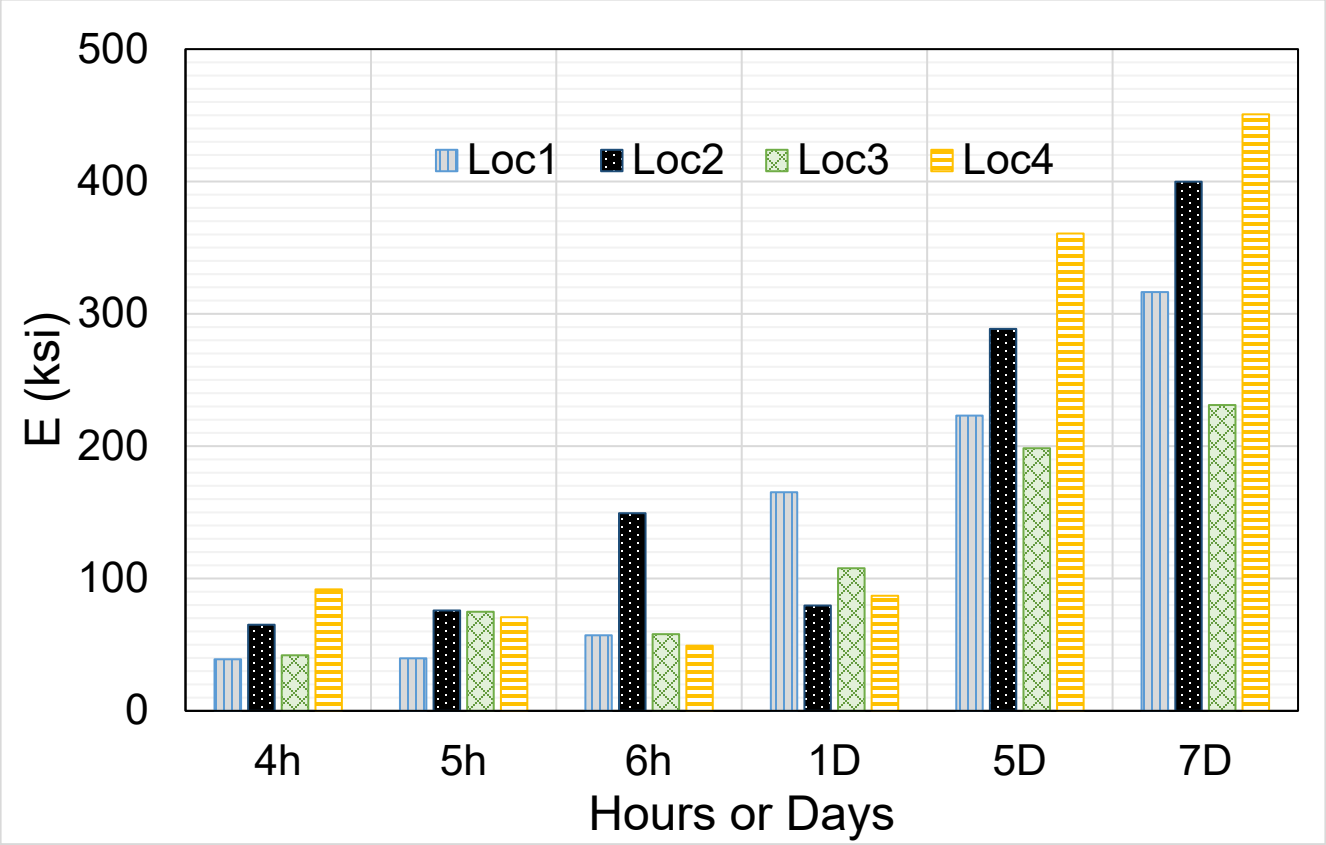

Figure 70. Chart. LWD test results for IL-61 locations 1–4.

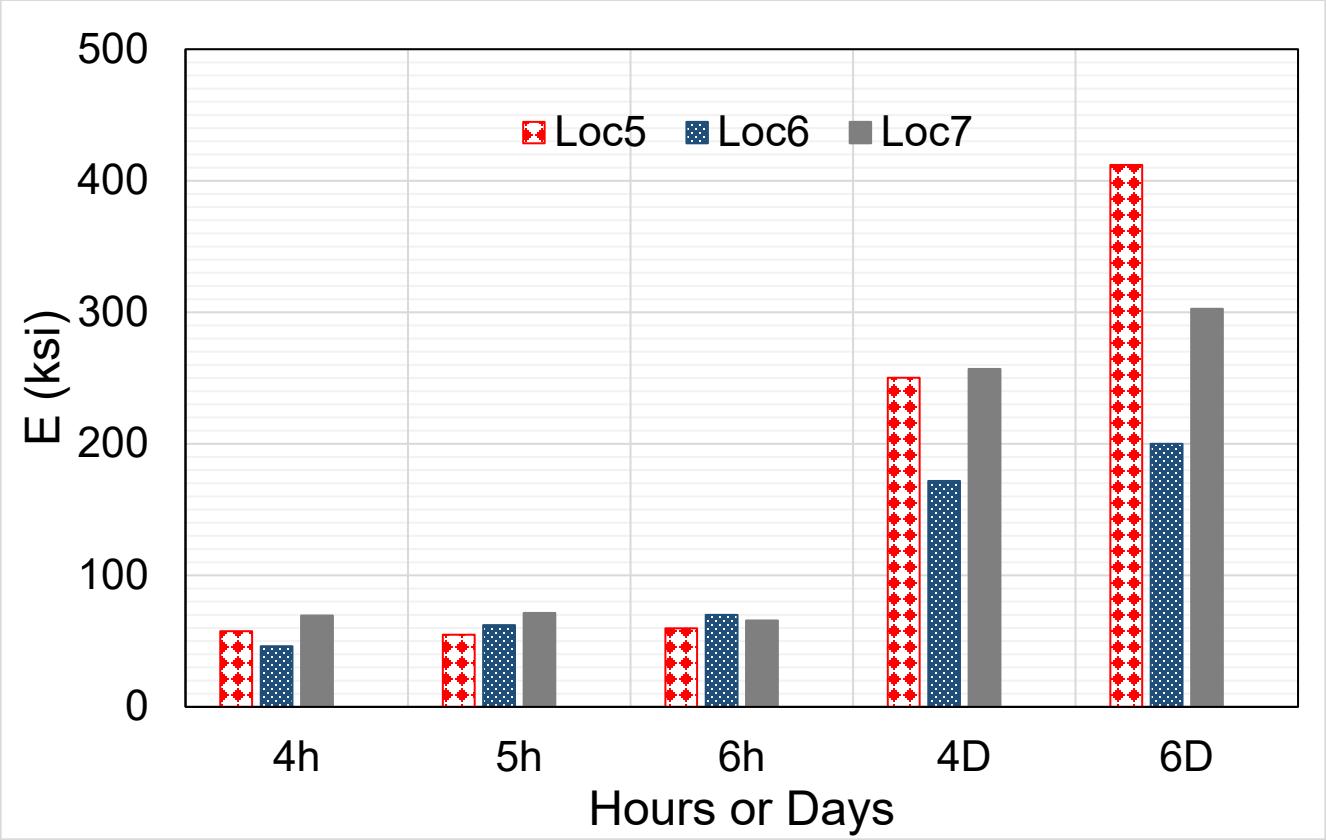

Figure 71. Chart. LWD test results for IL-61 locations 5–7.

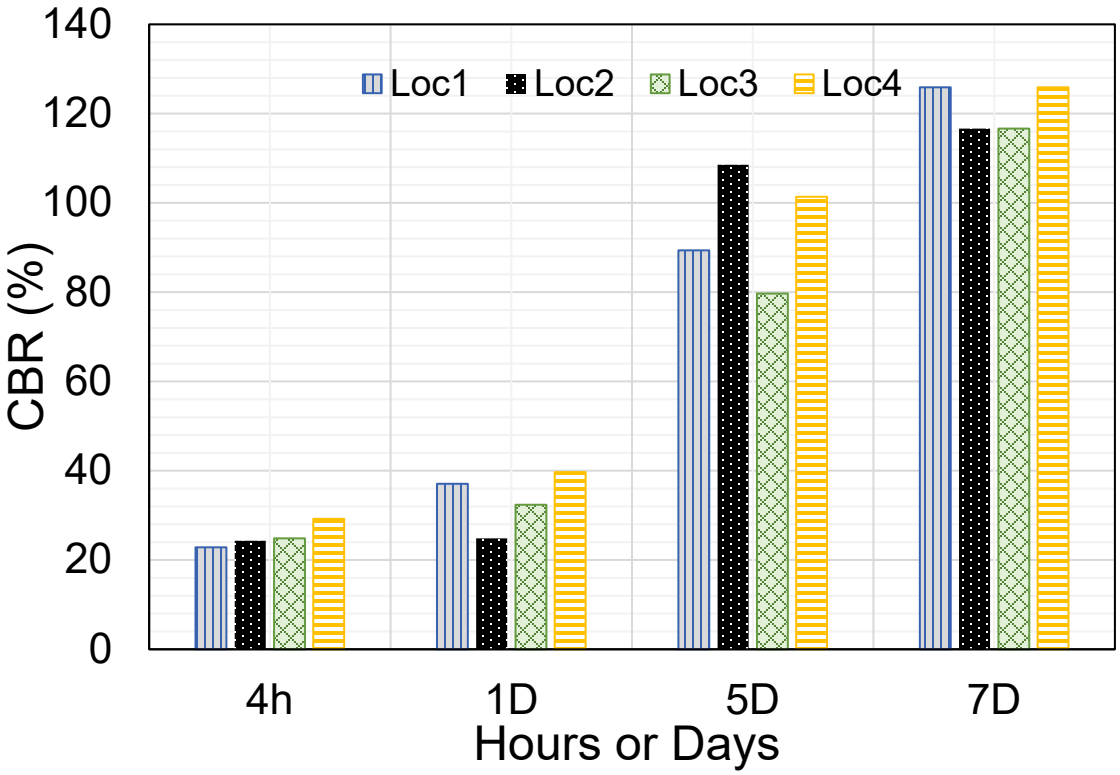

Figure 72. Chart. DCP test results for IL-61 locations 1–4.

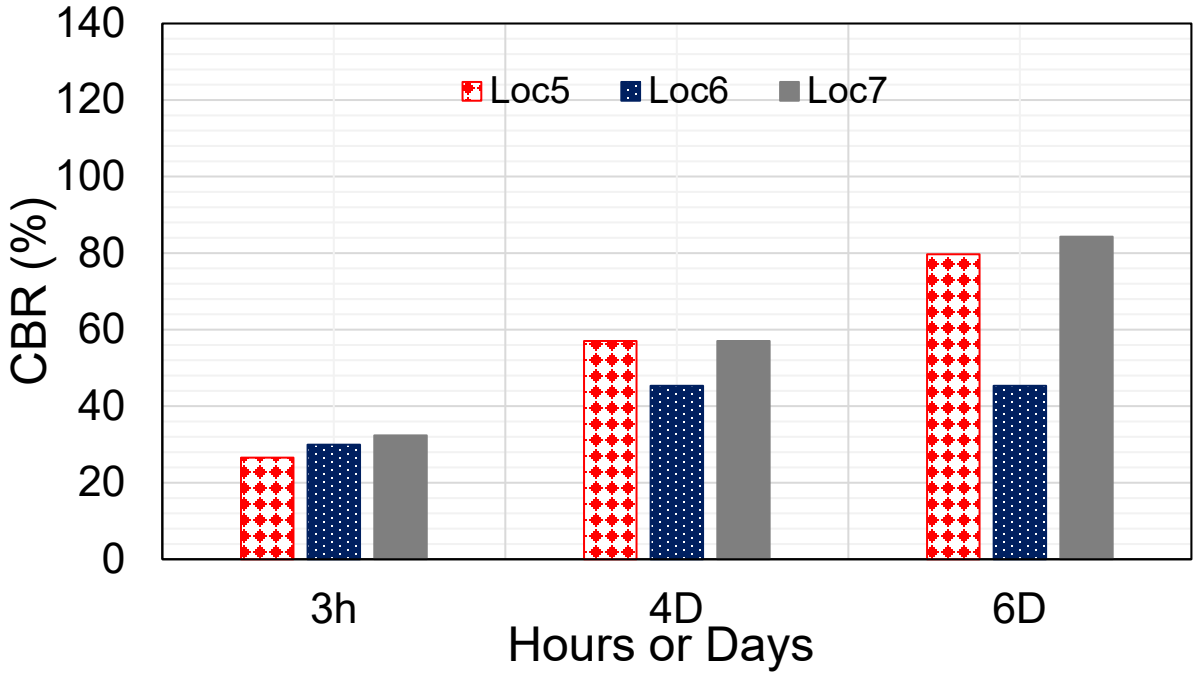

Figure 73. Chart. DCP test results for IL-61 locations 5–7.

Moisture content results:

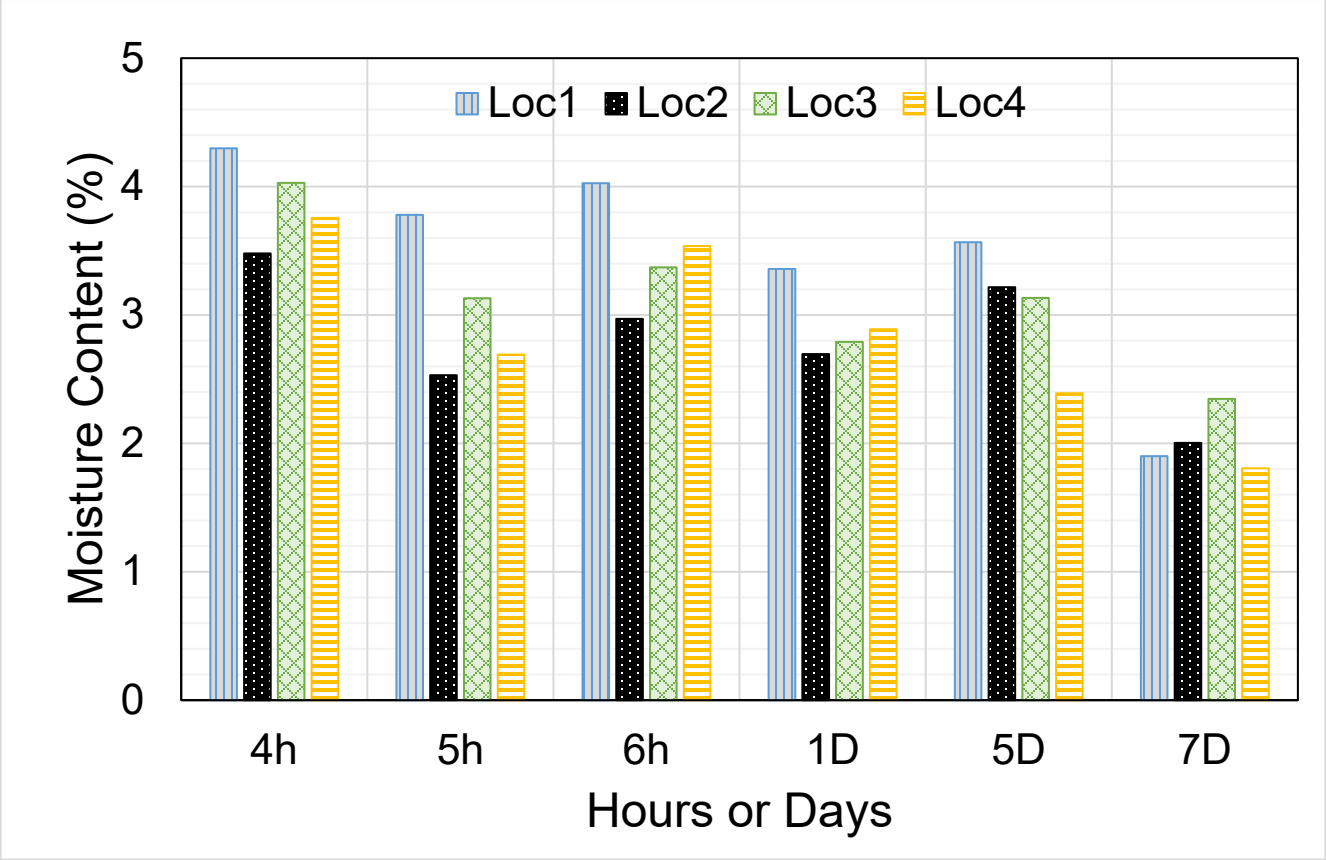

Figure 74. Chart. Moisture content results for IL-61 locations 1–4.

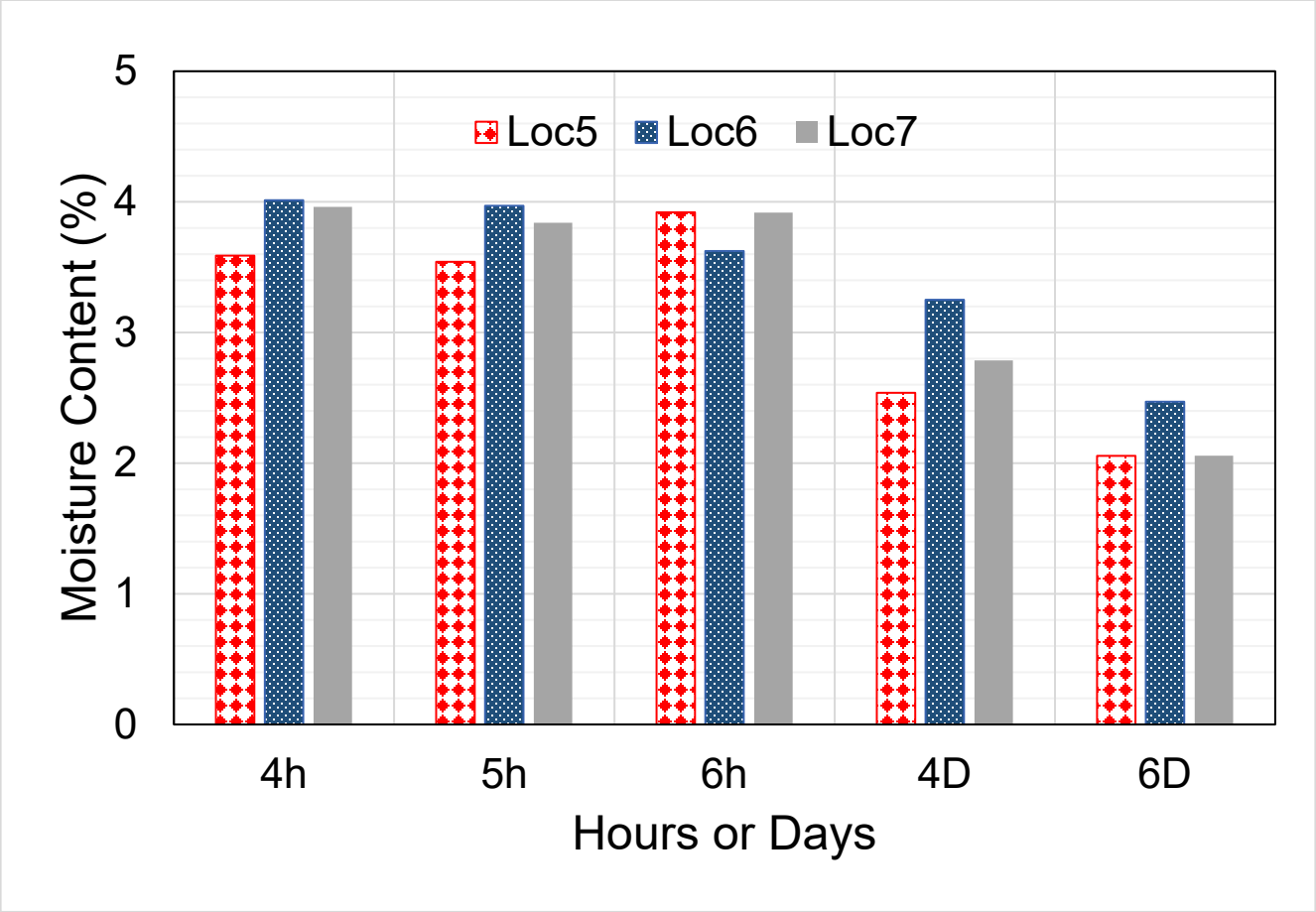

Figure 75. Chart. Moisture content results for IL-61 locations 5–7.

RT-509

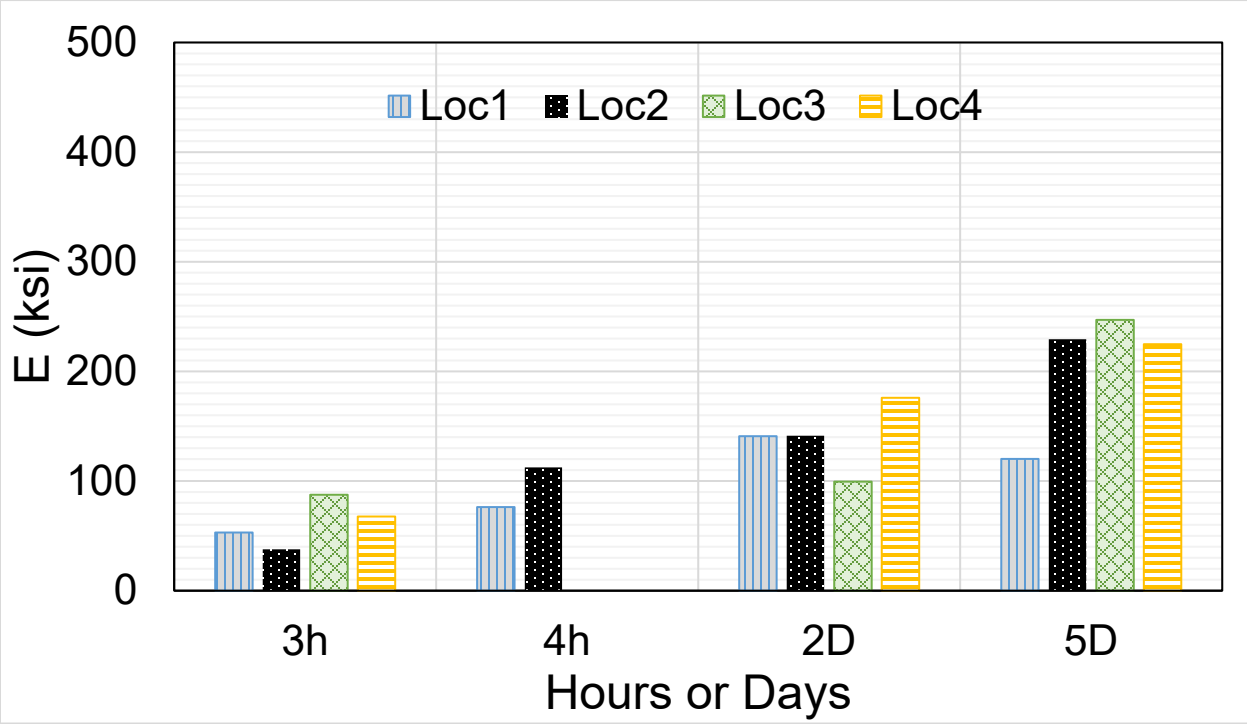

Figure 76. Chart. LWD test results for RT-509 locations 1–4.

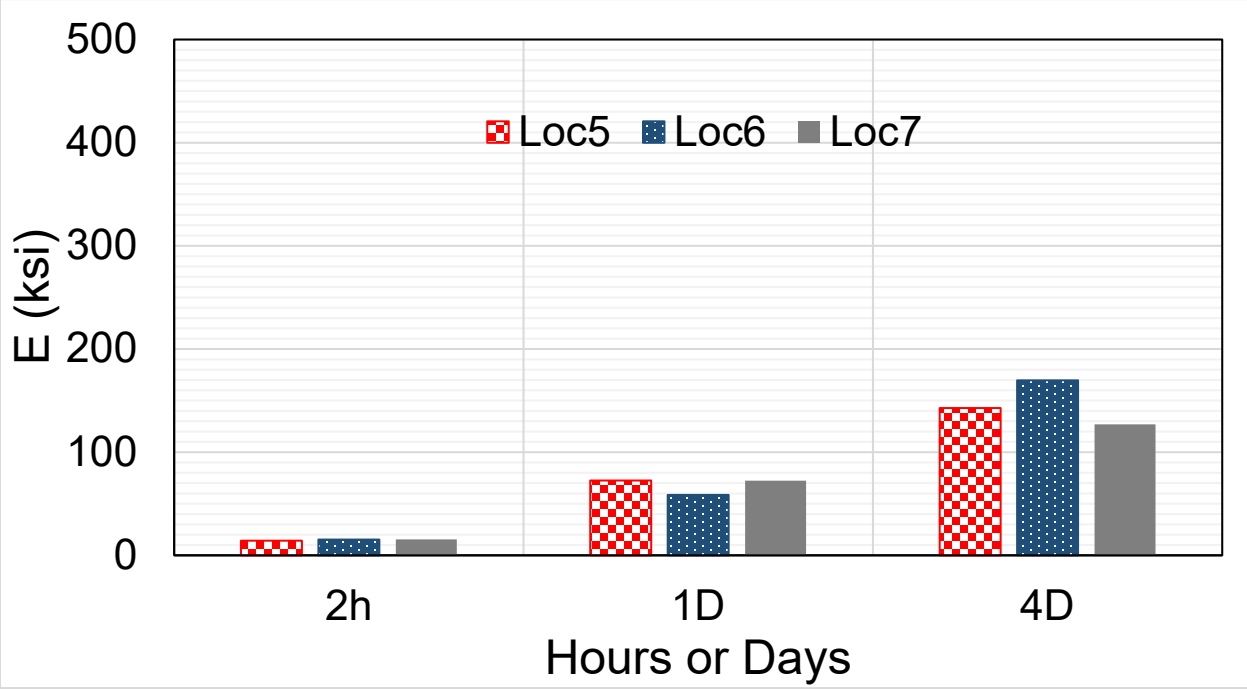

Figure 77. Chart. LWD test results for RT-509 locations 5–7.

California bearing ratio (CBR) from dynamic cone penetrometer (DCP):

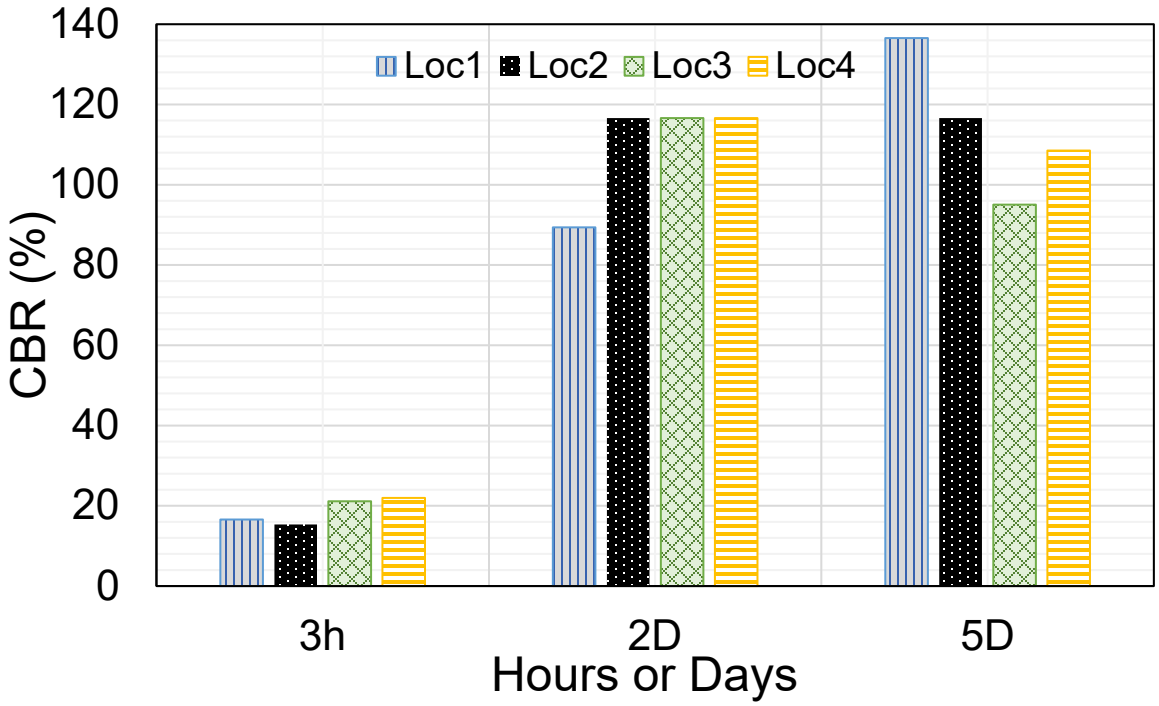

Figure 78. Chart. DCP test results for RT-509 locations 1–4.

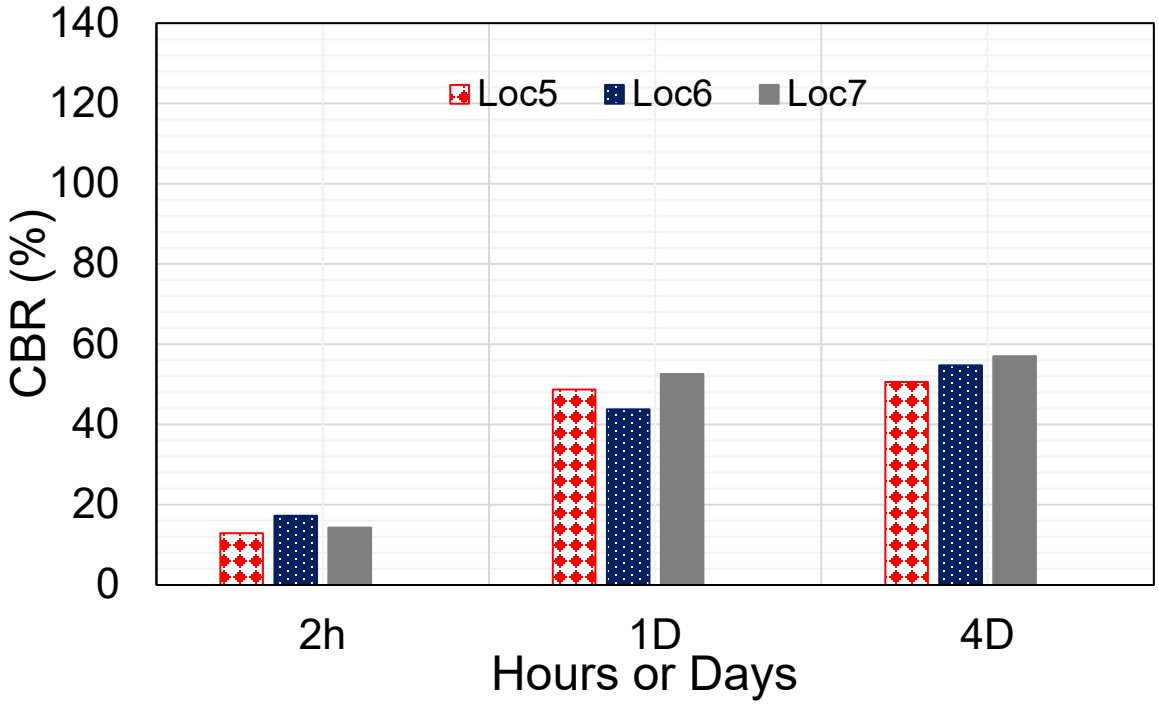

Figure 79. Chart. DCP test results for RT-509 locations 5–7.

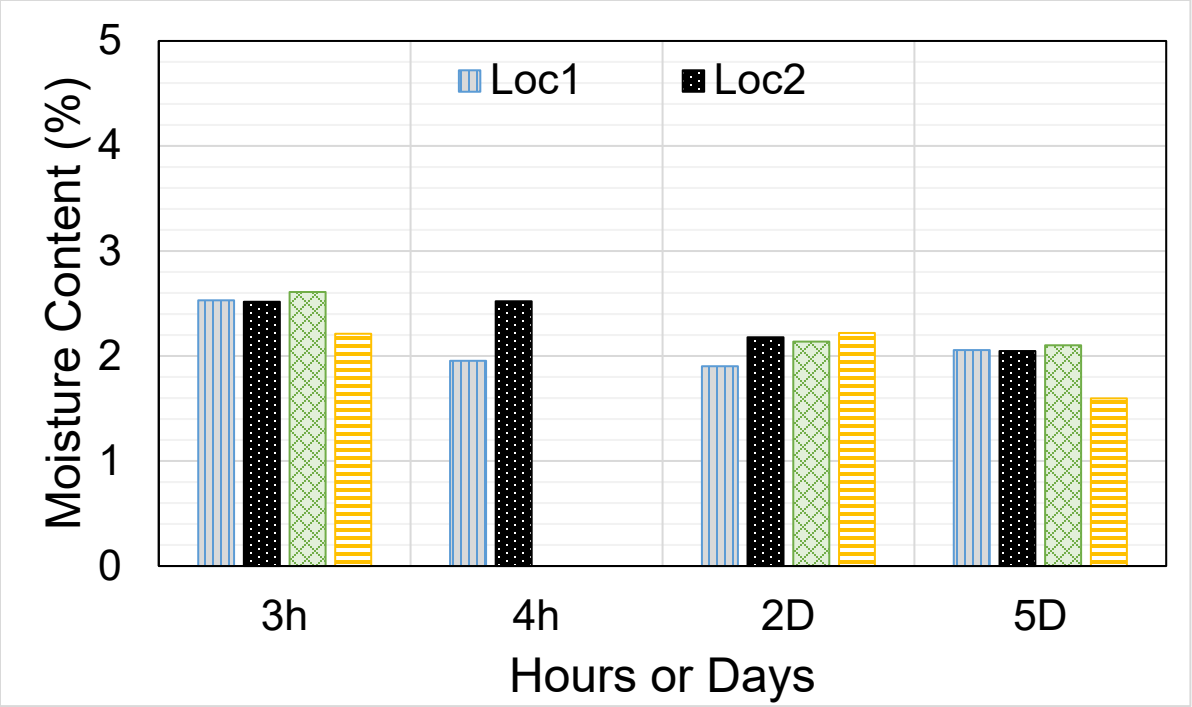

Figure 80. Chart. Moisture content results for RT-509 locations 1–4.

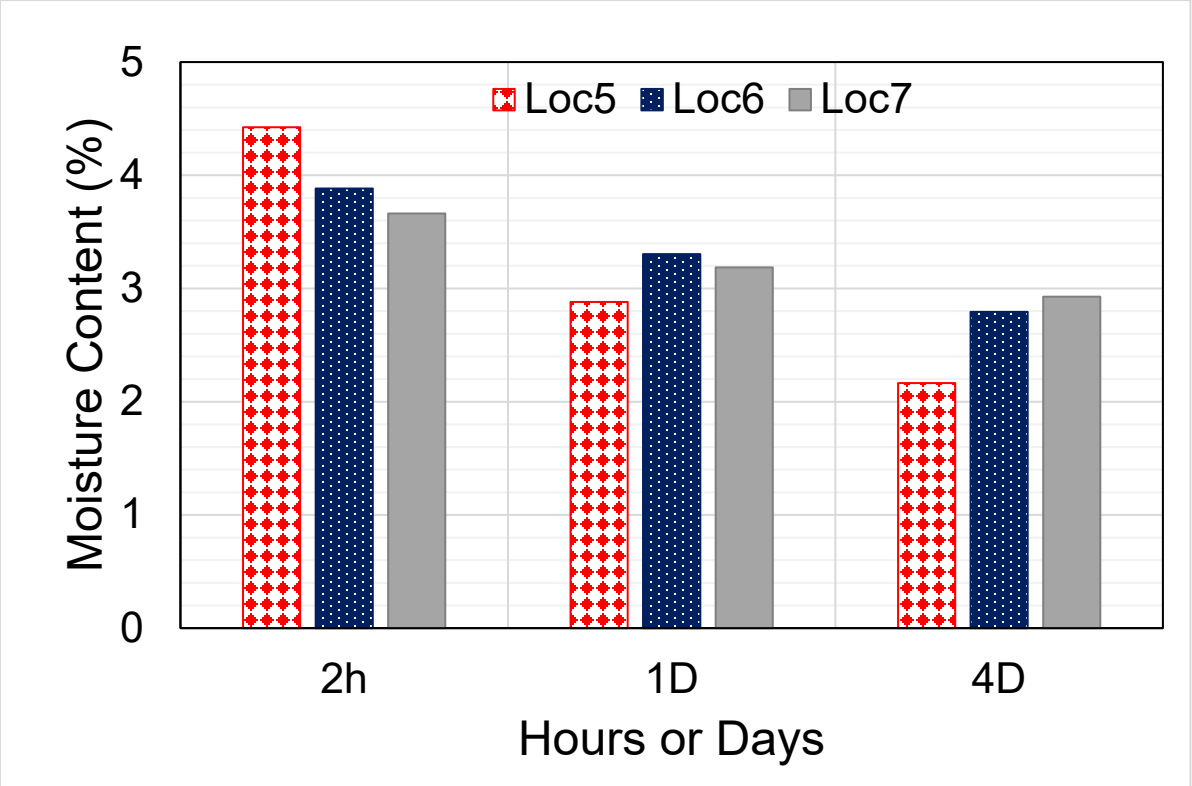

Figure 81. Chart. Moisture content results for RT-509 locations 5–7.

IL-100

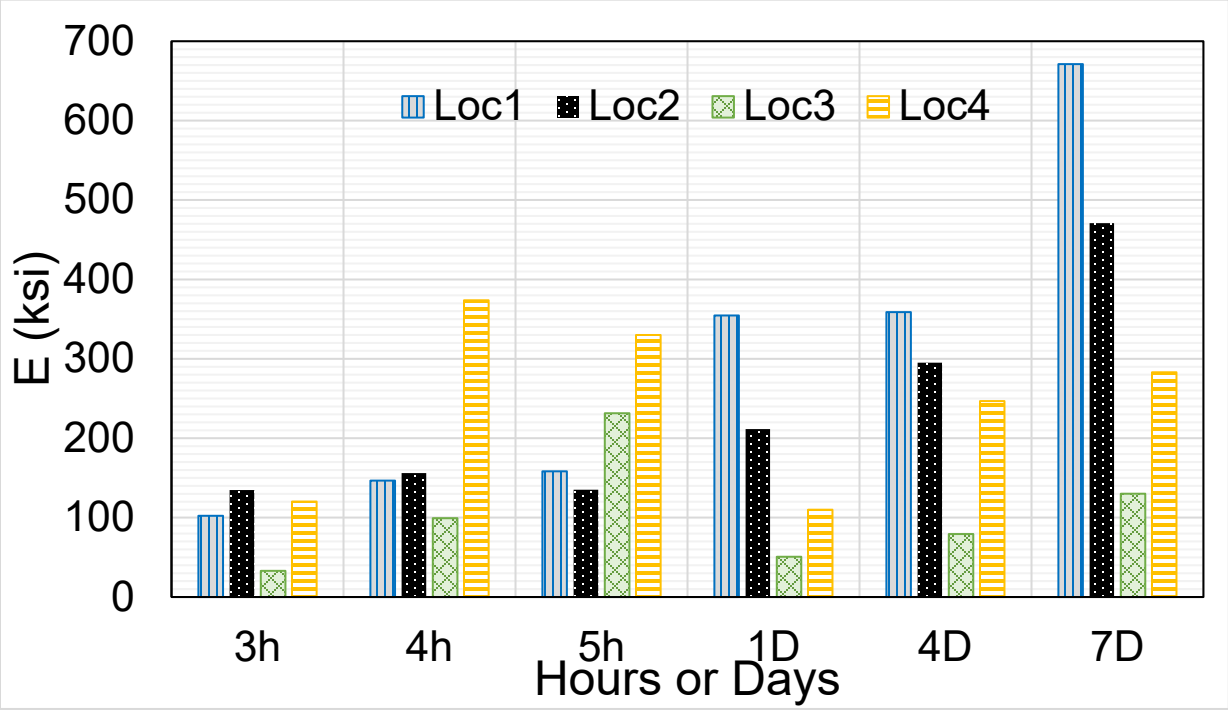

Figure 82. Chart. LWD test results for IL-100 locations 1–4.

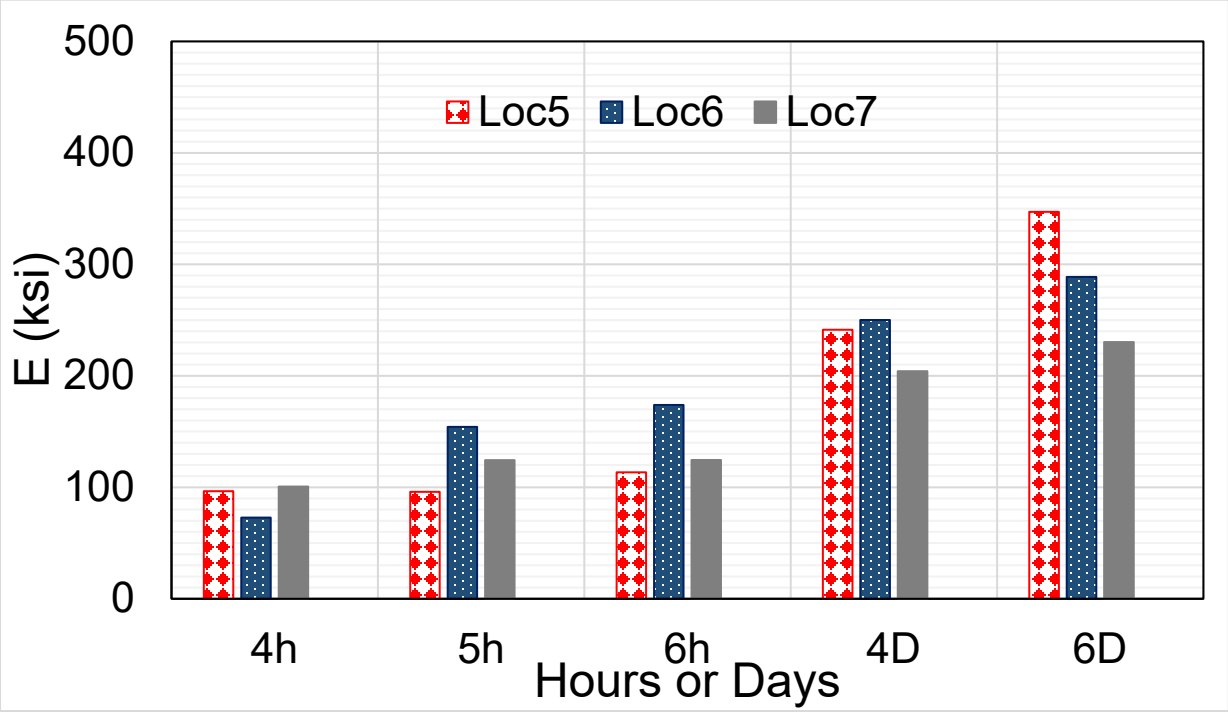

Figure 83. Chart. LWD test results for IL-100 locations 5–7.

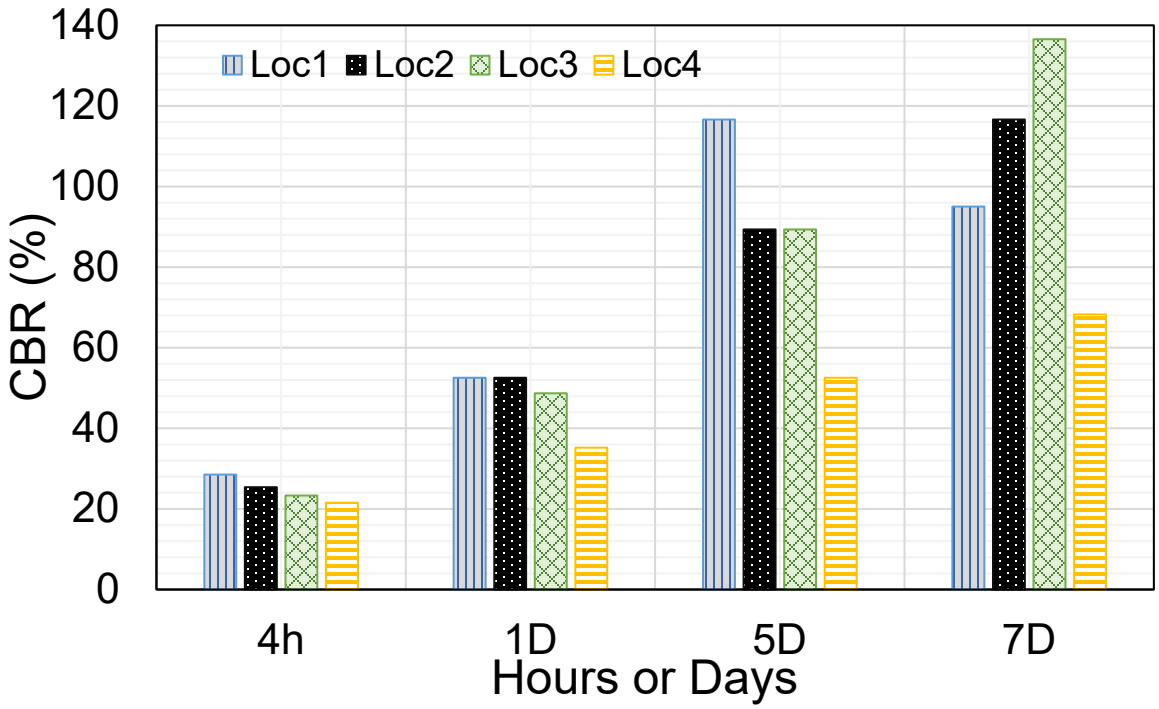

Figure 84. Chart. DCP test results for IL-100 locations 1–4.

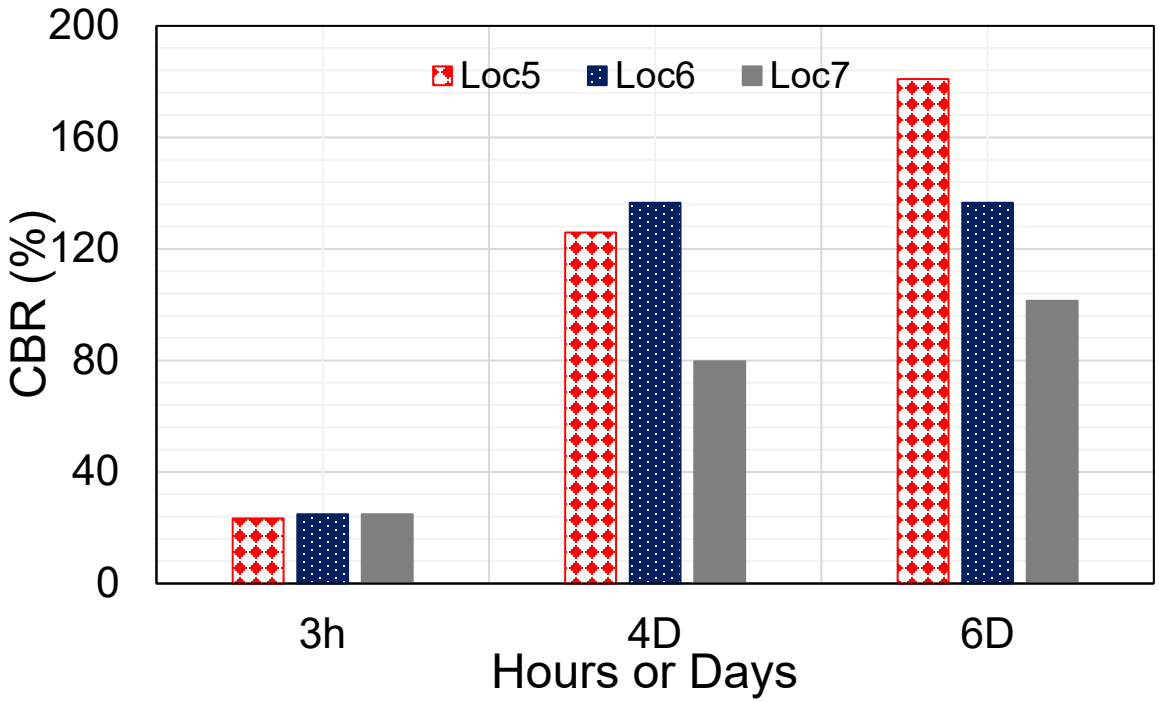

Figure 85. Chart. DCP test results for IL-100 locations 5–7.

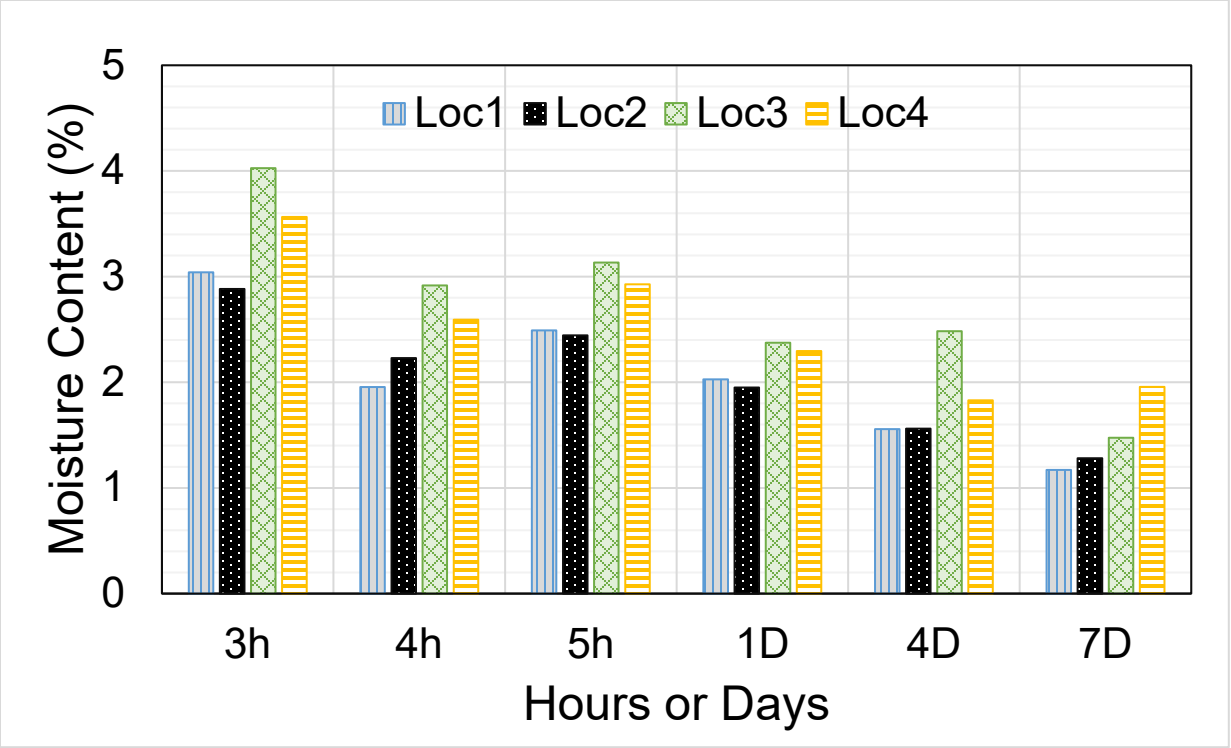

Figure 86. Chart. Moisture content results for IL-100 locations 1–4.

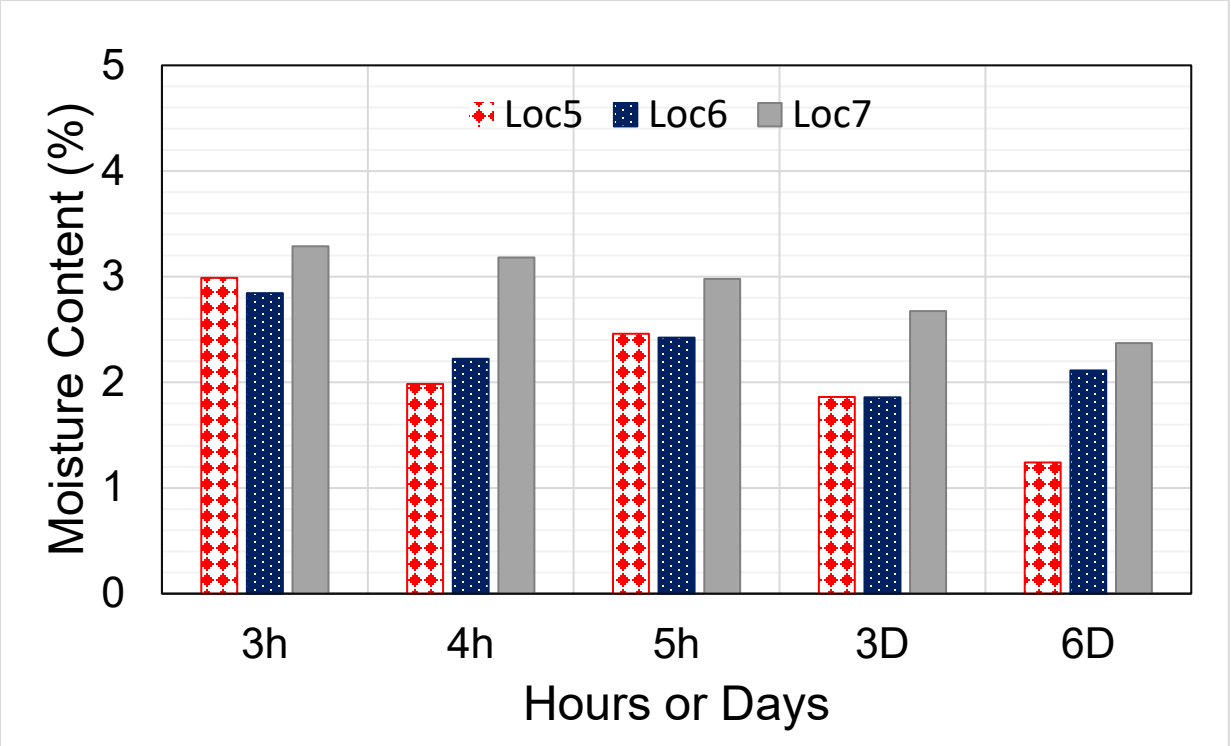

Figure 87. Chart. Moisture content results for IL-100 locations 5–7.

IL-116

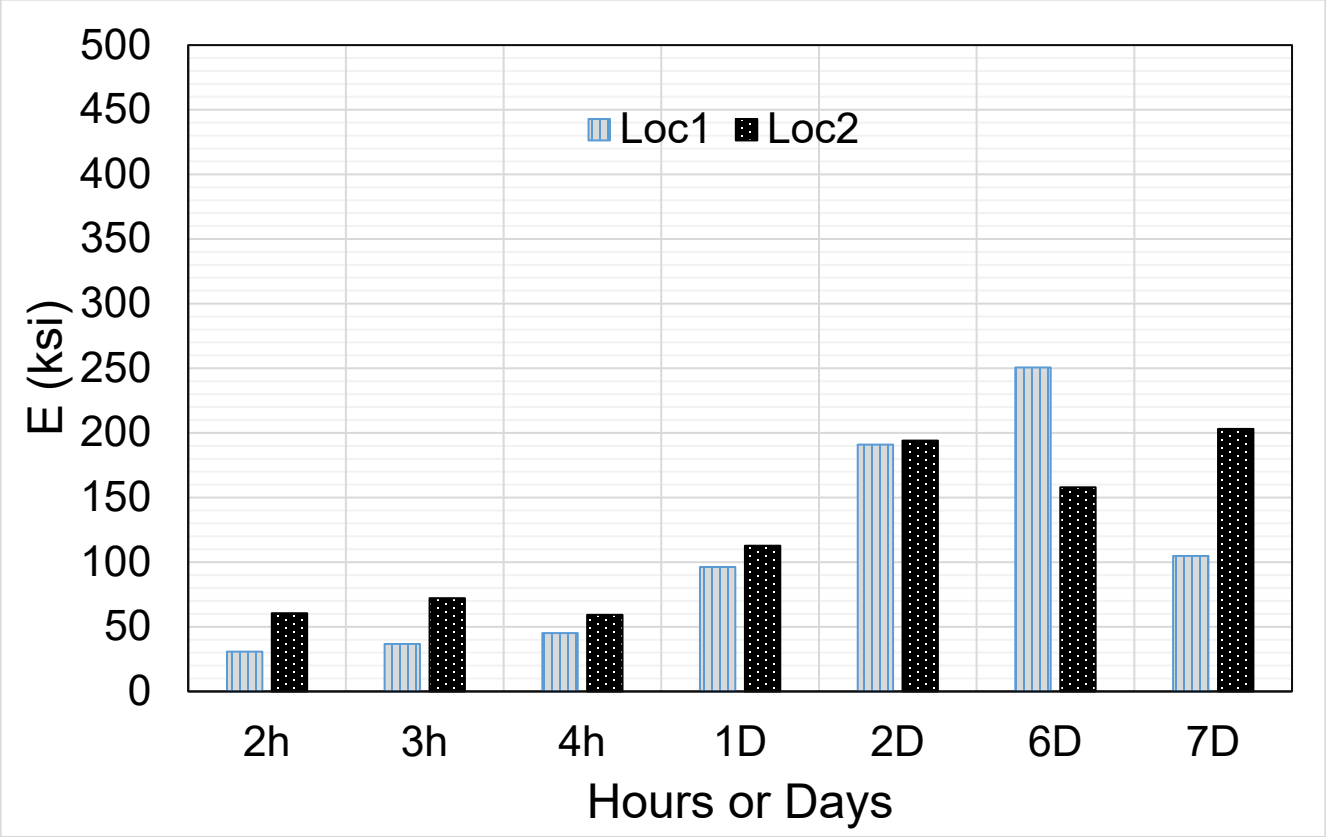

Figure 88. Chart. LWD test results for IL-116 locations 1–2.

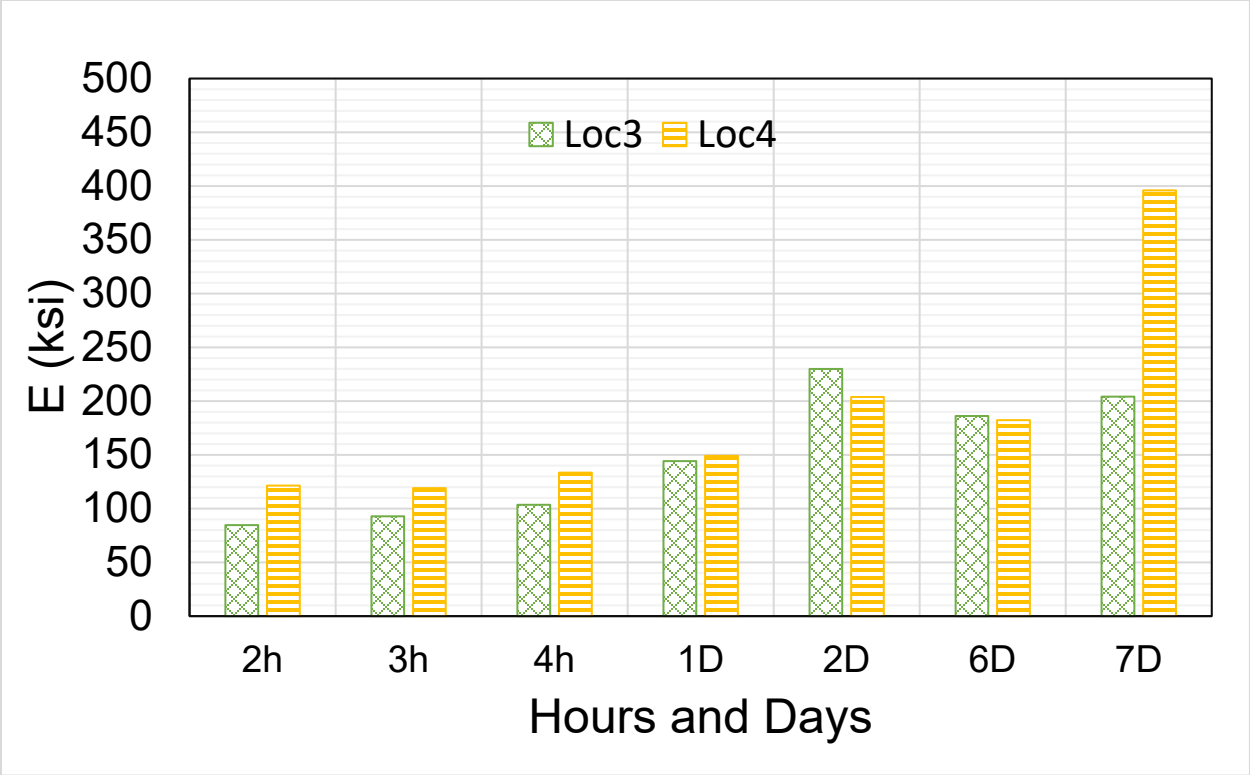

Figure 89. Chart. LWD test results for IL-116 locations 3–4.

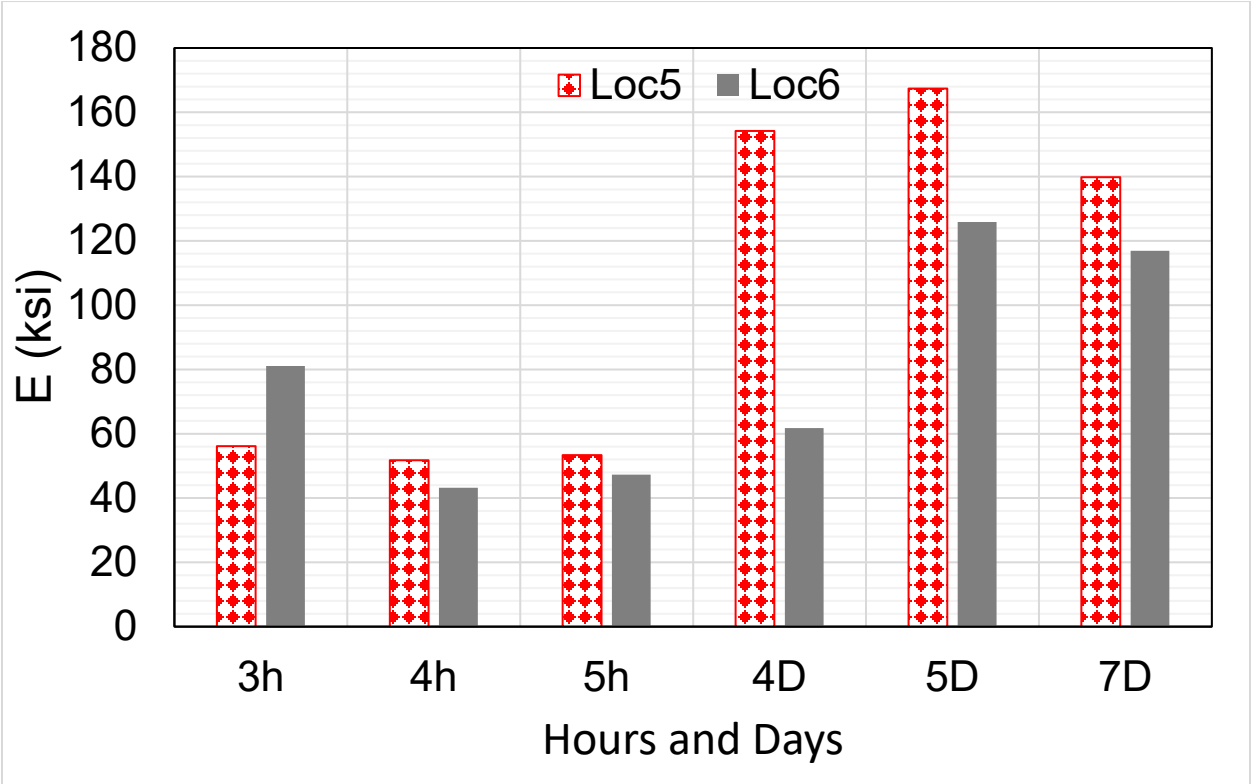

Figure 90. Chart. LWD test results for IL-116 locations 5–6.

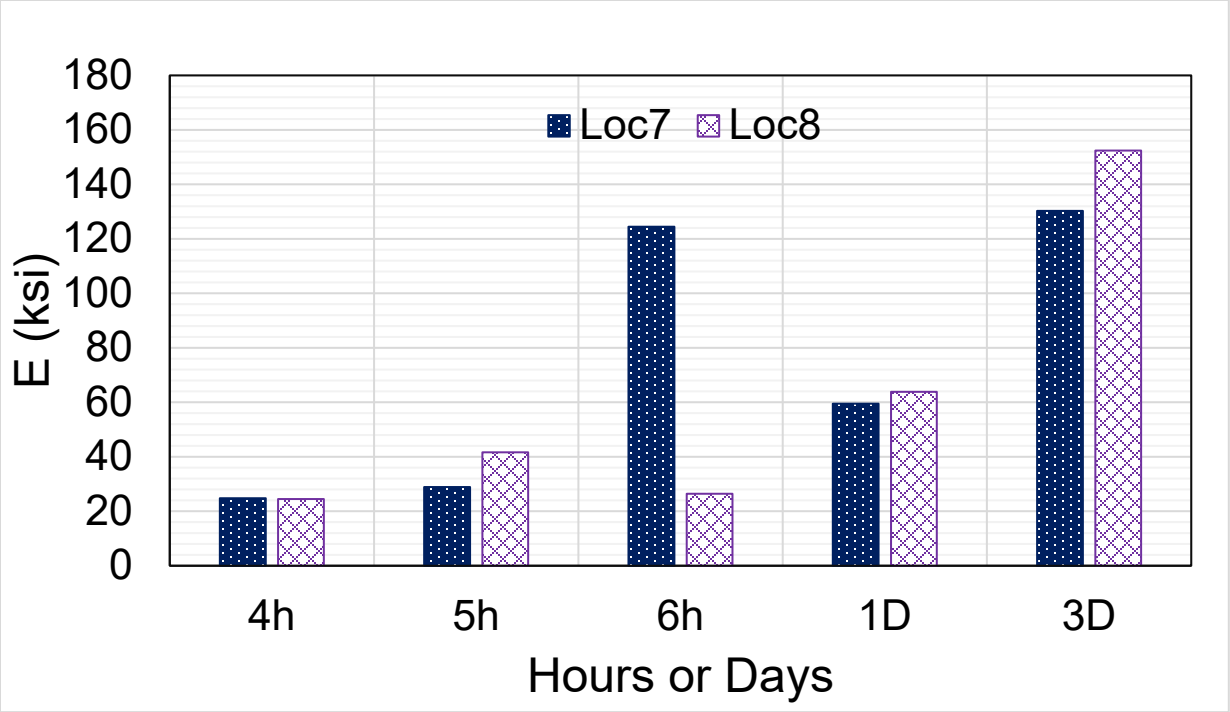

Figure 91. Chart. LWD test results for IL-116 locations 7–8.

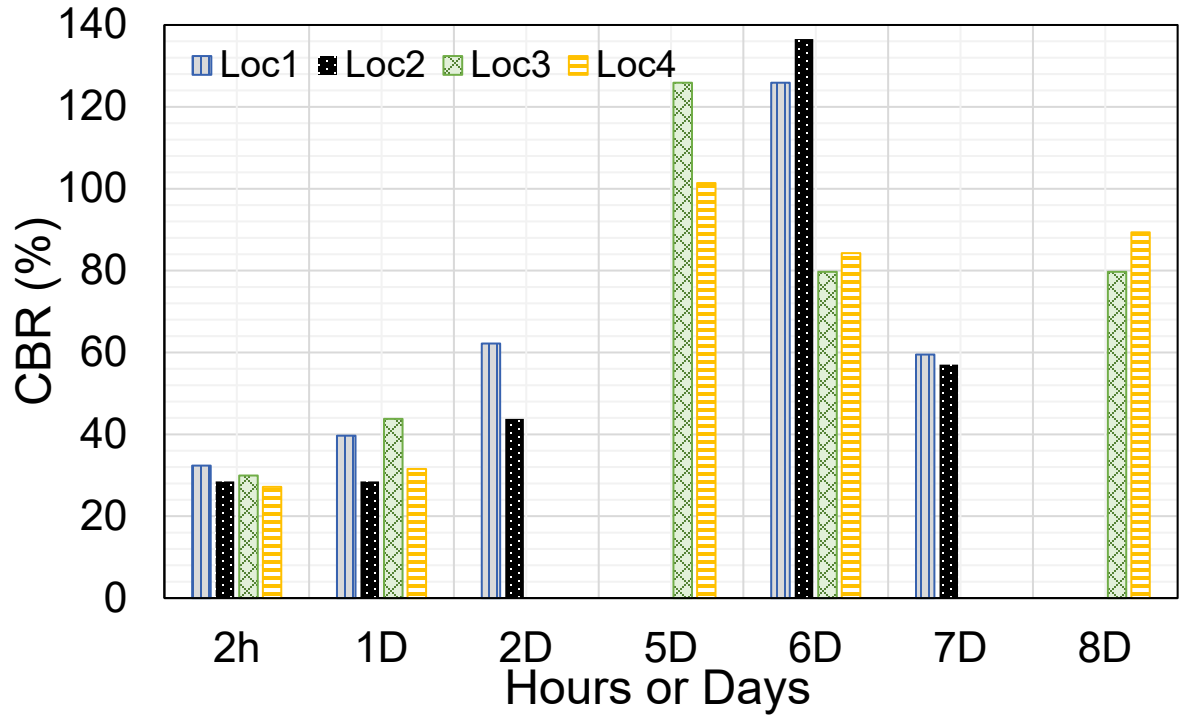

Figure 92. Chart. DCP test results for IL-116 locations 1–4.

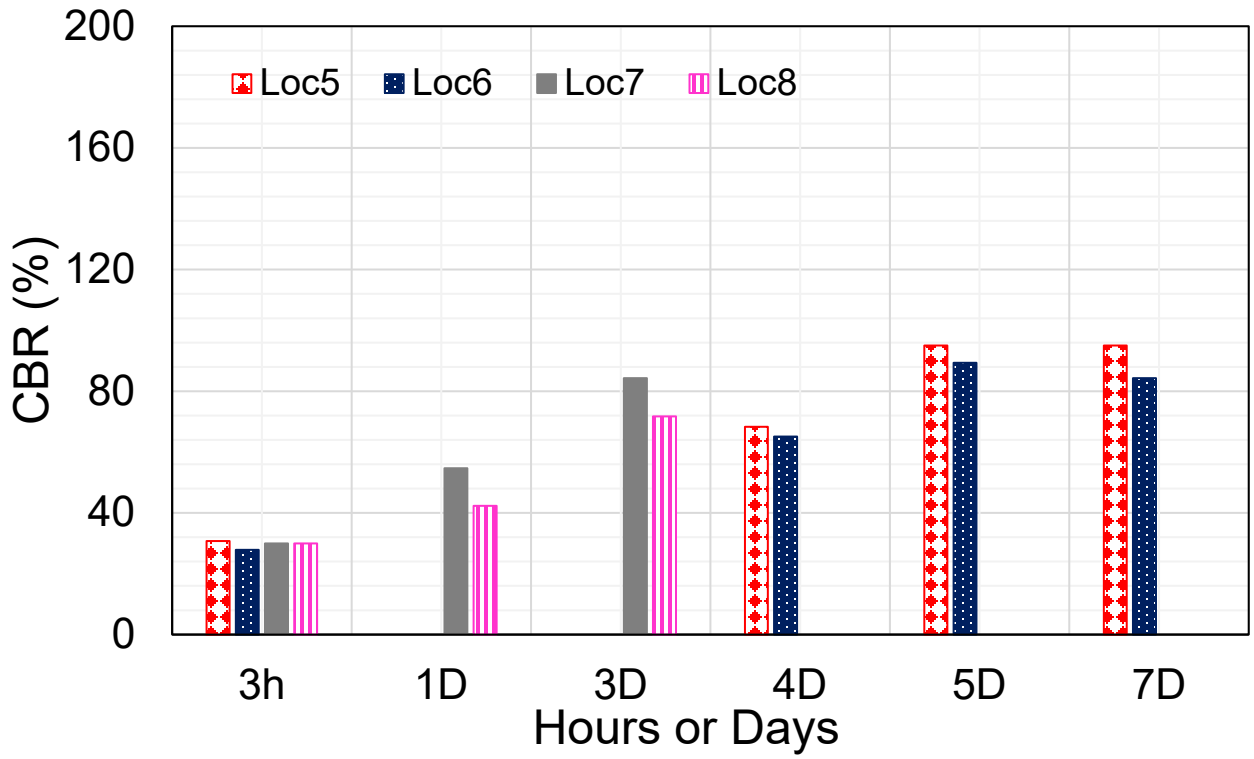

Figure 93. Chart. DCP test results for IL-116 locations 5–8.

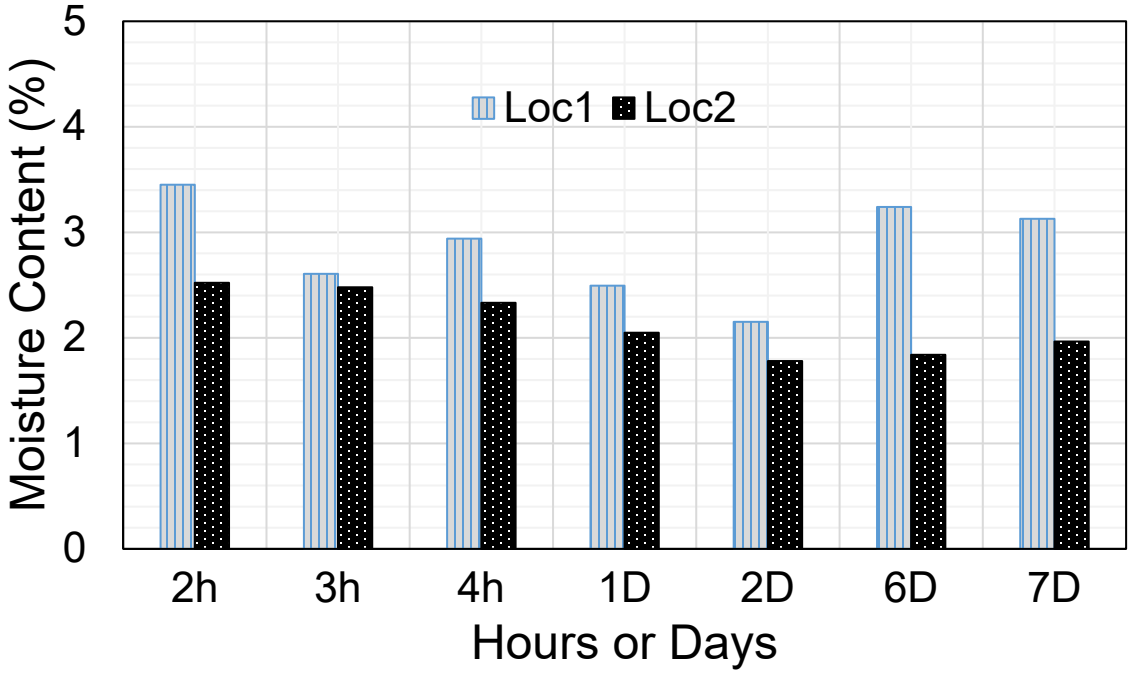

Figure 94. Chart. Moisture content results for IL-116 locations 1–2.

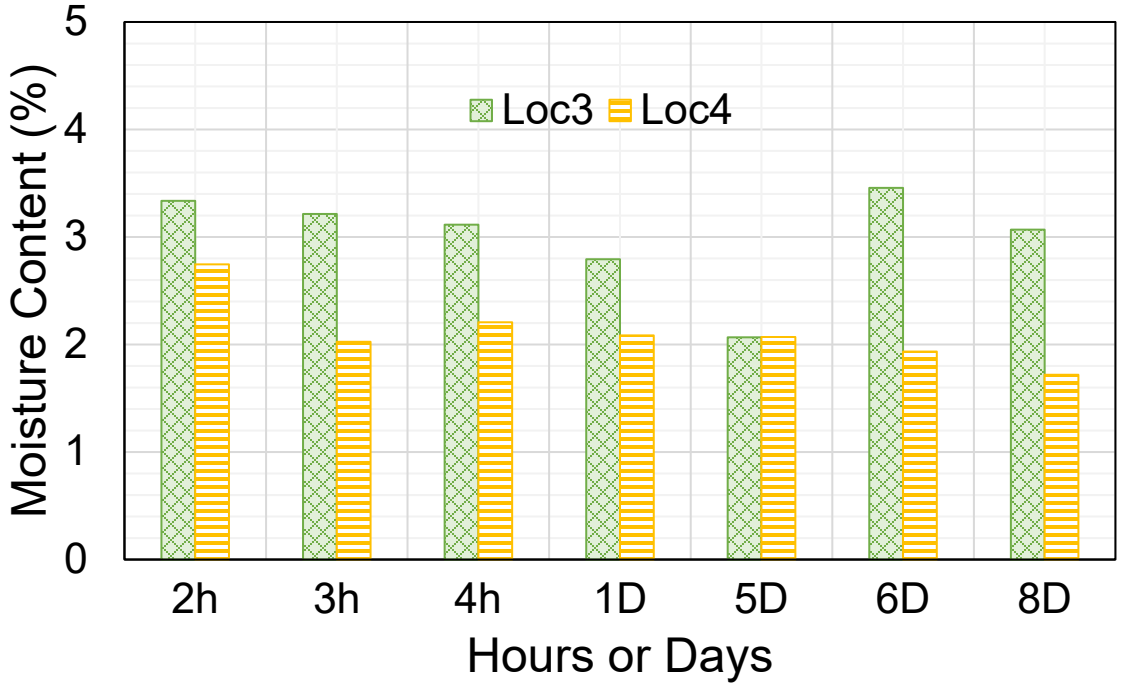

Figure 95. Chart. Moisture content results for IL-116 locations 3–4.

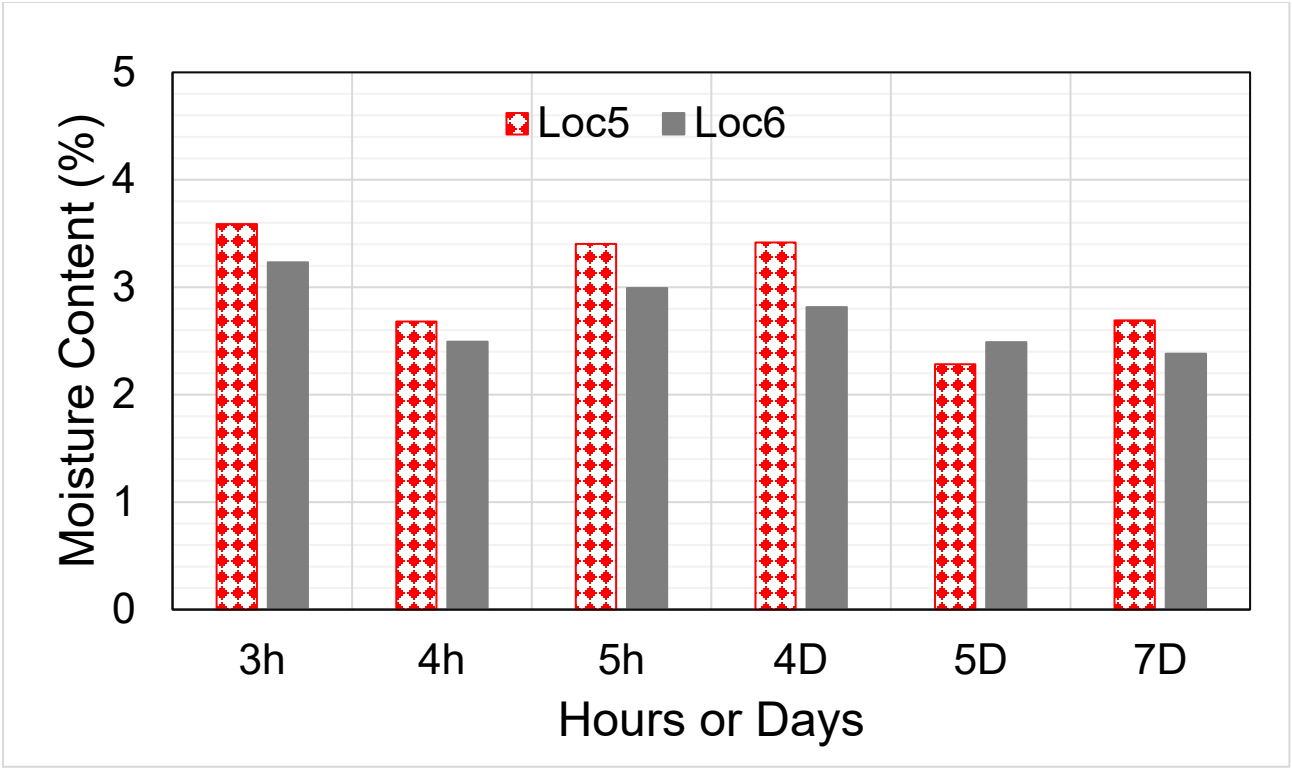

Figure 96. Chart. Moisture content results for IL-116 locations 5–6.

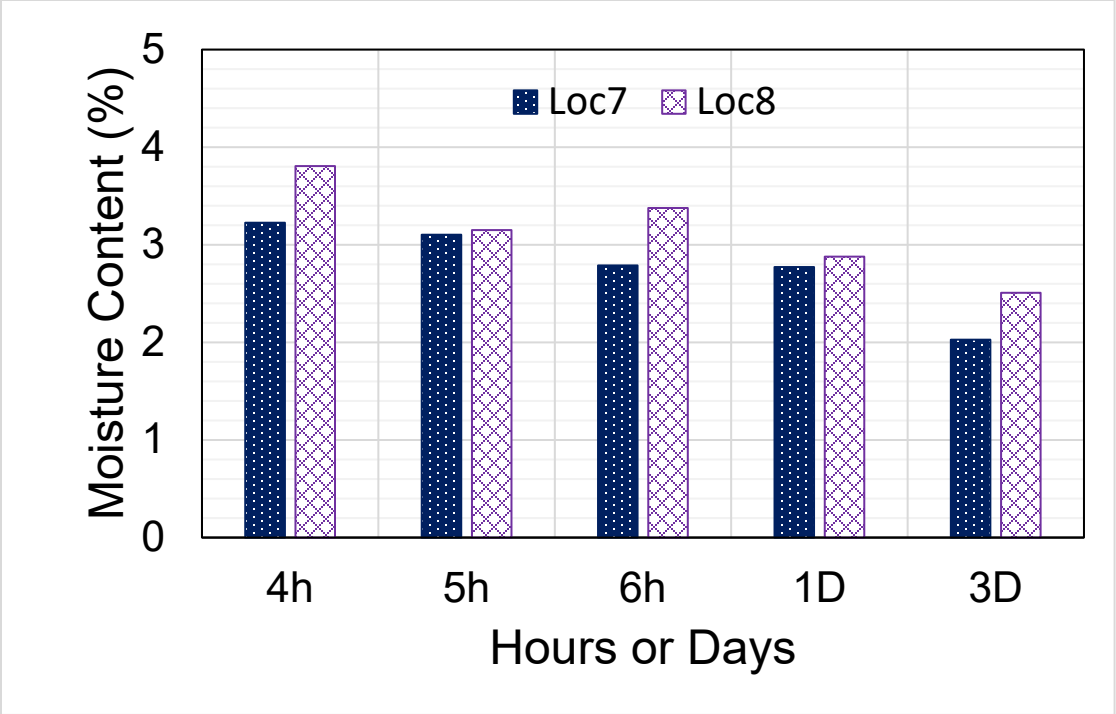

Figure 97. Chart. Moisture content results for IL-116 locations 7–8.

IL-64

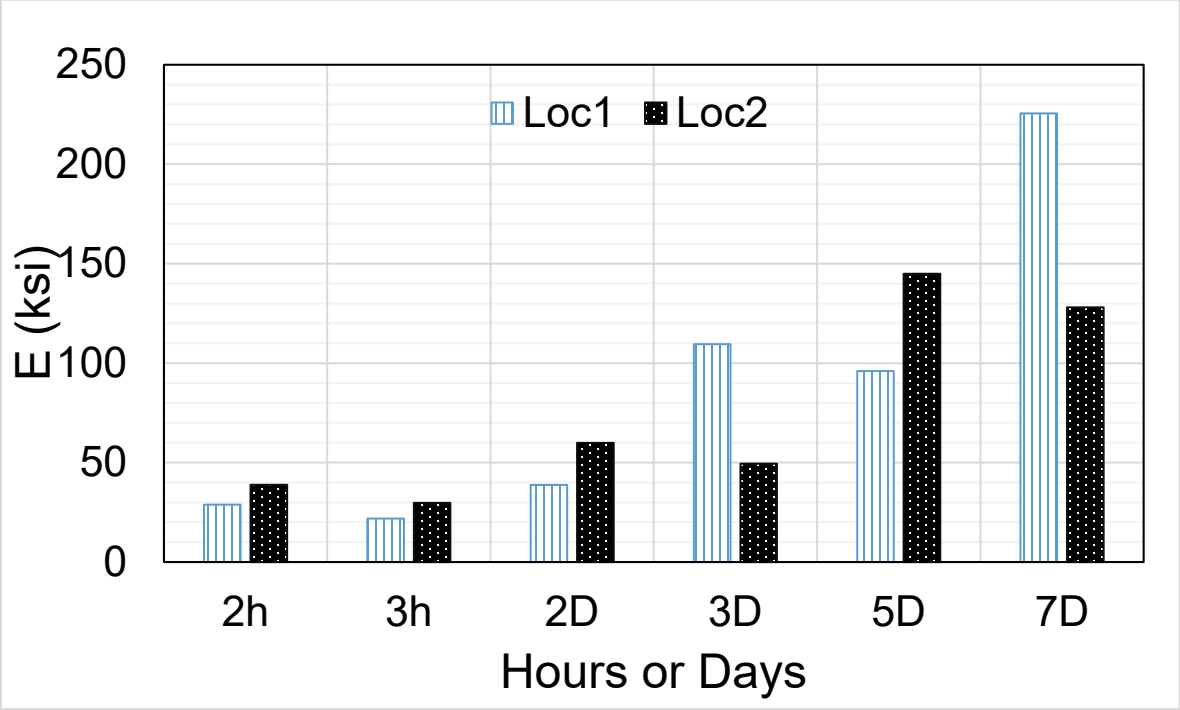

Figure 98. Chart. LWD test results for IL-64 locations 1–2.

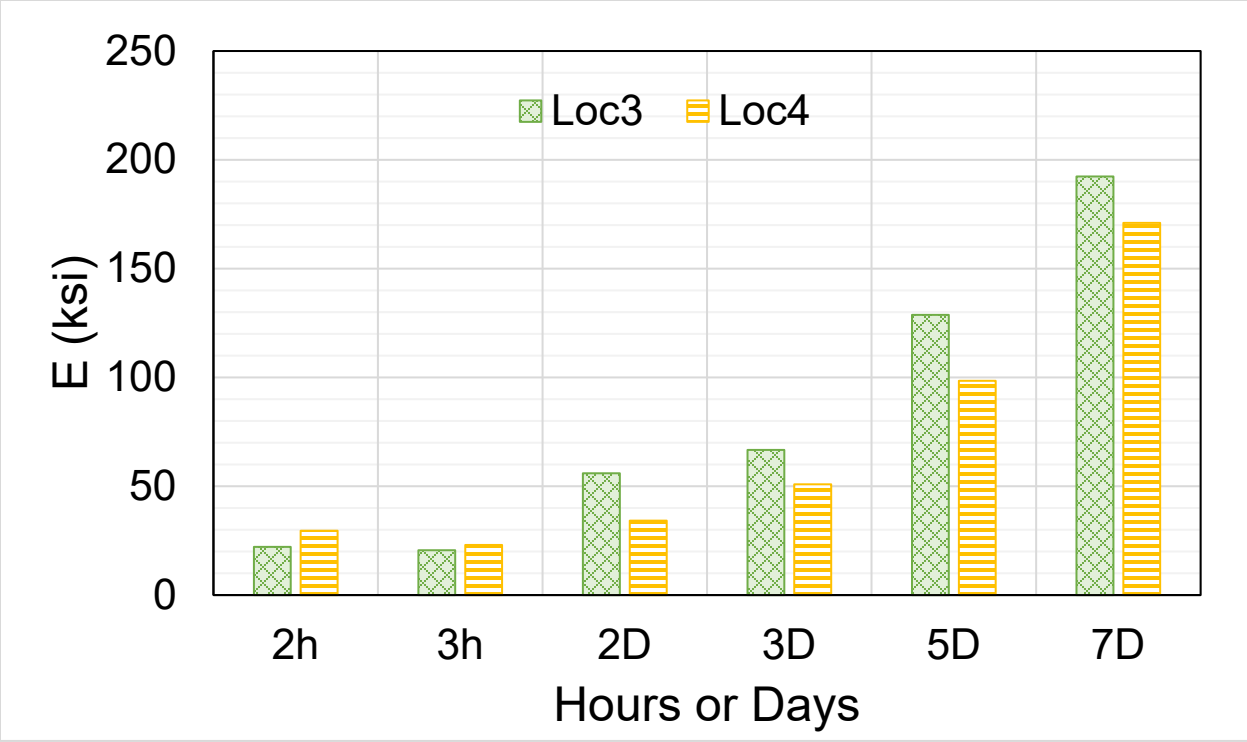

Figure 99. Chart. LWD test results for IL-64 locations 3–4.

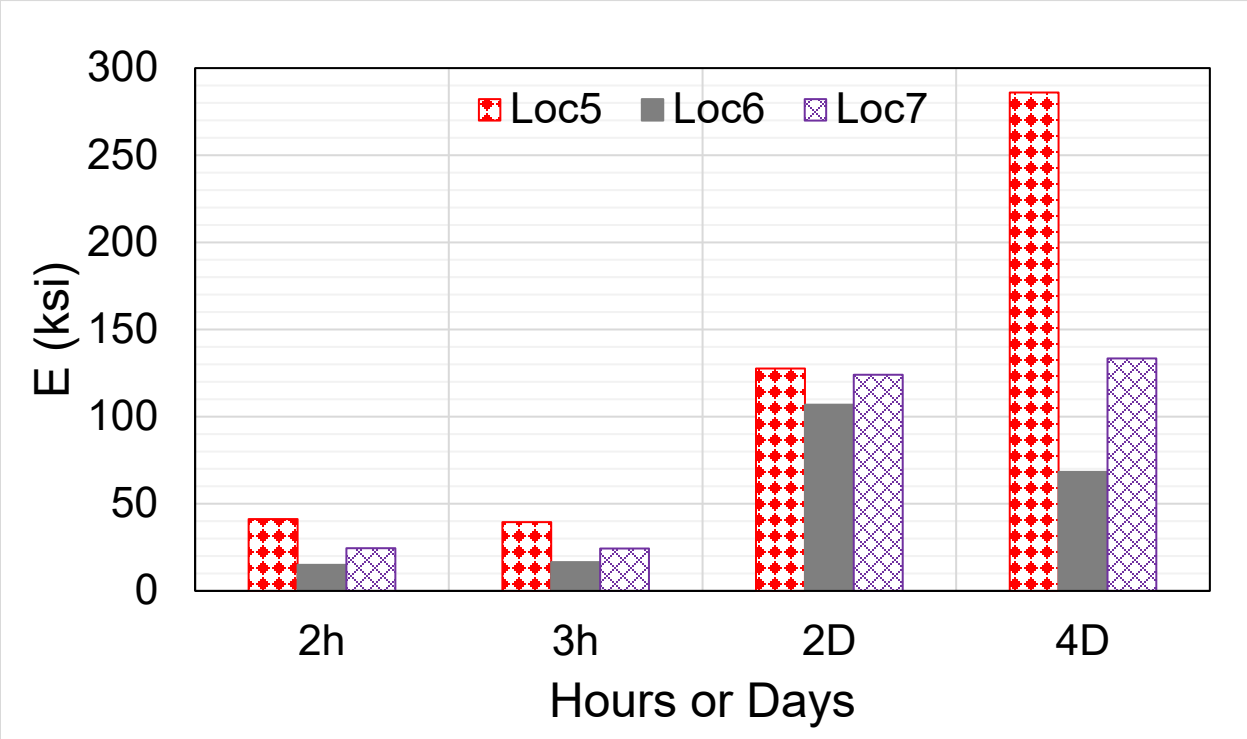

Figure 100. Chart. LWD test results for IL-64 locations 5–7.

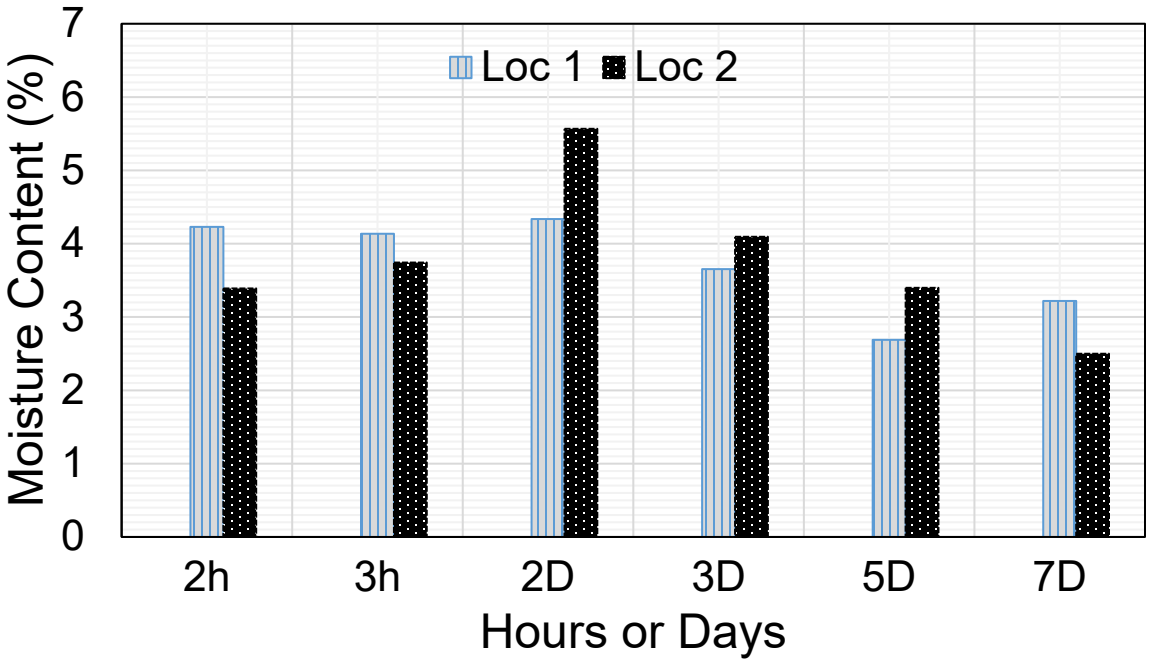

Figure 101. Chart. Moisture content results for IL-64 locations 1–2.

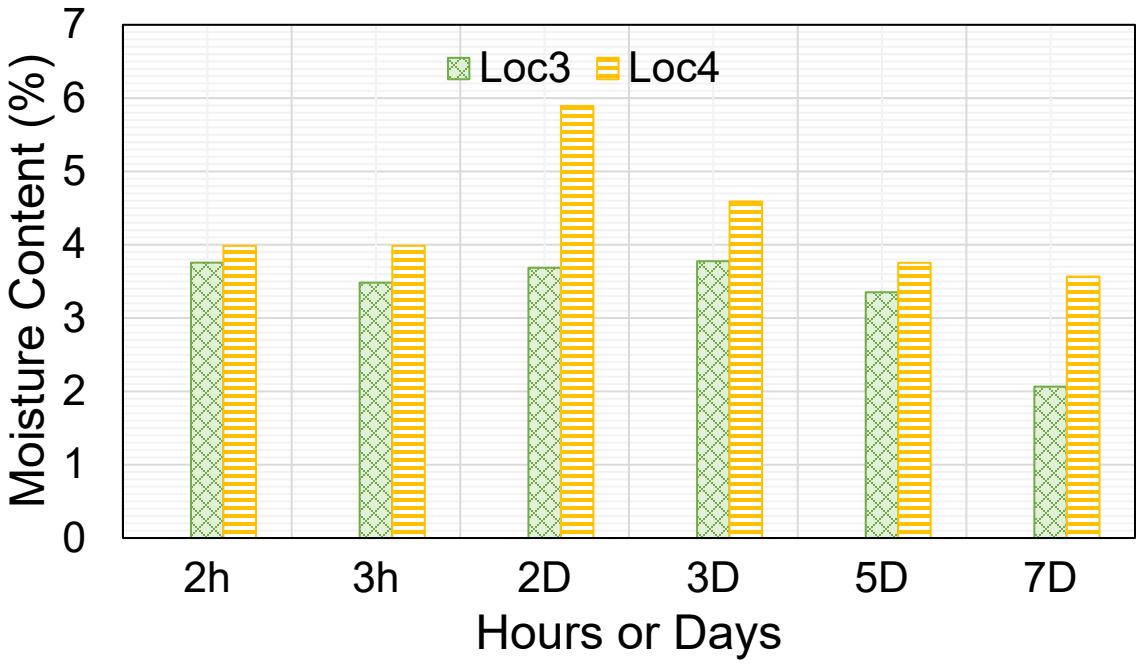

Figure 102. Chart. Moisture content results for IL-64 locations 3–4.

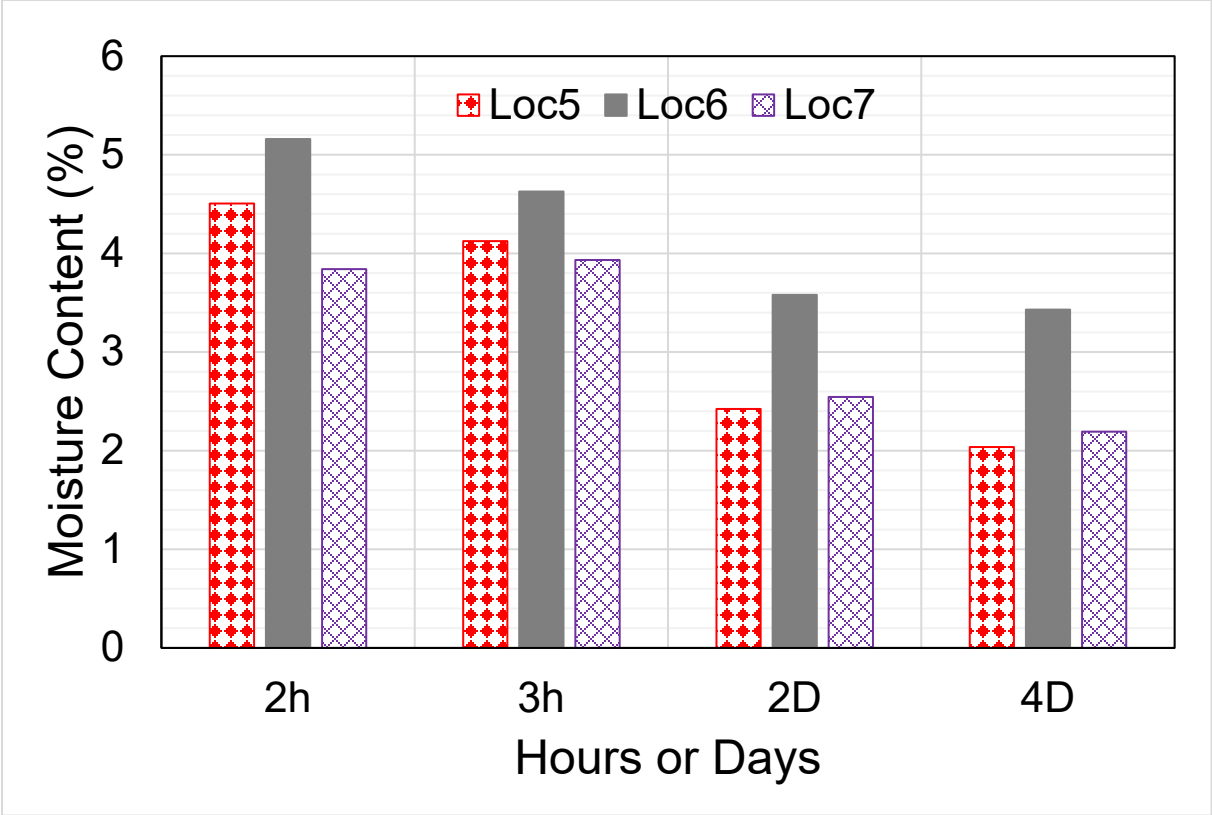

Figure 103. Chart. Moisture content results for IL-64 locations 5–7.

IL-91

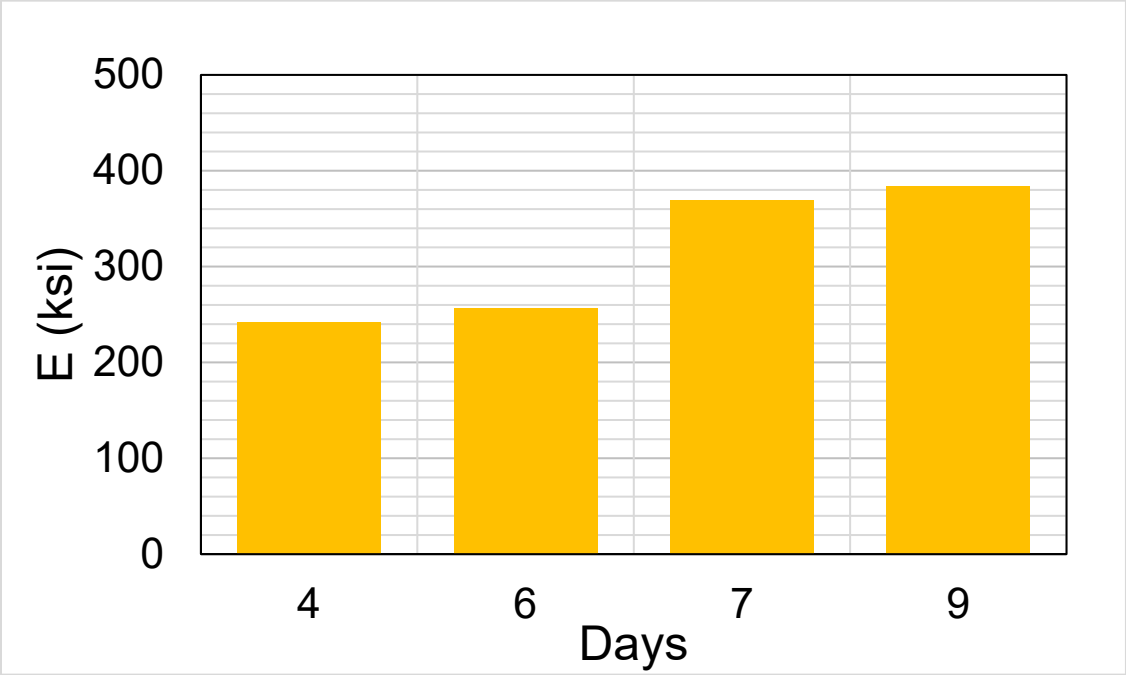

Figure 104. Chart. Moisture content results for IL-91 for one location.

APPENDIX C: TOOL USER GUIDE

INSTALLATION

Open the tool folder, open the “for redistribution” folder, and click the file with the “.exe” format.

Click “next” and the tool will be installed. Please allow the installation of MATLAB Compiler Runtime or MCR during the installation. That component helps install and execute the tool on a PC without MATLAB installation.

After installation, the icon of the GPR-Density tool is on the desktop and “start” app library of Windows 10.

USE PROCESS

Figure 105 presents the interface after opening the tool, which also represents mode 1.

Figure 105. Photo. GPR-Density tool initial interface, mode 1.

Figure 105 shows Module 1: Existing Pavement Evaluation. Users can change the module by clicking the corresponding radio button. This module is used for density prediction of dry existing pavements. The module applies the reflection amplitude method to calculate the dielectric constant, the wavelet transform decomposition approach to smooth the dielectric constant profile, and the ALL model to predict density.

Two files are required: a calibration file (on top of a perfect reflector like copper) and a pavement GPR scan. Additionally, some volumetric mix design values are needed: 1) binder content in decimal (P_b); 2) maximum theoretical specific gravity (G_{mm}); and 3) type of dominant aggregate. Typical aggregate types in Illinois are listed in the drop-down menu: limestone, dolomite, granite, and trap rock.

The dielectric constant and density profile will then be generated. Figure 106 shows an example of dielectric constant profile results, both raw and smooth curves are shown.

Figure 107 shows module 2, which is used to monitor HMA density during compaction. This module includes the reflection amplitude method for dielectric constant calculation, wavelet transform decomposition approach for dielectric constant profile smoothing, mean reflection amplitude method for surface moisture removal, and ALL model for density prediction. Notably, the mean reflection amplitude method transforms the signal into frequency domain, which results in higher computation time than other modules. Figure 107 illustrates an example of density profile results; the plot is acquainted by 92% and 97% density horizontal thresholds for practicality.

In addition to the previously defined parameters, the other inputs for module 3 (which is directly related to the project presented herein) are explained below:

- Total time (ns): length of an A-Scan in nanoseconds, usually 12 ns.
- Start time (ns): approximated start time of the main pulse (ns); this could be inferred from the x-axis in the plot after inputting the files.
- End time (ns): approximated end time of the main pulse (ns); this could be inferred from the x-axis in the plot after inputting the files.
- Central frequency (GHz): central frequency of the operated antenna in GHz, usually 1–2 GHz.

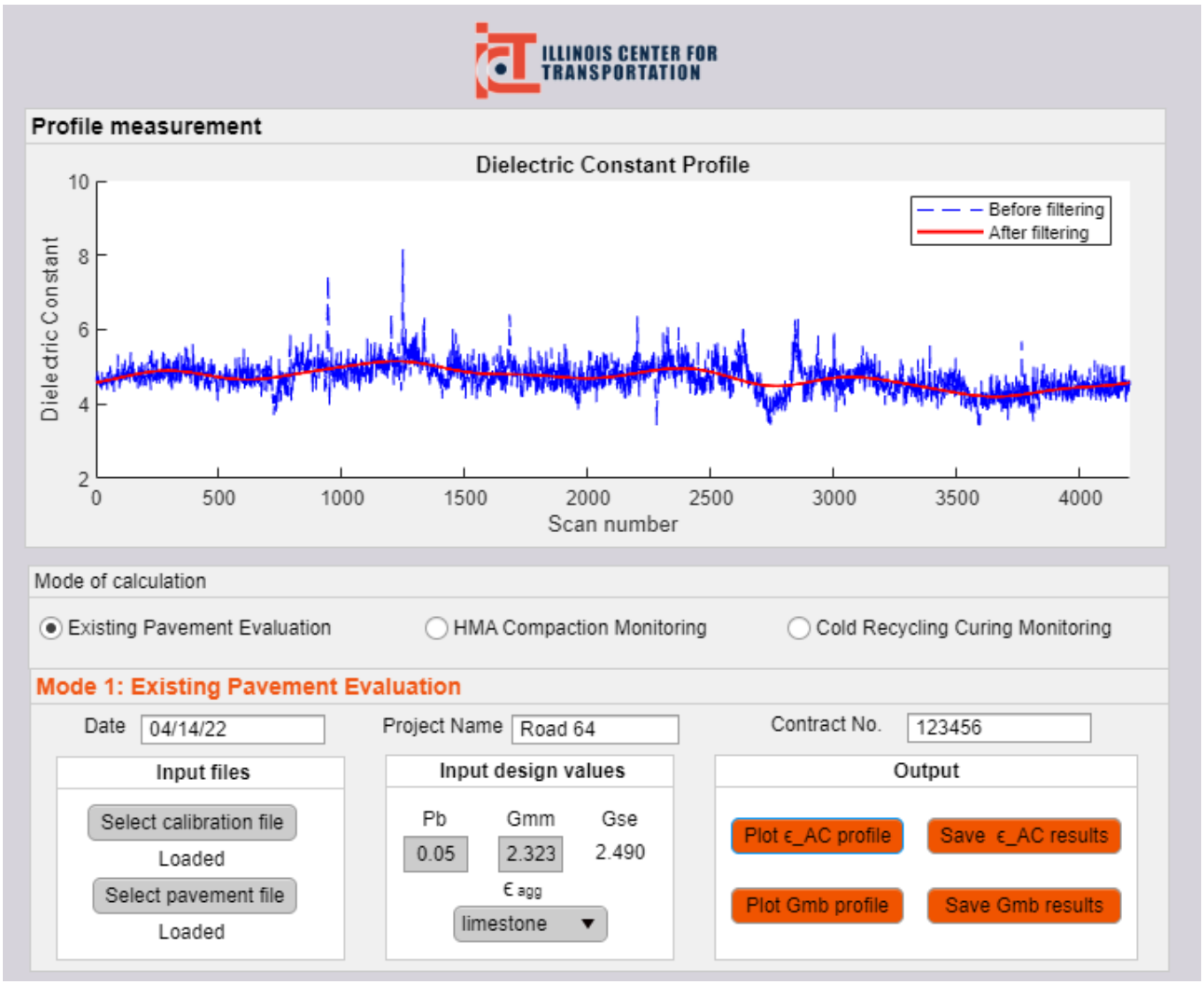

Figure 106. Photo. Dielectric constant profile results in mode 1.

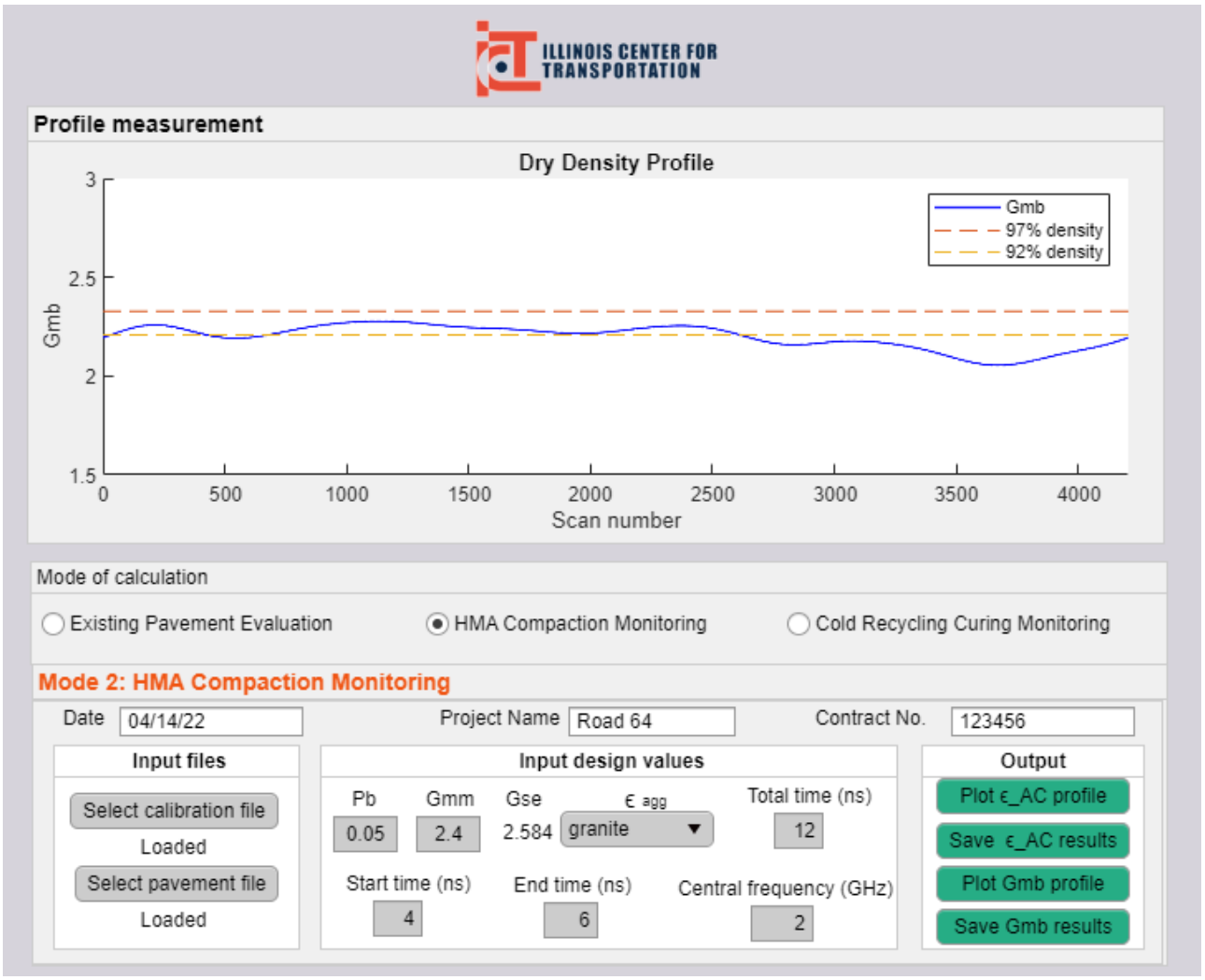

Figure 107. Photo. Mode 2: HMA compaction monitoring with density example.

APPENDIX D: XCMP METHOD REVIEW

Another method to predict the dielectric constant of a bulk asphalt mixture is the extended common midpoint (XCMP) method (Leng & Al-Qadi, 2014). The XCMP setup uses two 2 GHz air-coupled antennas for data collection, as presented in Figure 108. This method uses the antenna setup geometric information and two-way travel time of the transmitted signals to obtain the bulk dielectric constant value (see arrows in Figure 108).

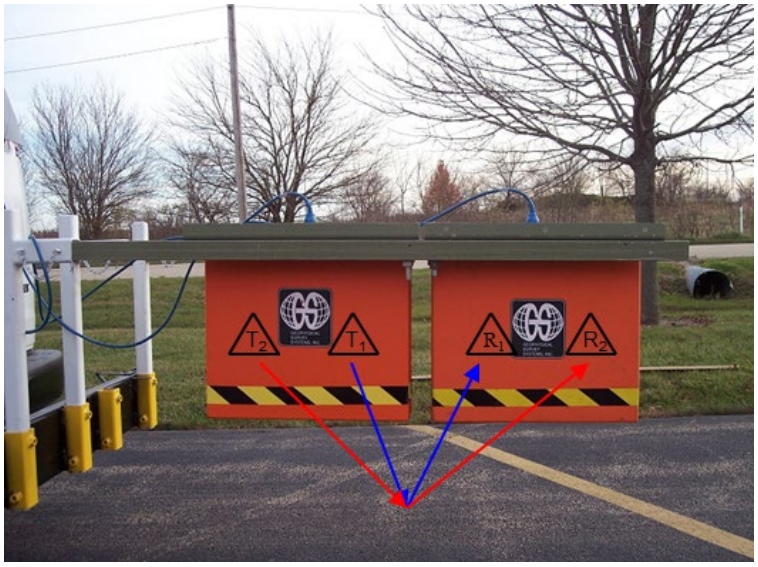

Figure 108. Photo. GPR test setup of XCMP approach.

Trial tests were performed at the Illinois Center for Transportation before using the algorithm in fields (Figure 109). Both air-coupled bistatic systems are set at height d_0 above the ground. *T* represents the transmitter, and *R* represents the receiver. The separation distance between the transmitter and receiver of the inner system (T1/R1) is x_{01}, and that of the outer system (T2/R2) is x_{02}. The distance between the incidence point and reflection point of T1/R1 is x_1, and that of T2/R2 is x_2. The XCMP method needs the reflections from the layer surface and bottom reflections. To magnify the reflection from the pavement layer bottom, steel sheets were embedded under the pavement surface layer. Figure 110 presents the collected signals from two antennas.

Figure 109. Photo. GPR measurements using the XCMP method.

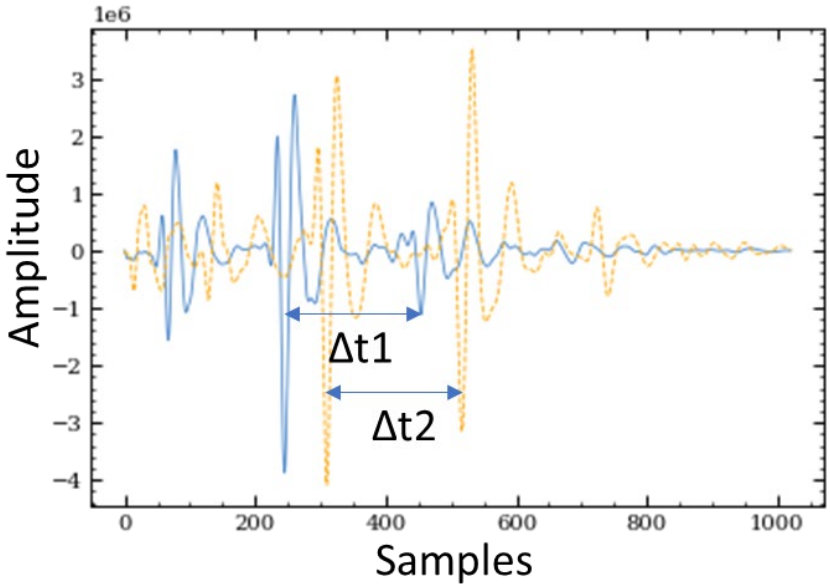

Figure 110. Chart. Collected GPR signals using the XCMP method.

According to Leng and Al-Qadi (2014), the dielectric constant and layer thickness can be calculated as presented in Table 11.

Table 11. Collected Signal Information and Corresponding Dielectric Constant and Layer Thickness

#	Time interval Δt1	Time interval Δt2	Original thickness	Calculated ϵ	Calculated thickness
1	2.99e-9	3.39e-9	6 in.	6.34	0.180 m
2	2.07e-9	2.39e-9	4 in.	–	–
3	1.02e-9	1.56e-9	2 in.	–	–
4	4.09e-9	5.62e-9	8 in.	8.74	0.208 m

Missing values in Table 11 are negative, which indicates numerical errors in the calculation of dielectric constants and pavement thickness using the XCMP method. The XCMP method performed well for pavement layers thicker than 4 in. However, for thin pavement layers, the XCMP method will be affected by the sampling rate limitation of GPR systems. For thin pavement layers, the difference between Δt1 and Δt2 is relatively small and will cause numerical error during the calculation. For non-dry asphalt pavement, the GPR signal is attenuated because of internal moisture; thus, the reflection from the bottom of pavement layer will be difficult to observe.

Considering the signal attenuation in the wet asphalt mixture and the thickness of the CIR layer, the XCMP method was not recommended in this study. Instead, the reflection amplitude method was applied to calculate the dielectric constant of the pavement layer.


Illinois Department
of Transportation


ILLINOIS